Development of Alkali-Activated Concrete Incorporating Carbonated Wood Biomass Fly Ash as a Sustainable Precursor

By

Abdellah Hussein

to obtain the degree of Master of Science in Civil Engineering
at the Delft University of Technology
to be defended publicly on 7th of July 2025 at 15:00.

Project duration:	May 2023 – July 2025	
Thesis committee:	Prof. Dr. Guang Ye	Chairman
	Dr.ir. Kees Blom	External Examiner
	Dr. MSc Xueyan Liu	External Examiner
	Dr. ir. Boyu Chen	Daily Supervisor
	MSc. Yu Zeng	Daily Supervisor

TU Delft Delft University of Technology

Acknowledgements

This thesis marks the final step of my master's journey in structural engineering, with a specialisation in concrete structures at the TU Delft. The work presented here reflects not only a period of research into carbonated biomass fly ash as a low-carbon alternative in concrete but also a period of significant personal and academic growth. Working at the intersection of sustainability and engineering has given me a new perspective on the responsibilities and possibilities we carry as structural engineers.

I would like to express my sincere gratitude to Prof. Dr. Ye, my thesis chairman, for his thoughtful guidance and steady support throughout this project. His feedback helped me keep sight of the bigger picture while pushing me to refine the details.

A special thank you goes to my daily supervisors, Dr. Boyu Chen and MSC. Yu Zeng, for their patience, encouragement, and continuous involvement throughout the experimental phase. Their clear advice and sharp critical thinking helped me stay grounded through all the ups and downs in this journey.

To the technicians and lab staff, your practical knowledge and willingness to assist, even on short notice, made a real difference. I especially want to thank Maiko van Leeuwen, Ton Blom, John van den berg and Arjan Thijssen for their support in the Stevin and Micro Labs; their contributions were crucial in making this work possible.

Finally, thank you to everyone, colleagues, friends, and family, who stood by me during this process. Your support kept me going, and for that I'm truly grateful. I hope this work adds something valuable to the conversation around sustainable construction and maybe even opens a door for the next person to take it a step further.

This work was supported by the funding received from the European Union's Horizon Europe research and innovation programme under grant agreement No 101058162 (AshCycle).

Abdellah Hussein

Delft, June 2025

Abstract

Concrete is one of the primary contributors to global carbon emissions, mainly due to the widespread use of Portland cement. Transitioning to more sustainable binder alternatives is therefore very crucial. The potential advantages of using wood biomass fly ash (BFA) as a sustainable precursor in the manufacturing of alkali-activated concrete is investigated in this study. Several biomass fly ashes (BFA1, BFA2, BFA3, and WA4) were characterised to identify the most suitable candidate for CO_2 sequestration. Focusing on the existence of reactive Ca- and Mg-bearing phases, the selection was based on both chemical composition and phase analysis using XRF and XRD, followed by a free lime content analysis. Among these investigated ashes, BFA1 showed the most interesting characteristics, particularly in regard to its possible CO_2 absorption capacity.

The selected biomass fly ash (BFA1) underwent a two-stage pretreatment process intended to improve its environmental performance as well as to improve its use in alkali-activated concrete. The first step involved a water-interaction treatment. This treatment was primarily meant to prevent the generation of hydrogen gas, an issue that typically originates from the reaction of metallic aluminium in the ash with the alkaline environment. In addition to that, this treatment also enables the immobilisation of heavy metals. The second pretreatment was an accelerated carbonation pretreatment. This is mainly focusing on an increase in the CO_2 sequestration by transforming reactive CaO and $Ca(OH)_2$ into stable carbonates such as calcite. In addition to carbon absorption, this carbonation process contributed further to the immobilisation of heavy metals.

The effectiveness of each of these methods was assessed. The main assessment criteria were the reduction in heavy metal concentration, removal of metallic aluminium, and overall carbonation efficiency. Both treatments effectively dropped heavy metal levels to below the Dutch Soil Quality Limit (SQL). Furthermore, the combination of both treatments proved most successful for totally mitigating metallic aluminium content. Hereby resolving major challenges for the safety of including BFA into concrete. The carbonation of the ash was carried out through two routes, a dry route and a wet route (L/S = 0.3). The effectiveness of the wet carbonation method exceeded the gas-solid method by achieving complete carbonation in just eight hours. In contrast, the gas-solid approach was significantly slower, and after two months, total carbonation was nevertheless not achieved. The persistent presence of free lime confirmed the limited efficiency of the gas-solid route. The CO_2 absorption capacity of BFA1 was eventually determined to be 6.59% by weight, highlighting the effectiveness of the wet carbonation method in facilitating carbon sequestration.

Combining QXRD, ICP-OES dissolution, FTIR and isothermal calorimetry allowed for the assessment of the reactivity of the pretreated BFA1 samples. Raw BFA showed the most reactivity among the various treatments, based on its largest cumulative heat release from the isothermal calorimetry test. Its finer particle size distribution and lower degree of particle agglomeration were mostly responsible for this increased reactivity. Raw BFA also showed the highest dissolution levels of alumina and silica in the ICP-OES test, further confirming its superior chemical reactivity in alkaline environments. On the other hand, the samples that underwent carbonation treatment showed a reduction in reactivity. This was clear from the lower total heat generated in the isothermal calorimetry tests and the lower dissolution of reactive elements in the ICP analysis. In addition to that, FTIR spectra showed the presence of gel-like structures in both water-treated and carbonated BFA1 samples, demonstrating the initial formation of reaction products. These early reactions reduce the reactivity of the material by consuming some of its available reactive content, thereby influencing the reactivity during subsequent alkaline activation.

Following the pretreatment process of the ash, the water-carbonation-treated BFA was incorporated into alkali-activated concrete mixtures by partially replacing slag at varying replacement levels. These concrete mixtures were developed and tested in order to meet the requirements for the production of sidewalk pavement blocks. Mechanical testing showed that a 25% replacement level of slag with treated BFA was sufficient to satisfy the compressive strength class of C30/37, as defined in the regulation. The reference mix (AAC-REF) reached a compressive strength of 49 MPa, while the mix including 25%

pretreated BFA showed a slightly lower strength of 46 MPa. Durability testing showed that the treated BFA significantly lowers freeze-thaw resistance. The mass loss resulting from freeze-thaw after 28 cycles increased from 3.63 kg/m² in the AAC-REF sample to 5.66 kg/m² in the BFA-containing mix at the 25% replacement level, a significant reduction in the long-term durability under freeze-thaw conditions.

Paste samples were prepared to analyse the impact of BFA addition on the microstructure and phase composition. FTIR analysis of the paste determined the degree of polymerisation, showing a slightly increased polymerisation degree in the BFA-containing paste. QXRD and TGA were applied to determine the amount of reaction products formed after alkali activation. Both pastes contained similar types of reaction products, but the reference paste contained a greater amount of amorphous phases. Lastly, SEM analysis was performed to examine morphological and compositional changes due to the incorporation of BFA. BFA incorporation resulted in the development of micro-cracks between the BFA grain and the surrounding matrix and within the BFA particle itself. SEM-EDX point analysis revealed that the reaction gel consisted mainly of C–A–S–H, although the BFA-containing specimens had a larger Ca/Si ratio, likely due to the high calcium level in the BFA and the existence of calcite.

A life cycle assessment (LCA) was conducted to measure the environmental benefits of including water-carbonation-treated BFA, with a focus on lowering its carbon footprint. The results showed that replacing 25% of slag with pretreated BFA reduced CO_2 emissions by 21.28% relative to the reference mix, which consisted of 100% slag. This shows the potential of using BFA as a sustainable alternative precursor in an alkali-activated system.

Finally, this thesis demonstrates that pretreated biomass fly ash can be utilised in alkali-activated binder systems, especially under combined water and carbonation treatments. Although these treatments might slightly reduce the reactivity of the ash, their environmental benefits, including CO_2 sequestration, metallic aluminium elimination, and heavy metal immobilisation, provide strong justification for their incorporation in sustainable building materials.

Table of content

List of Figures

List of Tables

1

Introduction

1.1 Background

Concrete is the most widely applied construction material globally. A material highly valued for its strength, durability, and capacity to accommodate a great range of structures and applications. Despite its advantages, the production of conventional concrete, notably Portland cement concrete, is a highly polluting activity, contributing about 8% of the total CO_2 emissions globally [1], [2]. In response, innovations in sustainable construction have aimed to minimise these emissions by turning to alternative precursor materials. Among these materials, biomass fly ash has demonstrated great potential as a viable alternative due to its reactivity in alkaline environments [2], [3], [4].

In the EU, an amount of 50 million tonnes of biomass ash is produced every year, with a large portion coming from the combustion of wood [5]. Currently, most wood BFA is either disposed of in landfills or used as a soil amendment in forestry [5], [6], [7]. Wood BFA contains a high quantity of calcium-bearing phases, like free lime and portlandite [8]. These phases can react with CO_2 to form stable carbonates such as calcite. Incorporating carbonated wood ash into alkali-activated binders can be beneficial, as it enables permanent CO_2 storage in concrete. Furthermore, it reduces the dependence on conventional precursors like slag. This is further helping to lower the embodied carbon content of concrete. This approach stands in contrast to the conventional applications of BFA as a soil amendment or landfill disposal, which do not ensure long-term CO_2 absorption and may involve heavy metal leaching risks.

1.2 Problem statement

Despite the potential benefits of incorporating biomass fly ash in concrete, several significant challenges stand against its widespread adoption. The most important of these is the variability of physical and chemical characteristics, which may cause unpredictable performance when added to concrete [9]. This variability comes from the differences in biomass sources, temperatures during the combustion, and the techniques of combustion [10]. Furthermore, the hazardous components that are found in biomass fly ash are complicating its widespread application. These components are heavy metals, metallic aluminium, and chlorides, which can negatively affect the mechanical properties and environmental performance of concrete [11], [12].

Although previous work has primarily addressed the environmental implications of carbonation, including CO_2 uptake and immobilisation of heavy metals [13], [14], [15], a gap in the literature remains regarding the application of carbonated BFA in alkali-activated systems. A deeper understanding is necessary for how carbonated BFA will function in these systems. In particular, how it will react with other mix ingredients and how it will contribute to the overall performance of the resulting concrete. This study aims to close this gap by investigating the carbonation of BFA, optimising its application in alkali-activated mix designs, and assessing the mechanical and durability properties of the resulting material.

1.3 Research aim and objectives

This research explores the viability of utilising carbonated biomass fly ash as a partial precursor to alkali-activated concrete. The research is focused on several main objectives:

- To determine the raw biomass fly ash characteristics regarding carbon capture potential and select one among various BFA ashes based on its absorption potential.
- To identify the optimal pre-treatment methods to remove metallic aluminium from the raw biomass fly ash and increase the BFA's CO_2 uptake capacity. The influence on leaching of the heavy metals as well as the reactivity of the ash, will also be taken into consideration.
- Incorporate pre-treated biomass fly ash in different concrete mixtures and investigate the mechanical and durability properties. Additionally, microstructural analysis of the paste binders will be conducted to identify modifications caused by the addition of the pre-treated BFA.
- Performing a life cycle assessment to measure the CO_2 reduction after the incorporation of BFA into various concrete mixtures.

1.4 Scope and limitations

Several limitations determine the scope of this research:

- This study will only consider biomass fly ash as a partial binder replacement for slag.
- The evaluation of concrete properties will be limited to 28 days of curing.
- Concrete and paste samples are cured at a room temperature of 20 °C and a relative humidity of ≥95%.
- No superplasticizers or any additional chemical admixtures will be used in the concrete and paste mixtures.

1.5 Thesis structure

The structure of this thesis is presented in Figure 1.1.

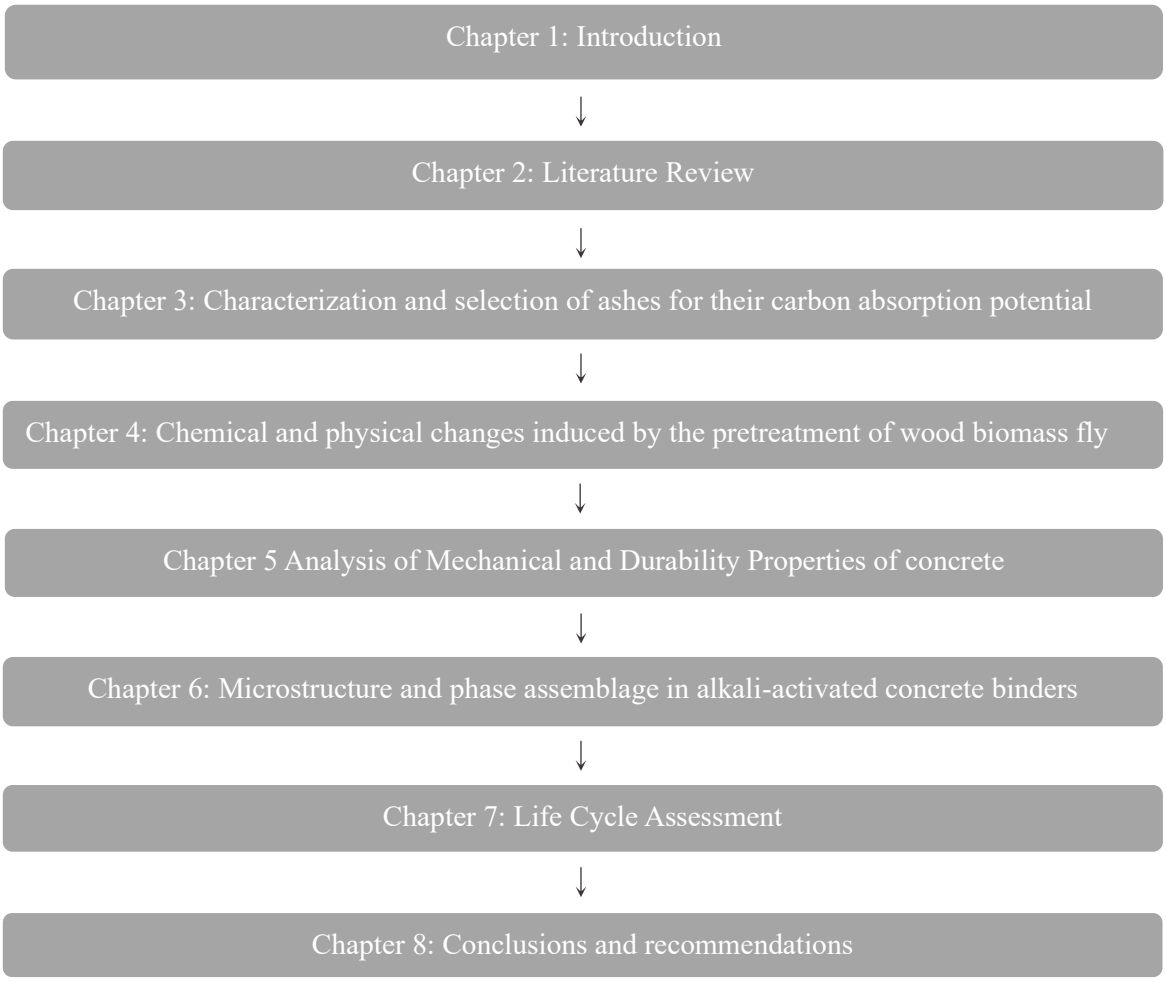

Figure 1.1: Outline of the thesis.

2

2 Literature review

2.1 Biomass fly ash

Biomass is a renewable energy source originating from natural sources, which include plants, trees, and agricultural wastes. Currently, it accounts for about fifteen percent of the global energy consumption, with projections suggesting it could reach up to 50% of the world's energy needs by 2025 [16]. The combustion of biomass generates ash as a waste product. This ash is classified into two types, which are biomass bottom ash (BBA) and biomass fly ash (BFA), as shown in Figure 2.1 [17]. Biomass bottom ash consists of the heavier and coarser fraction that gathers at the bottom of the combustion furnace [18]. Biomass fly ash is much finer and is carried with the flue gases before being captured by the filtration systems [17]. Biomass fly ash is an interesting alternative as a precursor for the production of alkali-activated materials due to its relatively low organic content and its fine texture [17].

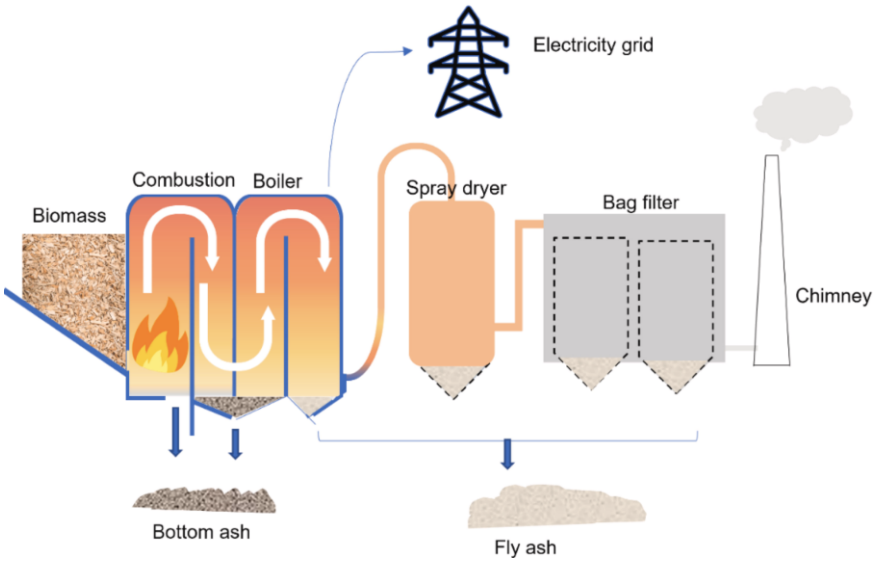

Figure 2.1: Flow diagram of biomass combustion system showing energy production and ash separation into bottom ash and fly ash [8].

Low-carbon binders such as alkali-activated materials offer a more sustainable alternative to conventional Portland cement. Aluminosilicate-rich precursors are activated with an alkaline solution that produces a hardened binder through a process called geopolymerization [19]. AAMs traditionally depend on precursors including slag, coal fly ash, and metakaolin. But since these materials are byproducts of manufacturing processes that are themselves undergoing change or decline, their availability is increasingly uncertain [20]. This makes the search for alternative precursors more crucial, and BFA is one of the candidates with great potential. Using BFA as an alkali-activated material also poses certain challenges. Although BFA contains reactive amorphous phases that could be involved in the alkali activation process, its overall reactivity is lower than that of more established precursors [21]. This is due to the lower amorphous content in the ash, which is necessary for the alkali activation process [22]. One notable characteristic of BFA is the relatively higher loss on ignition (LOI) content, which reflects the presence of unburned carbon. High LOI causes challenges since it increases water demand

and can negatively impact the mechanical properties of the produced final product [23]. Furthermore, BFA may contain impurities like chlorides and heavy metals, which can cause environmental risks. The presence of metallic aluminium in BFA is also adding more challenges to its use in concrete. This metallic aluminium can react in an alkaline environment and generate hydrogen gas, which results in concrete expansion and cracking. As a result, pretreatment of the ash is essential in order to resolve these issues.

2.2 Pretreatment of biomass fly ash

Different pre-treatment techniques are utilised on biomass fly ash (BFA) to address issues such as lower reactivity and the presence of compounds like chlorides, sulphates, metallic aluminium, and heavy metals. The pretreatments are designed to improve the suitability of the ash as a precursor for application in alkali-activated systems. The most common pretreatment methods include grinding, thermal activation, accelerated carbonation, and washing. These techniques are applied to a wider range of incineration ashes, including biomass fly ash, coal fly ash, and municipal solid waste incineration (MSWI) fly ash, in order to improve their reactivity and remove contaminants.

These methods and their addressed problems are summarised in Table 2.1. Some of the treatments, including thermal activation and grinding, are effective but energy-intensive processes. Their application can raise the total carbon footprint of the produced concrete. Other methods, including chemical treatments, use chemicals like sodium hydroxide that are themselves hazardous to the environment and can interfere with the alkali activation reaction. The selection of a pre-treatment strategy should therefore be based on a balance between enhancing performance and reducing environmental impacts.

Table 2.1: Summary of BFA pre-treatment methods and the problems they address.

Pre-treatment Method	Problems Addressed
Accelerated carbonation	Immobilizes heavy metals and enables permanent CO_2 storage
Grinding and milling	Increases surface area and reactivity, improves workability
Sieving	Removes coarse particles and unburnt LOI content, enhances reactivity
Thermal activation	Enhances reactivity, reduces heavy metal content, oxidizes metallic aluminium
Water treatment and washing	Mitigates metallic aluminium, removes chlorides and sulphates contaminants
Chemical treatment (NaOH)	Mitigates expansion caused by metallic aluminium

2.2.1 Methods for metallic aluminium removal

Various methods for removing metallic aluminium have been extensively discussed in the literature. In one of these methods, the ash is immersed in an alkaline solution, allowing the metallic aluminium to react and produce hydrogen gas. A common approach to remove metallic aluminium is the use of sodium hydroxide (NaOH) solutions [24], [25], [26], which stabilizes aluminium and generates hydrogen gas rapidly through the following reaction [26]:

$$2Al + 2NaOH + 6H_20 \rightarrow 2Na[Al(OH)_4] + 3H_2 \quad pH > 11.75$$

Although this method is effective, it was deemed unsuitable for this study because the use of sodium hydroxide could interfere with the carbonation process, a critical step in this research. Additionally, immersing the ash in a NaOH solution initiates an alkaline activation process, during which certain reaction products are formed. This reduces the ash's reactivity in subsequent concrete mix designs.

Thermal treatment is also a discussed method in the literature that can be used to remove metallic aluminium. In this method, the ash is heated to reach 1000 ◦C to oxidize the metallic aluminium [27]. Although this method succeeds in reducing the metallic Al to 90 wt%, it is not preferable, as this addition of energy lowers the environmental advantage of the ash, and the higher temperature can change the chemical and mineralogical composition of the ash.

Instead, the aluminium-water interaction method is the most promising method [28], [29], [30].This method takes advantage of the intrinsic alkalinity of biomass fly ash to initiate aluminium-hydrogen reactions. This approach eliminates the need for external chemicals while leveraging the naturally high pH environment provided by compounds in the ash.

The reactions involved in aluminium-water interaction are [29]:

$$2Al + 6H_2O \rightarrow 2Al(OH)_3 + 3H_2$$

$$2Al + 4H_2O \rightarrow 2AlO(OH) + 3H_2$$

$$2Al + 3H_2O \rightarrow Al2O_3 + 3H_2$$

These reactions produce aluminium hydroxides and release hydrogen gas. Additionally, under alkaline conditions, reactions involving calcium hydroxide also contribute as follows [29]:

$$2Al + 6H_2O + 2Ca(OH)_2 \rightarrow 2CaAl(OH)_5 + 3H_2$$

The reaction forms hydrated calcium aluminates, $CaAl(OH)_5$, while calcium hydroxide is regenerated through the following reaction [29]:

$$2CaAl(OH)_5 \rightarrow 2Ca(OH)_2 + 2Al(OH)_3$$

The overall reaction can thus be summarized as [29]:

$$2Al + 4OH^- + 2H_2O \rightarrow 2Al(OH)_3 + H_2$$

This cycle ensures that metallic aluminium is stabilized while maintaining the alkalinity of the ash, making it suitable for further treatments like carbonation.

2.2.2 Accelerated carbonation pretreatment for carbon sequestration

Accelerated carbonation is used to promote CO_2 sequestration within cementitious materials. This process transforms CO_2 into stable carbonates by reactions involving calcium-rich phases. This process makes long-term storage of CO_2 in concrete possible. Biomass fly ash contains a very high amount of calcium and magnesium-bearing phases. These phases are essential for the carbonation process [31]. Fly ash carbonation involves various chemical interactions, which result in the formation of calcium carbonate. This process is shown in three steps, Figure 2.2 [32]:

- In the first step, the calcium and magnesium ions (Ca^{2+} , Mg^{2+}) are released from the solid fly ash matrix into the water through dissolution [33].
- In the second step, the CO_2 dissolves in water to form carbonic acid, H_2CO_3. This weak acid subsequently transforms into carbonate ions, CO_3^{2-} [33].
- In the last step, the released carbonate ions react with the dissolved calcium ions to form $CaCO_3$ [33].

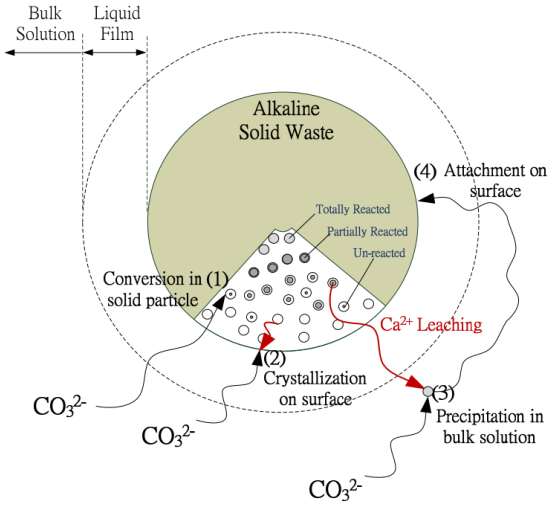

Figure 2.2: Mechanism of accelerated carbonation in alkaline waste ashes [34].

Mineral carbonation follows two main pathways: direct and indirect carbonation, as can be seen in Figure 2.3.

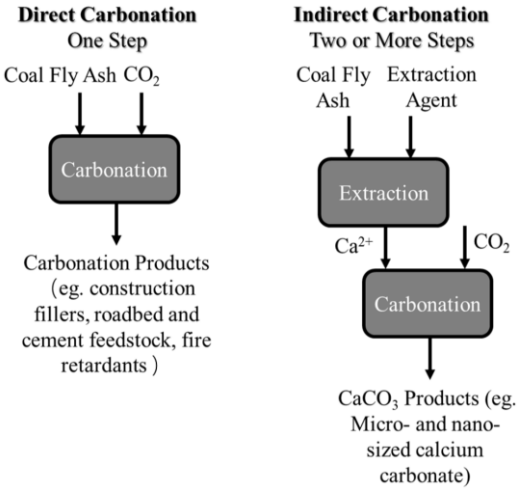

Figure 2.3: Schematic representation of the direct and indirect carbonation routes for mineral CO_2 sequestration [35].

Direct Carbonation occurs within a single chamber and utilizes either dry or wet methods. The primary advantage of this pathway is its simplicity, making it a promising technique for using fly ash in CO_2 sequestration. There are two key techniques under this pathway [32], [36], [37]:

1. **Gas-Solid Carbonation**: In this technique, fly ash is directly exposed to gaseous CO_2 in a controlled environment. This method is favoured for its simplicity, However, the reaction rates tend to be slower due to limited CO_2 mobility through the solid material. Reaction speeds can be enhanced by increasing CO_2 concentration, temperature, and pressure, which help to accelerate CO_2 diffusion and carbonate formation.
2. **Aqueous Carbonation**: This method involves mixing fly ash with water, followed by exposure to CO_2 gas. Aqueous carbonation is generally more effective than gas-solid carbonation because of the better dissolution of CO_2 in water and faster ion exchange in the liquid phase.

Indirect carbonation is a multi-step process where calcium and magnesium ions are first extracted from the fly ash using a leaching agent, such as acids or ammonium salts [37], [38], [39]. After extraction, these calcium-rich solutions are reacted with CO_2 to produce pure carbonate products [38]. This method allows for more controlled carbonation and typically results in higher-purity carbonate products.

Various leaching agents, including sulphuric acid (H_2SO_4), acetic acid (CH_3COOH), formic acid (HCOOH), and nitric acid (HNO_3), as well as HCl, have been tested for the leaching of magnesium for mineral carbon sequestration [40]. Kodama et al employed ammonium chloride (NH_4Cl) as an extraction agent for the extraction of calcium, thereby achieving up to 99% efficiency in the selectivity of calcium extraction [41]. While indirect carbonation can produce purer carbonate products, making them suitable for higher-value applications, it involves more complex processing stages and higher costs, which could hinder scalability for concrete production.

2.2.2.1 Factors influencing accelerated carbonation

Several factors influence the rate and extent of carbonation in fly ash materials. These factors can be broadly categorized into external factors, which relate to the conditions under which carbonation occurs, such as CO_2 partial pressure, temperature, and moisture content [42] and internal factors, which are inherent to the properties of the fly ash itself. The most significant internal factors include the chemical composition of the ash and its particle size distribution, both of which directly affect the ash's reactivity and its ability to sequester CO_2.

CO_2 partial pressure

The kinetics of the carbonation reaction in fly ash depend on the partial pressure of CO_2. The carbonation process proceeds slowly at low CO_2 pressures, particularly in the gas-solid route. Calcium carbonate forms within the pores and blocks them, hindering further CO_2 diffusion into the pores [32], [36], [43]. Increasing the CO_2 pressure enables additional carbonation by improving gas penetration and reopening of the blocked pore. In the case of wet carbonation, the CO_2 pressure is also very significant, since it affects the CO_2 gas solubility in the water. Henry's Law governs this relationship since it states that the partial pressure of a gas in a liquid determines its solubility. Higher CO_2 pressures therefore result in a higher concentration of dissolved CO_2 in the pore solution, thereby increasing the amount of reacting agent available for carbonation [34], [36]. This relationship is described by the next equation:

$$CO_2 = kCO_2)$$

Where CO_2 is the concentration of CO_2 dissolved in water, kCO_2 is Henry's constant, and $P(CO_2)$is the partial pressure of the CO_2 gas [34].

Experimental studies support these theoretical relationships. Dananjayan et al. investigated the effect of CO_2 pressure on the carbonation capacity of fly ash [36]. Their results showed that increasing CO_2 pressure significantly enhanced reaction kinetics in the gas-solid route, with a maximum carbonation capacity of 26.33 g CO_2/kg achieved at 10 bar, Figure 2.4 (left). The CO_2 pressure increase was also beneficial for the wet carbonation route. However, in this route, lower pressure was required to reach higher CO_2 absorption. The maximum carbonation capacity reached 50.3 g CO_2/kg at 4 bar, showing the efficiency of adding moisture to the mix rather than increasing the CO_2, Figure 2.4 (right).

Ukwattage et al. published results in another study on aqueous carbonation [44]. Their study verified that although increasing CO_2 pressures speed up the carbonation process, the total gain in sequestration capacity is negligible. A saturation point is eventually reached, beyond which further increases in pressure yield no significant improvement in carbonation efficiency. [36].

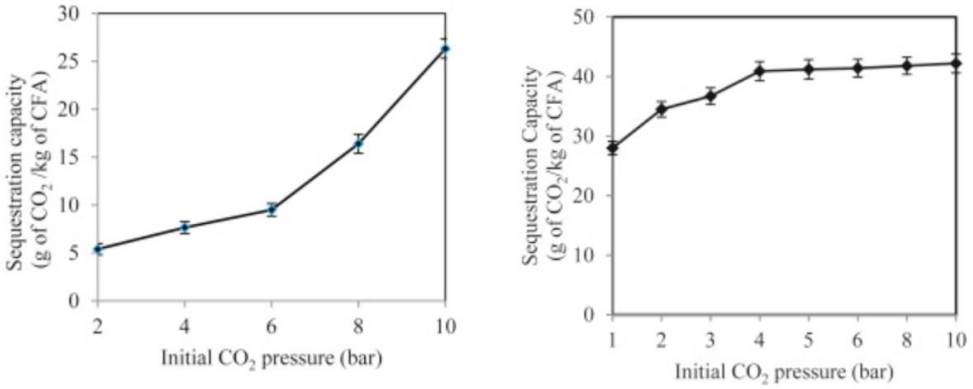

Figure 2.4: This Figure illustrates the relationship between CO_2 pressure and sequestration capacity in both gas–solid (left) and aqueous carbonation routes (right) [36].

Temperature

The rate of carbonation reaction is significantly affected by temperature. Ukwattage et al. investigated the effect of temperature on aqueous carbonation and found that raising the temperature improves reaction rates, thus allowing the maximum carbonation capacity to be reached more quickly[33]. However, the total amount of absorbed CO_2 did not increase significantly [33]. For instance, the absorption was lowest at 20 °C and showed a slight improvement at 40 °C, but temperatures beyond 60 °C led to a decline in carbonation efficiency. This indicates that while kinetics improve, absorption capacity plateaus or even declines at elevated temperatures, Figure 2.5. Similar results were reported by Chang et al [45], who observed that CO_2 uptake accelerates in the temperature range of 30–60 °C, but further heating above 60 °C reduced the overall carbonation conversion rate.

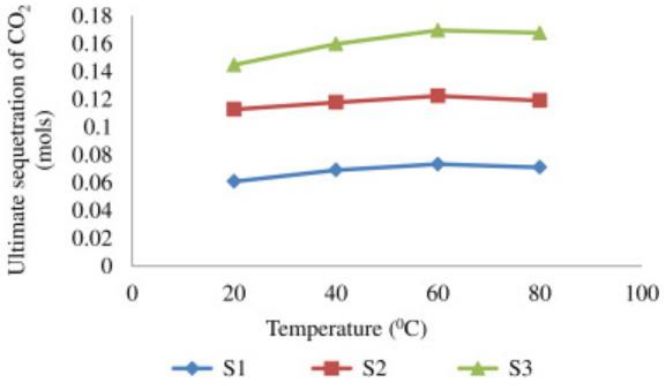

Figure 2.5: Ultimate CO_2 sequestration at varying carbonation temperatures for different fly ash samples [45].

At higher temperatures, the solubility of CO_2 in water decreases. This limits the amount of dissolved CO_2 for carbonation reactions [37]. As illustrated in Figure 2.6, CO_2 solubility is inversely related to the temperature increase [32]. Although higher temperatures can accelerate reaction kinetics, mainly by increasing the leaching of calcium ions [46], [47]. The lower availability of dissolved CO_2 at these higher temperatures could still limit the overall carbonation process. Faster reaction rates at higher temperatures also produce calcium carbonate ($CaCO_3$) rapidly on the surface of fly ash particles. This blocks the internal pore structure and reduces further CO_2 diffusion into the particles. Consequently, limited CO_2 gas transport reduces the long-term carbonation potential even if initial carbonation is accelerated [32], [43].

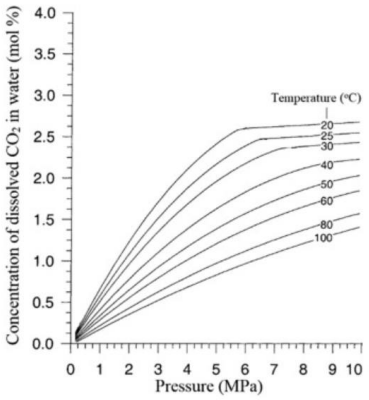

Figure 2.6: Effect of temperature on CO_2 solubility in water under different pressures [32].

Water content

Determining the carbonation rate depends on the water content in fly ash. Water facilitates the dissolution of CO_2 and the leaching of Ca^{2+} ions from the ash material. The dissolving of CO_2 depends on a certain amount of water to produce carbonate ions (CO_3^{2-}) that react with the leached calcium ions to generate calcium carbonate. However, as noted by Ukwattage et al. (2014) [33], too little water leads to dry conditions that slow down ionization and calcium leaching, while too much water inhibits CO_2 diffusion by blocking the pores of the matrix.

Wang et al reported that in slurry carbonation systems, the liquid-to-solid (L/S) ratio is a key parameter [48]. For wet carbonation of fly ash, an L/S ratio of 0.25 L/kg was found to be optimal in reaching the highest absorption capacity. This L/S ratio was also optimum for increasing the reaction speed, thus reaching the highest potential in less time. Increasing the L/S ratio beyond this value resulted in a reduction of carbon absorption due to hindrance of the CO_2 diffusion into the pores of the solid, Figure 2.7.

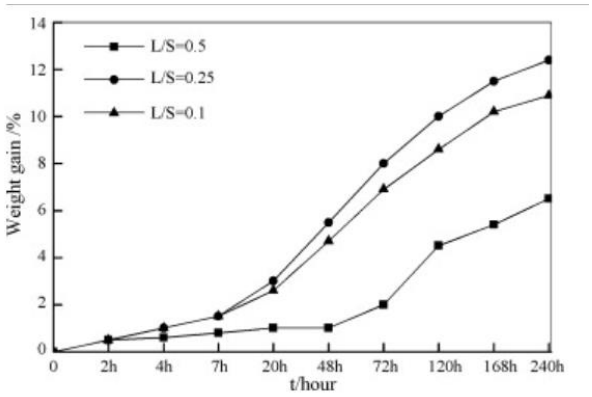

Figure 2.7: Carbonation Progress at Different Liquid-to-Solid Ratios [48].

Several studies have investigated the optimal solid-to-liquid ratio for maximizing CO_2 absorption under aqueous carbonation conditions [49], [50]. There is broad agreement in the literature that the ideal water-to-solid ratio lies between 0.2 and 0.3, as the presence of water is essential to promote the dissolution of CO_2 and facilitate the carbonation reaction. In the absence of moisture, carbonation is minimal, and reaction rates are significantly reduced. As illustrated in Figure 2.8, gas-solid carbonation can still occur without water, but the process is much slower and far less efficient compared to aqueous carbonation.

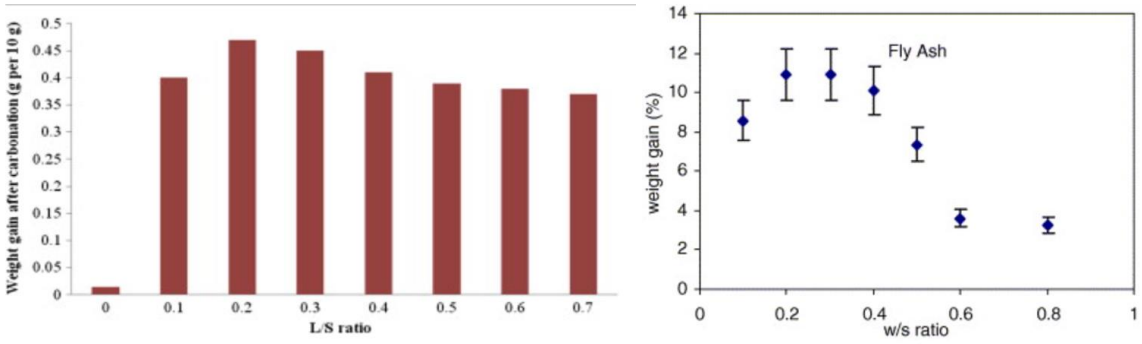

Figure 2.8: Relationship Between Water Content and Weight Gain During Aqueous Carbonation [49] [50].

Ash-dependent factors

The chemical and physical properties of the ash itself can be considered internal influence factors that have an effect on the potential for carbon sequestration. The presence of calcium and magnesium-bearing compounds directly affects the CO_2 sequestration capacity. Fly ash with higher concentrations of free lime (CaO) and portlandite $Ca(OH)_2$, shows faster carbonation rates and greater CO_2 uptake potential [51].

The particle size and surface area of the cementitious material are also crucial factors in the kinetics of carbonation in ash materials [33]. Smaller particles provide a larger surface area for CO_2 diffusion, enhancing the reaction rate. Polettini et al. investigated the carbonation of slag with various particle sizes [52]. With the particle size reducing from 1000 to approximately 80 µm, the CO_2 uptake of the slag was found to increase exponentially, Figure 2.9. With the further reduction in the particle size, the CO_2 uptake capacity decreased. This reduction is likely due to particle agglomeration, which reduces the effective reactive surface area. Additionally, the rapid formation of a calcite layer on the particle surface at finer sizes may block pore structures, further hindering CO_2 diffusion and limiting the progression of the carbonation reaction.

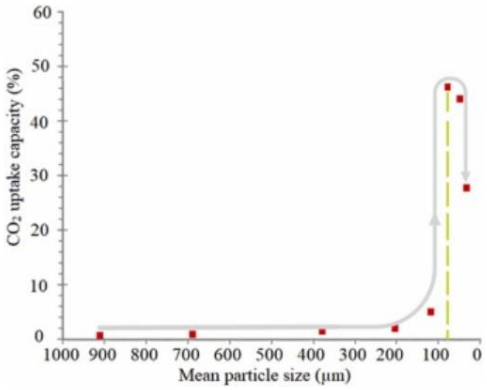

Figure 2.9: the particle size of slag and the corresponding carbon uptake [32].

2.2.3 Pre-treatment methods to improve the ash reactivity

Various methods have been mentioned in the literature to increase the reactivity of fly ash. These methods include mechanical grinding, sieving, and thermal activation. Sajay et al. [53] reported an increase in ash reactivity after milling, mainly due to the reduction in particle size. Reactivity improves when the average particle size decreases below 5–7 µm. Temuujin et al. investigated the mechanical activation of fly ash using a vibration mill [54]. When this mechanically activated fly ash was used to prepare geopolymer paste cured at ambient temperature, an 80% increase in compressive strength was achieved compared to geopolymer made from raw fly ash. This improvement was linked to the smaller particle size after mechanical activation, which enabled higher dissolution rates of the ash particles.

It was also reported that grinding could improve reactivity due to an increase in the amorphous content. This phenomenon is linked to localised high-temperature spots generated at the points of collision during grinding, which can induce partial melting of crystalline phases [55]. Consequently, even non-reactive phases such as quartz may become partially reactive, thereby improving the overall reactivity of the ash.

Thermal activation is also used to increase the reactivity of BFA. In this method, high temperatures, mainly between 600 and 900°C, are used to decompose crystalline phases and increase the amorphous content. Faried et al. reported that burning rice husk ash at 700°C produced the highest amount of amorphous silica, thereby increasing the ash reactivity [56]. In addition to that, the thermal treatment removes unburned carbon content. This carbon content negatively impacts strength development, as unburned carbon can absorb water and negatively influence the hydration process. Zeyad et al have confirmed in their study that heat treatment at temperatures up to 700°C can effectively eliminate unburned carbon [57]. His approach enabled the increase of BFA to 25% by weight of the binder without a reduction in the mechanical performance.

Popławski et al. [58] also studied sieving to enhance the reactivity of BFA. Following the removal of the coarse particles, the process of sieving resulted in more reactive element concentration in the finer ash. It enhanced the reactivity of the ash, with a corresponding early and long-term gain in strength. Compressive strength of the samples containing 15% of the sieved ash was equal to or even surpassed that of the control samples. The results revealed that the process of sieving is quite an effective and simple method for enhancing the performance of biomass fly ash.

2.2.4 Pre-treatment methods to immobilize heavy metals in fly ash

Accelerated carbonation has also been shown to reduce heavy metal leaching [48], [59]. During carbonation, the pH of the ash drops to around 9. This pH is favourable for immobilising a wide range of heavy metals [60]. Tian Sicong et al. reported that the leaching solution pH is the dominant factor for heavy metal dissolution. The leaching concentrations of Pb, Zn, Cu, and Se showed a U- or V-type relation with the pH. The minimum leaching occurred under slightly alkaline to neutral conditions in the range of pH from 8 to 10. This pH range is achieved after carbonation treatment. Qixin Yuan et al. examined the influence of carbonation pressure on heavy metal leaching [61]. It was found that increasing carbonation pressure to 5 MPa reduced the leaching concentrations of Cr, Cd, Pb, and As by 18.25%, 4.66%, 9.98%, and 8.10%, respectively. Further increasing the pressure to a supercritical state of 8 MPa decreased the concentrations by 34.94%, 7.00%, 15.28%, and 35.85%, respectively. Carbonation results in the formation of $CaCO_3$, which blocks the pores and encapsulates these heavy metals.

Different studies revealed that mechanical grinding in combination with carbonation has the potential to further immobilize heavy metals. Mechanical activation increases the surface area of the ash, thus allowing more of the heavy metal particles to react. Chen et al found that carbonated and ball-milled fly ash achieved a heavy metal stabilization efficiency of up to 99.8% for Pb and 98.5% for Zn, which was significantly higher than that of untreated fly ash [62].

Thermal activation is also used for heavy metal removal. The principle involves heating the ash to high temperatures so that metals are vaporised and condensed into a separate fraction [63], [64], [65]. Metals such as Zn, Pb, Cu, and Cd are targeted in these processes. Other metals, for example, As, Cr, and Ni, are generally non-volatile, whereas Hg is volatile and difficult to condense [66]. Nowak et al. thermally treated fly ash at 1050°C for 10 minutes and found that over 95% of Cu, Pb, and Zn have been removed [66]. An increased temperature and longer duration enhance removal efficiency. But when the temperature is above the melting point range of the ash, evaporation of the metals may be reduced by altering the ash viscosity and sintering.

2.3 Incorporation of biomass fly ash in concrete mixture

Incorporating biomass fly ash (BFA) in concrete may affect its mechanical and durability characteristics, based on the reactivity of the ash and its behaviour when combined with other mix elements. Various studies have assessed the effects of BFA at different replacement levels for conventional binders, including cement, slag, or fly ash from coal. Some have reported enhanced performance in the concrete, while others have reported detrimental effects, which are highly reliant on the particular ash characteristics. This variation in results further emphasizes the need for knowledge of BFA material characteristics and its behaviour in the binder system. The following section summarizes relevant studies examining how BFA influences important properties in concrete, including compressive strength, tensile strength, and durability.

Ercan et al. studied the effect of ground wood ash on the mechanical properties of alkali-activated mortars [23]. Wood ash was used to partially replace slag at 0%, 10%, and 20%. The ash was ground for 10 and 20 minutes using a planetary ball mill, and sodium silicate (Na_2SiO_3), sodium carbonate (Na_2CO_3), and sodium hydroxide (NaOH) were used as activators. The results showed that mechanical grinding improved the reactivity of the ash, showing that a 10-minute grinding duration was optimal, Figure 2.10. Among all activators, sodium silicate produced the highest compressive strength at both 7 and 28 days. In contrast, untreated wood ash reduced compressive strength due to its high unburned carbon content and the presence of larger and less reactive particles. The sodium silicate activated samples, with ash contents (10%), ground for 10 minutes, achieved a strength gain of 19.72% at the age of 28 days. Grinding for 20 minutes resulted in a strength gain of 6.45%. All the other activators presented similar results. Despite these gains, a higher ash content (20%) still showed a reduction in strength. The loss in strength resulted from dilution of the reactive binder. This study confirmed that grinding improves the reactivity of wood ash in alkali-activated systems, regardless of the used activator.

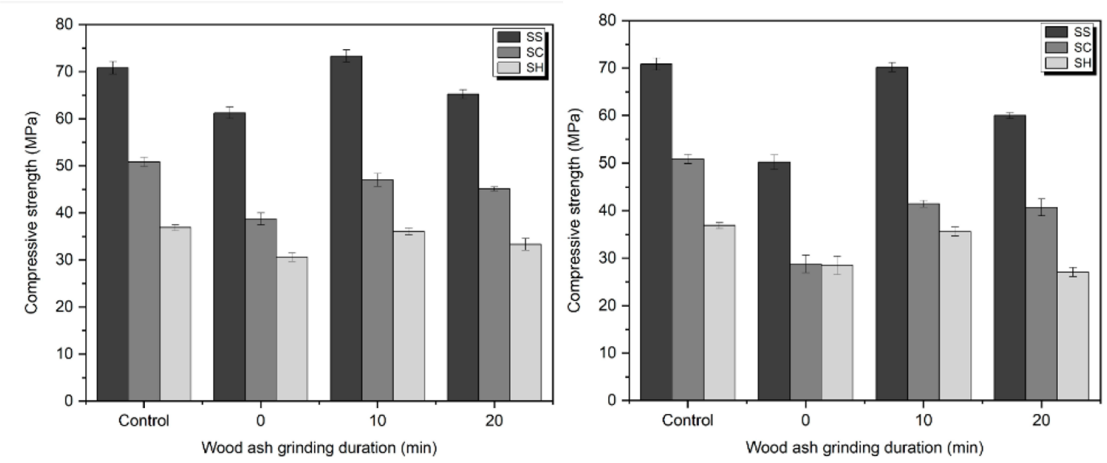

Figure 2.10: Compressive strength of GGBFS mortars containing wood ash at different grinding durations and activated with various alkali activators. Left: 10 wt% wood ash at 28 days; Right: 20 wt% wood ash at 28 days. SS = sodium silicate, SC = sodium carbonate, SH = sodium hydroxide.

Gabrijel et al. investigated the use of wood fly ash (WFA) as a partial binder replacement in concrete, using two types: WFA1 (rich in pozzolanic oxides) and WFA2 (high in CaO), at 15% and 30% replacement levels [67]. The results showed a reduction in 28-day compressive strength: 6–14% at 15% replacement, and 25–34% at 30%, mainly due to reduced binder content, as WFA has limited reactivity and functions primarily as a filler, Figure 2.11. Also, the type of ash showed little effect on strength variation. Moreover, 2-year strength gains were minimal, confirming the low long-term pozzolanic activity of both ash types.

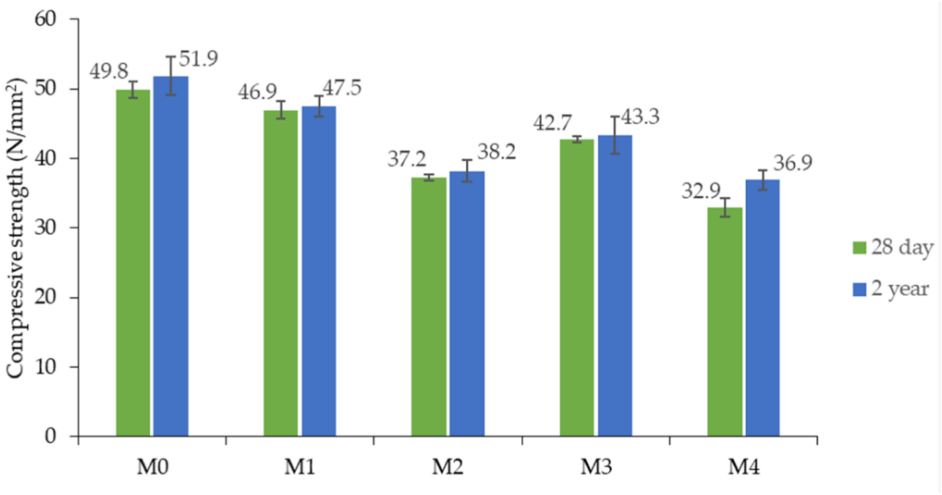

Figure 2.11: Compressive strength of concrete mixtures at 28 days and 2 years. WFA1 is rich in pozzolanic oxides, while WFA2 contains a higher proportion of calcium oxide. Mixes M1 and M2 represent concrete incorporating 15% and 30% WFA1, respectively, while M3 and M4 correspond to mixes with 15% and 30% WFA2. M0 is the reference mix without wood fly ash.

Ghorpade et al. investigated the use of wood waste ash (WWA) as a partial binder replacement in concrete at levels ranging from 0% to 30% by weight [68]. Both compressive and split tensile strength were evaluated at 28 and 90 days, Figure 2.12. The study showed a decrease in compressive strength with increasing WWA levels. However, an increase in the 90-day strength was observed at 10% WWA. This was attributed to delayed pozzolanic activity. In contrast, 20 to 30% replacement levels of WWA led to greater strength reductions, showing a limited reactivity at higher levels.

Tensile strength followed a similar trend as the compressive strength. It typically decreased with a higher WWA content, yet the mixtures containing 10% WWA reported improvements from 28 to 90 days. These were correlated with a more favourable microstructure and better packing of particles. Lower tensile performance at higher replacement levels was again correlated with weaker pozzolanic reactions and lower hydration product formation.

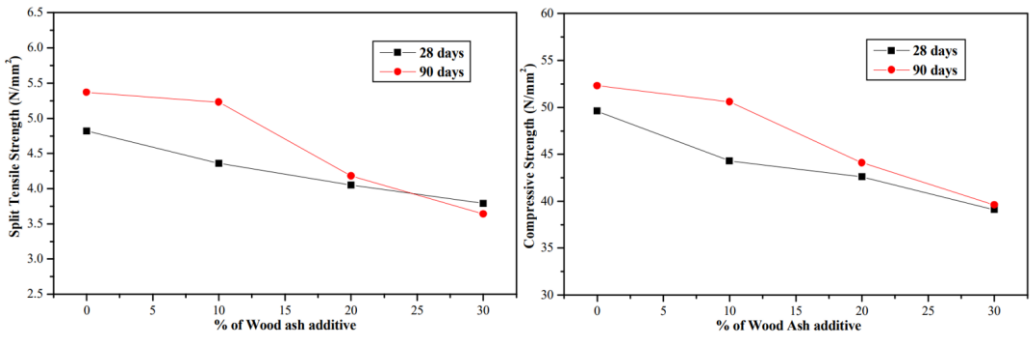

Figure 2.12: Effect of biomass fly ash incorporation on mechanical performance of concrete. Left: split tensile strength Right: compressive strength.

Another study on the incorporation of waste rice husk ash (RHA) in concrete was carried out by Givi et al [69], where 95 µm and 5 µm-sized particle sizes of fly ash were added to the concrete mixture, Table 2.2-2.3. The addition of RHA resulted in a gain in compressive strength over the control sample at 28 days, and this continued until 90 days. Improvement in strength was seen in both particle size fractions.

The study further showed that replacement of the binder by 20% of RHA did not negatively influence the strength of the concrete. This could be attributed to the high pozzolanic activity of the ultra-fine RHA with a SiO_2 composition of 88%, showing a high pozzolanic reactivity. The use of fine RHA particles resulted in improved particle packing, which reduced the volume of larger pores within the cement matrix, thus enhancing the overall microstructure.

Table 2.2 : Compressive strength of concrete incorporating waste rice husk ash (RHA) with particle size of 95 µm at various replacement levels.

Mix designation	RHA (%)	Compressive strength (MPa)		
		7 days	28 days	90 days
U1[a]	5	27.4	39.9	45.8
U2	10	28.3	43.8	51.2
U3	15	25.9	39.1	44.4
U4	20	24.6	38.3	42.8

Table 2.3 : Compressive strength of concrete incorporating waste rice husk ash (RHA) with particle size of 5 µm at various replacement levels.

Sample designation	RHA (%)	Compressive strength (MPa)		
		7 days	28 days	90 days
C0 (control)	0	27.3	36.8	42.3
M1[a]	5	25.7	38.7	43.5
M2	10	25.1	40.6	46.1
M3	15	23.7	37.9	42.7
M4	20	21.5	36.7	41.3

Nagrockienė et al. investigated the use of biomass fly ash (BFA) as a partial cement replacement in concrete, focusing on both mechanical properties and freeze–thaw durability [70]. Their results showed that increasing BFA content up to 25% did not negatively impact compressive strength, Figure 2.13. In fact, at a 5% replacement level, a 17.8% increase in strength was observed compared to the control mix.

The same study also examined freeze–thaw performance and found that low BFA dosages (5–10%) significantly improved durability, with the highest resistance of 800 cycles recorded at 5% replacement, Figure 2.14. This enhancement was attributed to the formation of closed pores, which help alleviate internal stresses caused by freezing. In contrast, higher replacement levels (25–30%) resulted in a substantial drop in freeze and thaw resistance to approximately 300 cycles, due to increased open porosity and reduced matrix integrity. Overall, the findings indicate that low BFA contents can enhance both strength and durability, while higher amounts may compromise long-term performance due to poorer pore structure and weaker binder connectivity.

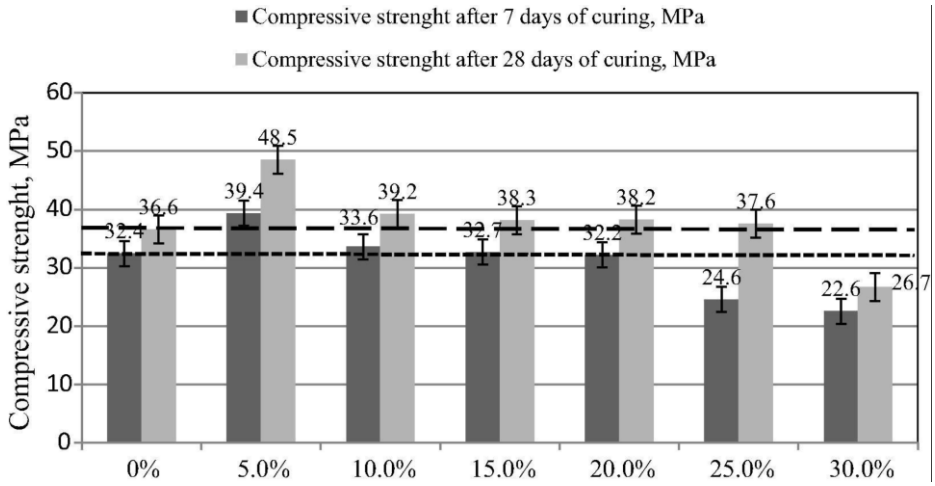

Figure 2.13: Compressive strength of concrete at 7 and 28 days with varying biomass fly ash content.

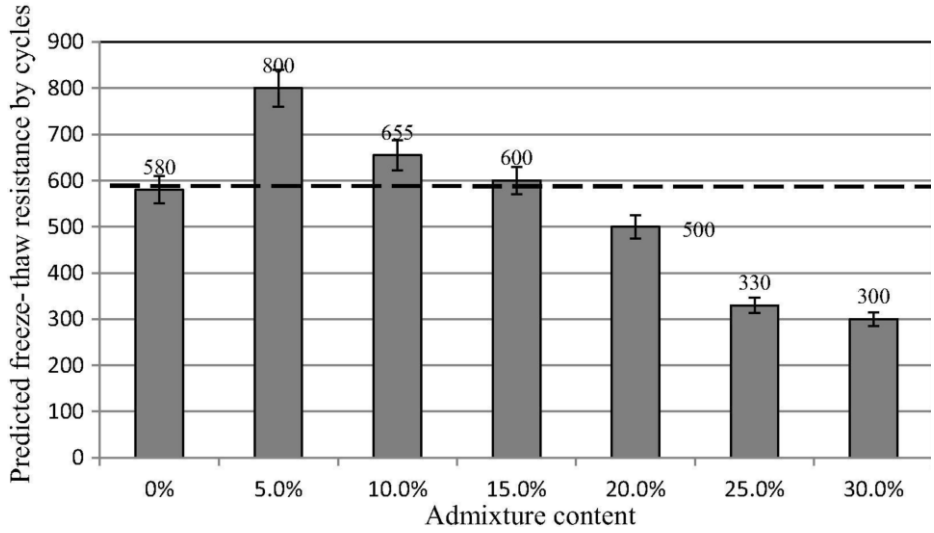

Figure 2.14: Freeze–thaw resistance of concrete as a function of biomass fly ash content.

Conclusion.

As more concern grows over the future availability of conventional precursor materials like slag and coal fly ash, biomass fly ash presents a promising alternative. BFA comes with a unique set of challenges that need to be addressed. Unlike other precursors, it shows a lower reactivity during alkali activation, and it often contains various contaminants that can pose environmental risks and mechanical degradation when incorporated into concrete. These contaminants include heavy metals, chlorides, loss on ignition (LOI), and metallic aluminium. These challenges must be solved through appropriate pre-treatment strategies before incorporating BFA into concrete.

Incorporation of BFA in concrete has been reported in previous studies, but no study to date has focused on using carbonated BFA in alkali-activated systems. Carbonation not only stores CO_2 permanently in the concrete matrix but can also affect the reactivity and behaviour of the ash. The purpose of this study is to fill this knowledge gap by investigating how carbonated BFA performs when integrated into alkali-activated concrete.

3

3 Characterization and selection of ashes for their carbon absorption potential

3.1 Introduction

In this chapter, an analysis will be conducted on three biomass fly ashes and one wood ash. Only one will be selected for use in the making of concrete. These tested ashes are BFA1, BFA2, BFA3 and WA4. The main criterion for the selection procedure is the ash ability to sequester the highest amount of carbon, through the presence of free lime. Thereby is this carbon stored permanently in stable carbonate forms. XRF and XRD techniques will be used to assess the mineralogical and phase composition of the selected ashes. Additionally, the free lime content, an essential component for carbon absorption, will be measured through chemical experimentation. These methods should give us information about the various ashes capacity for carbon sequestration potential.

3.2 Materials and methods

3.2.1 materials

BFA1, BFA2, BFA3 and WA4 were provided from different wood incineration plants in the Netherlands. These ashes are used in the selection phase.

3.2.2 Methods

Chemical composition

The chemical composition of BFA1, BFA2, BFA3, and WA4 is determined using a PANalytical Axios MAX WD-XRF spectrometer. This technique provides the major oxide contents in the selected ashes. before the testing, samples were dried at 105 °C and then ground to a fine powder. This is done to make sure the tested sample is representative. The LOI content, which represents the unburned organic content, is measured following NEN-EN 1744-7 (2010) at a temperature of 550 °C.

Mineralogical composition

The mineralogical composition in the raw BFA1, BFA2, BFA3, and WA4 ashes was identified with XRD technique, using a Bruker D8 Advance diffractometer. Each of the ash samples was manually ground with a mortar and pestle to achieve a particle size between 1 and 5 µm. The data was collected over a 2θ range of 5° to 110°, with a step size of 0.04°. The analysis for the identification of the crystalline phases in the ashes was done with the Bruker software DiffracSuite.EVA.

Free lime content

The measurement of the free lime content in fly ash is important for the determination of the potential of the ash to absorb carbon. The quantification of the free lime content is done according to the chemical method from the NEN-EN 451-1 standard [71]. The method is detailed below and illustrated in Table 3.1. The free lime content is calculated through the following equation:

$$W_{CaO} = \frac{M \cdot c \cdot V}{m \cdot 1000} \cdot 100$$

where:
M = the molar mass of CaO, c = the concentration of the HCL solution, V = the volume of the HCL solution.
m = the mass of the ash sample.

Table 3.1: Schematic representation of the experimental procedure for determining free lime content in fly ash.

Step 1: Sample Preparation
20 grams of fly ash is ground using a mortar and pestle. The ground ash is then sieved through a 63-micrometer sieve. From this sieved sample, only 1 gram is taken for the chemical analysis.

Step 2: Reaction Setup
This 1 gram of fly ash is placed in a 250 mL flask. 12 mL of ethyl acetoacetate and 80 mL of butan-2-ol are added to the flask. This mixture should react with the ash to release the free lime.

Step 3: Heating and Condensation
The flask is fitted with a water-cooled condenser and a rubber stopper with a single hole to allow condensed solution to cool down. The whole setup is placed on a heating plate with stirring. The heating with stirring lasted for 3 hours.

Step 4: Filtration
After heating, the mixture is still warm. It is then filtered through a filter crucible with an 8µm filter paper. This filter paper helps to remove any solid impurities. The residue left in the flask is then washed with 50 mL of propan-2-ol. After this filtration process, the solution consists of a yellow filtrate.

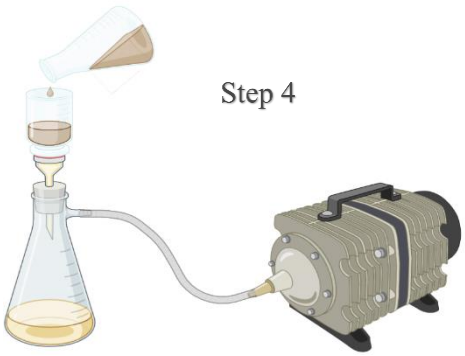

Step 5: Titration
12 drops of bromophenol blue indicator are added to the filtrate. The solution is titrated with a 0.1 M hydrochloric acid solution until a colour change is reached. This indicator changes the solution from yellow to blue. The volume of the HCL solution is recorded and used to calculate the free lime content, according to the given equation.

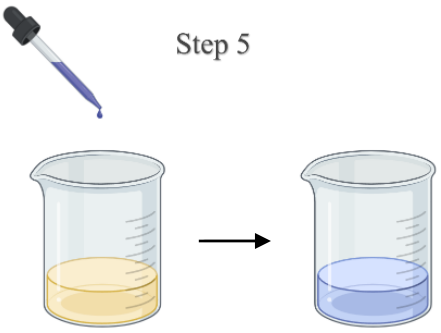

3.3 Results and discussion

3.3.1 Chemical composition

Results for XRF analysis of the selected ashes are presented in Table 3.2. The most significant oxide elements which have been detected in all ashes are CaO, MgO, SiO_2, Al_2O_3, Fe_2O_3, SO_3, Na_2O, K_2O, and P_2O_5. CaO is the major oxide, most notably in BFA1 at 51.12% and WA4 at 46.81%. This high concentration suggests a high carbon adsorption potential. BFA2 and BFA3 show a lower CaO content at 27.26% and 18.25%, respectively. Despite this, they still have sufficient calcium for further testing. MgO can also enhance the carbonation capacity as it can also react with carbon to form stable carbonates. However, its low concentration across all the ash samples shows a very little influence on the carbonation performance overall.

SiO_2 is an important oxide found in many precursors. This oxide provides reactive silica that is necessary for the alkali activation process. The content of this oxide is higher in BFA3 and BFA2 at 53.58% and 39.73%, respectively. This shows a stronger potential for alkali activation reactivity in these ashes, while BFA1 and WA4 have relatively lower content, at 9.77% and 4.21%, respectively.

Heavy metal content in the ashes can cause environmental concerns. They can leach out from the ash or the concrete samples incorporating this ash. For this reason, the ash with the lowest content of these metals should be considered the most suitable choice. WA4 has the highest concentration of heavy metals, with a concentration of lead reaching 1.11% and zinc at 4.66%. The concentration of these elements is high and enhances the leaching potential. BFA1 has detectable amounts of lead at a concentration of 0.40% and a concentration of zinc at 0.88%. BFA2 has a similar zinc content at 0.91% and lower lead content at 0.18%. Overall, WA4 shows the highest environmental risk due to its highest heavy metal content. By contrast, BFA3 appears to be the most environmentally favourable option, with the lowest content of these elements.

Table 3.2: XRF analysis showing the chemical composition in oxides for biomass fly ash samples BFA1, BFA2, BFA3, and WA4.

Chemical	BFA1	BFA2	BFA3	WA4
CaO	51.12	27.26	18.25	46.81
Cl	4.95	1.36	0.15	9.41
Na2O	0.34	2.10	1.14	7.13
SiO2	9.77	39.73	53.58	4.21
SO3	9.74	3.19	5.50	6.20
K2O	8.51	2.09	1.61	3.31
ZnO	0.88	0.91	0.14	4.66
Al2O3	2.69	4.62	9.23	1.05
Fe2O3	2.86	4.37	6.20	1.80
P2O5	2.42	2.07	0.69	0.62
TiO2	2.14	8.00	0.84	1.08
MgO	2.68	2.91	2.12	1.51
PbO	0.40	0.18	0.04	1.11
CuO	0.09	0.11	0.03	0.12
BaO	0.00	0.39	0.12	0.21
MnO	0.42	0.41	0.12	0.30
SrO	0.15	0.09	0.06	0.08
Cr2O3	0.05	0.12	0.03	0.09
ZrO2	0.03	0.07	0.06	0.00
LOI	0.64	0.00	0.00	9.76
Sum	100	100	100	100

3.3.2 Mineralogical composition

XRD measurements for raw biomass fly ash samples BFA1, BFA2, BFA3, and WA4 indicate the presence of several crystalline phases, Figure 3.1 and Table 3.3. Calcium carbonate ($CaCO_3$) is the most frequently occurring crystalline among the four samples. The abundant presence of calcite implies that natural carbonation may have occurred during storage or ash handling.

Anhydrite ($CaSO_4$) is consistently present across all samples. This calcium-bearing phase is important because it contains reactive calcium, which could potentially help in the carbonation reactions. However the literature[48] [72] shows that this phase is less involved in direct CO_2 uptake reactions. It is therefore not considered to be a major focus for carbonation potential in this work.

The primary phase significant in the carbonation process is lime (CaO). It is detected in BFA1, BFA2, and WA4, but not in BFA3. This can be due to that BFA3 may have undergone more extensive carbonation prior to the analysis. The lack of lime considerably lowers the suitability of BFA3 as a potential ash for carbon sequestration.

Portlandite ($Ca(OH)_2$) that is present exclusively in BFA1 indicates that this ash has been partially hydrated. This gives BFA1 an advantage in the carbonation process, as the presence of portlandite has been associated with enhanced CO_2 uptake

In addition, additional phases are identified in the ashes. Rutile (TiO_2) in BFA1 and BFA2 is consistent with the moderate titanium contents obtained through XRF. Sylvite (KCl) occurs in BFA1 and WA4, consistent with their higher K_2O values at 8.51% and 3.31%, respectively. Syngenite occurs in BFA1 alone. Halite (NaCl) is exclusively found in WA4. Hematite (Fe_2O_3) is only seen in BFA2, consistent with BFA2's higher iron value (4.37%), whereas albite ($NaAlSi_3O_8$) is present in BFA3.

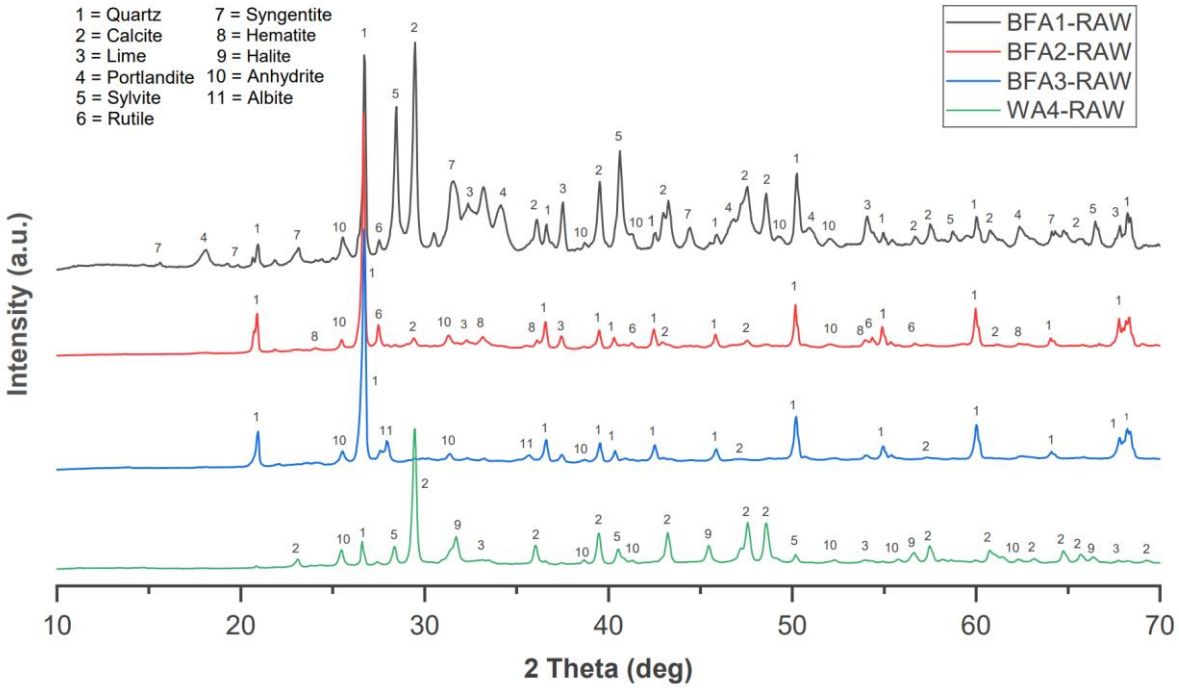

Figure 3.1: XRD patterns of raw ash samples from BFA1, BFA2, BFA3, and WA4, displaying the crystalline phases found in the various samples.

Table 3.3 : Identified crystalline phases and their corresponding ICSD reference codes.

Phases	ICSD codes
Quartz	PDF 00-005-0490
Calcite	PDF 01-083-0578
Lime	PDF 04-004-5476
Portlandite	PDF 01-076-0571
Sylvite	PDF 00-041-1476
Rutile	PDF 00-034-0180
Syngentite	PDF 00-028-0739
Hematite	COD 9000139
Halite	PDF 01-070-2509
Anhydrite	PDF 04-008-0191
Albite	COD 9002197

3.3.3 Free lime content in the raw ashes

The chemical analysis revealed the total free lime content in the raw ash samples BFA1, BFA2, and WA4, Figure 3.2. This content represents the combined amount of free lime and the lime portion originating from portlandite. The results show that BFA1 is the best-performing ash, as it has the highest content among the ashes, at 5.61%. This content is exceeding that of BFA2 and WA4, which are at 1.43% and 1.01%, respectively. Though the XRF data shows that WA4 has a higher total CaO content than BFA2, its free lime content stays the lowest. This shows that most of WA4's CaO content is found in stable minerals, like calcite.

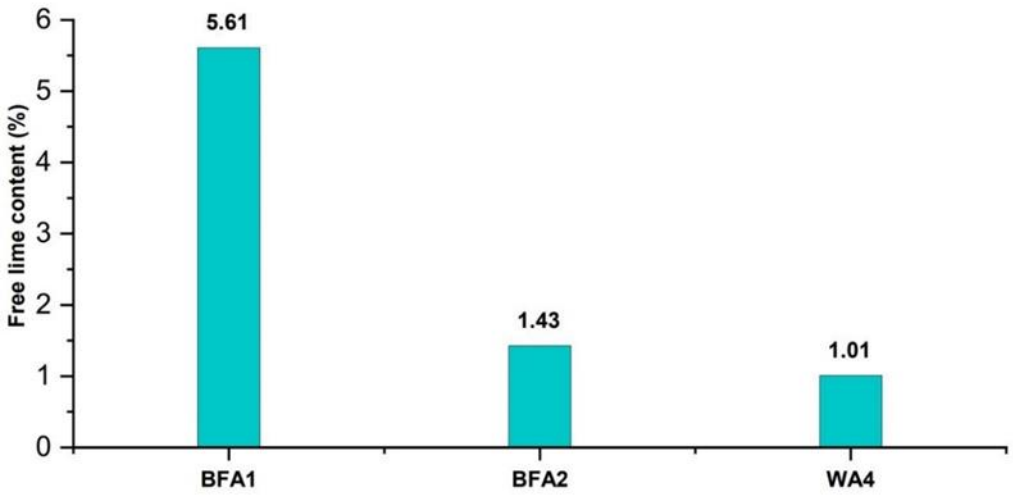

Figure 3.2: Distribution of free lime content across uncarbonated BFA1, BFA2, and WA4 samples.

3.4 Conclusion

BFA1 is the best candidate for carbon dioxide absorption due to its superior free lime content, reaching 5.61%, Figure 3.2. This high level of free lime is crucial in the carbonation process. Furthermore, XRD analysis of BFA1 has shown the presence of portlandite in the ash. This serves as an extra form of available lime content that has not undergone carbonation. The presence of portlandite in BFA1 suggests that it has undergone less pre-existing carbonation than other examined ashes.

In contrast, BFA3 has no lime or portlandite detected in the XRD analysis. This indicates that it lacks the essential components needed for effective carbon sequestration. The results for BFA2 and WA4 are also not promising. The chemical analysis shows a very low free lime content for BFA2 at 1.43% and for WA4 at 1.01%.

Furthermore, the magnesium content from the XRF analysis in BFA1, BFA2, BFA3, and WA4 is shown to be too low to have any impact on carbon sequestration.

4

4 Influence of pretreatment on the characteristics of wood biomass fly ash

4.1 Introduction

The biomass fly ash (BFA1) used in this study has undergone two pre-treatment processes to improve its use in concrete.

The first pre-treatment method is the water-interaction treatment. This method addresses the presence of reactive metallic aluminium in BFA1. Metallic aluminium found in the ash reacts in an alkaline environment to produce hydrogen gas. This gas creates internal stresses and cracking in concrete. The water-interaction treatment allows for the formation of this hydrogen gas, thus preventing its negative impacts during concrete production. This treatment also has a secondary role in the immobilization of heavy metals found in the ash. This is further reducing the risk of heavy metal leaching.

The second pre-treatment involves carbonation mineralization. This process is meant to improve carbon sequestration by enhancing the synthesis of stable carbonate compounds inside the ash. This process not only helps in the long-term storage of carbon within concrete but also helps to immobilize heavy metals present in BFA1, so reducing possible environmental hazards related to their leaching.

4.2 Materials and methods

4.2.1 Materials

The various ashes and their treatments are referred to in the next section as follows, Figure 4.1:

- BFA-RAW: Refers to the untreated raw biomass fly ash BFA1
- BFA-H: Refers to the water-treated biomass fly ash BFA1
- BFA-C: Refers to the carbonation-treated biomass fly ash BFA1, through the wet carbonation route.
- BFA-H-C: Refers to the biomass fly ash BFA1 that has undergone a combination of water treatment and carbonation treatment.

These labels are used in every Figure, table, and discussion in the next part.

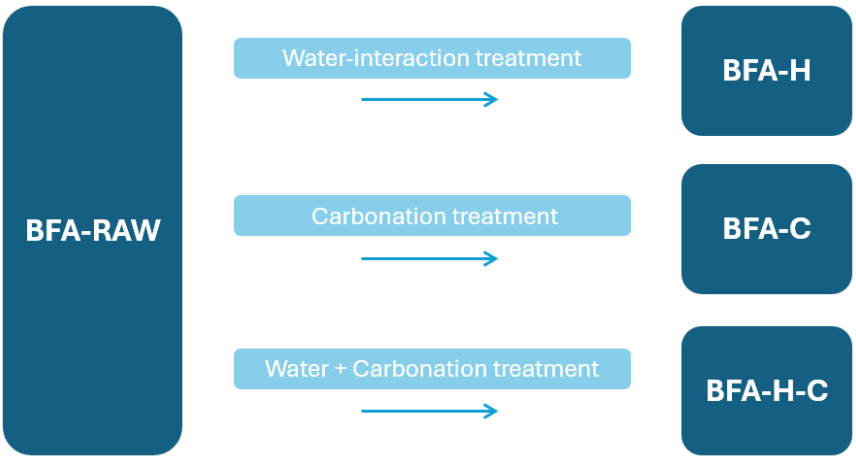

Figure 4.1: Pre-treatment routes of BFA-RAW: water (BFA-H), carbonation (BFA-C), and combined treatment (BFA-H-C).

4.2.2 Pre-treatment methods

4.4.2.1 Water-interaction pre-treatment of biomass fly ash

The presence of metallic aluminium in biomass fly ash creates challenges in the production of concrete. This metallic aluminium can react with water or an alkali solution and produce hydrogen gas. This gas can cause undesirable effects in concrete, including expansion and cracking. Thus, reducing the mechanical and durability properties [29], [73], [74]. Therefore, this metallic aluminium content in fly ash should be stabilized before being incorporated in concrete. The main purpose of the water-interaction treatment is to ensure that hydrogen gas generation is fully completed prior to incorporating the ash into concrete.

To conduct this treatment, the ash was mixed with water at a water-to-solid (w/s) ratio of 0.3 and placed in a sealed container for seven days at room temperature (22°C). The duration of the treatment was selected based on prior research, which shows that hydrogen gas generation slows significantly after 7 to 10 days [29]. This timeframe ensures the complete reaction of metallic aluminium while avoiding excessive treatment durations.

4.4.2.2 Carbonation pre-treatment of the biomass fly ash

The carbonation pre-treatment BFA1 was carried out using both the wet and the dry carbonation methods, so enabling a comparison of their efficiency in improving the ash's carbon absorption. These techniques were used over different carbonation times to evaluate the effect of exposure time on carbon sequestration potential. The dry carbonation process was done by exposing BFA1 to CO_2, thereby promoting the direct gas-solid carbonation. Although slower than wet carbonation, this technique has benefits in terms of controlling moisture content, which would help to prevent secondary reactions, possibly changing the microstructure of the ash. Furthermore, the addition of water can influence the particle size distribution of the ash by causing agglomeration of the ash particles.

Under the wet carbonation process, BFA1 is exposed to CO_2 in the presence of water, so increasing elements diffusion and reaction kinetics. This technique improves the dissolution of carbon and other reactive oxides, so encouraging the formation of stable carbonate phases.

The implementation of the carbonation methods is done through the preparation of small-scale samples. For the dry method, 10 grams of fly ash was evenly spread in a plastic container with an estimated 5 mm thickness, leaving the top open to the air condition. As shown in Figure 4.2, the wet method proceeded the same way except adding water to the ash prior. Based on earlier studies showing the efficiency in increasing carbonation [48], [49], [50], a L/S ratio of 0.3 was chosen. To examine the influence of carbonation duration, the pre-treatment was conducted over various time periods. All

samples were subjected to a standardized carbonation environment within a closed carbonation chamber. The parameters were fixed at 1% CO2 concentration, a temperature of 20°C, and a relative humidity of 60%.

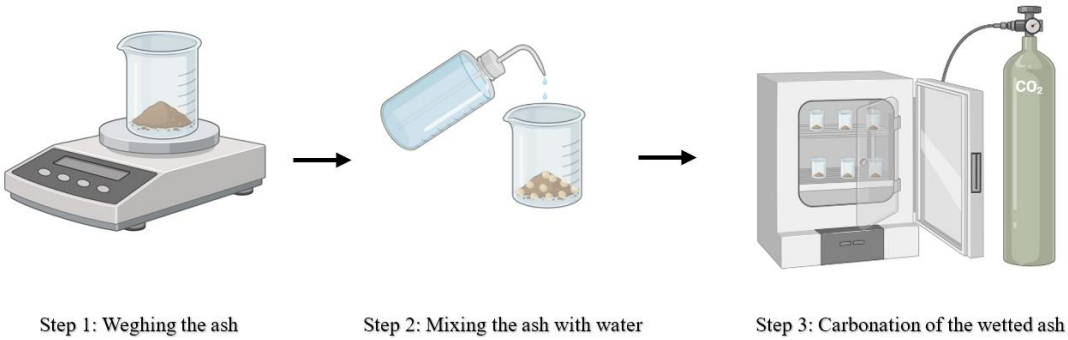

Figure 4.2: Schematic representation of the wet carbonation route for BFA1, showing the steps from initially weighing, through mixing with water, to CO2 treatment in the carbonation chamber.

Large-Scale Carbonation Pre-treatment

The next phase included upscaling the carbonation process to generate enough carbonated biomass fly ash for concrete production, Figure 4.3. Following a technique similar to that used for smaller-scale samples, larger plastic trays were used for this larger-scale preparation to hold significant quantities of ash.

5 kg of biomass fly ash was weighed and placed in a large bucket. Water was then added at a L/S ratio of 0.3, similar to the small-scale samples. To guarantee complete and even mixing, hand mixing was used; special attention to the bucket's corners helps to preserve a consistent water-to-ash ratio throughout the mixture. After mixing, the ash was evenly spread over the trays. These trays were placed in the carbonation chamber following the same parameters.

Figure 4.3: Setup for large-scale carbonation of BFA1, displaying plastic trays for extensive carbonation.

4.2.3 Ash characterization methods

XRD and QXRD

The mineralogical phases were identified through XRD using a Bruker D8 Advance diffractometer. The samples were manually ground with a mortar and pestle to achieve a particle size between 1 and 5 µm. The data was collected over a 2θ range of 5° to 70°, with a step size of 0.04°. The analysis of the data was performed using the Bruker software DiffracSuite.EVA. For the quantitative analysis, a 10 wt% of silicon powder was mixed with the ground ash and used as an internal standard. The identification and quantification of the phases were performed using the Profex-BGMN software.

TGA

Thermogravimetric analysis was performed using a TG 449 F3 Jupiter instrument. Around 30 mg of ash was placed in an open aluminium crucible and heated from 40 °C to 1000 °C at a rate of 10 °C/min under an argon gas atmosphere. The mass loss was continuously recorded to identify thermal decomposition stages.

Particle size distribution

The particle size distribution of the solid precursors was analysed using a laser diffraction technique. The measurements were carried out with a DIPA 2000 laser diffraction analyser, which can detect particle sizes up to 250 µm. Ethanol was used as the dispersing medium because it does not react with the precursor materials and ensures good dispersion. Approximately 0.5 g of dried powder was mixed into 500 ml of ethanol, which was introduced into the instrument system for measurement.

FTIR chemical bond

Fourier-Transform Infrared (FTIR) spectroscopy was employed to identify the functional groups and chemical bonds present in the raw and treated biomass fly ash (BFA) samples. The model of the instrument is PerkinElmer Spectrum 100. Each sample was scanned in the mid-infrared range of 4000–600 cm^{-1}, with a spectral resolution of 1 cm^{-1} .

ICP-dissolution Test

The ICP dissolution test is aimed at measuring the reactivity of the ash after the various treatments. 1 gram of ash was dissolved in 1 Liter of 5M NaOH solution. This mixture was stirred in a polypropylene container for 24 hours at room temperature (22°C). The objective of this test was to measure the solubility of key elements such as Ca, Si, Al and Mg, which are essential for the formation of reaction products during alkali activation. The filtered solutions were diluted with 0.2 vol% nitric acid and analysed using inductively coupled plasma-optical emission spectroscopy (ICP-OES), PerkinElmer Optima 5300DV model.

Isothermal calorimetry

Isothermal calorimetry experiments were performed using a TAM Air-314 isothermal conduction calorimeter. The preparation of the samples was done through the mixing of the alkaline activator solution with the solid precursor and mixed for one minute at 150 rpm using a head-mixer. This was followed by hand mixing for an additional 1 minute, and a final mix at 500 rpm for one minute to ensure homogeneity. Approximately 5 grams of the freshly mixed paste was then introduced into a small glass ampoule, which was immediately loaded into the calorimeter alongside a reference ampoule. Each mixture was prepared in duplicate, and the heat release was continuously recorded over a period of 160 hours.

Metallic aluminium

The metallic aluminium content in fly ash is determined by the water displacement method, Figure 4.4 [26], [28]. In this method, a representative ash sample is dried at 105 °C and sieved to 125 µm. It is then mixed with NaOH in a sealed flask, connected via a rubber tube to a graduated cylinder filled with water.

Hydrogen gas released from the reaction displaces the water, allowing direct measurement of gas volume. The hydrogen volume at room temperature is calculated using [27] :

$$f_{Al} = \frac{2\Delta V(\frac{273}{273+T})}{3V_0}\frac{M_{Al}}{m_{BA}}$$

In this equation, ΔV represents the volume of hydrogen gas released during the reaction, measured at room temperature T (expressed in degrees Celsius), while V_0 denotes the molar volume of an ideal gas under standard conditions (P_0 = 101.3 kPa and T_0 = 273 K). The term M_{Al} refers to the molar mass of aluminium, and m_{BA} corresponds to the mass of the biomass fly ash sample used in the experiment.

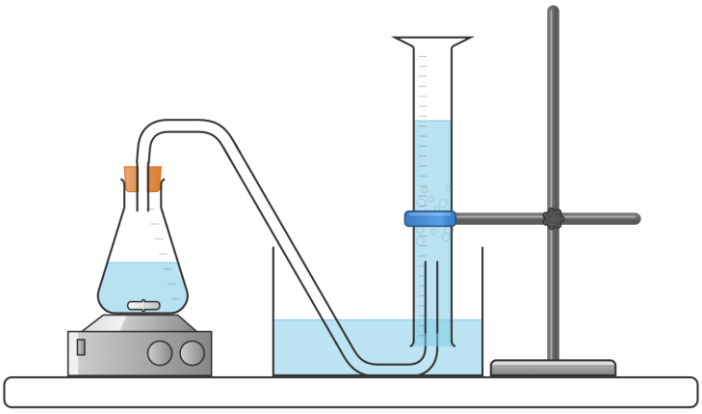

Figure 4.4: Experimental setup for water displacement to measure metallic aluminium content in fly ash.

4.3 Results and discussion

4.3.1 Results of the carbon sequestration potential

4.3.1.1 Mineralogical composition

The XRD analysis after carbonation for BFA1 provides important information on the different degrees of carbonation attained by the gas-solid and the aqueous carbonation processes. This analysis primarily focuses on the gas-solid carbonation process. This process would be preferable if it could achieve complete carbonation. The Addition of water can alter the phase composition and particle size of the ash. However, if gas-solid carbonation alone is not sufficient for complete carbonation, the addition of water becomes important to enhance the carbonation process.

Figure 4.5 shows the XRD results for both the gas-solid and the wet carbonation routes of BFA1. The focus here is primarily on the lime portlandite phases. The disappearance of these phases means the completion of carbonation. After two months of gas-solid carbonation, lime can still be detected, which is an indication of incomplete carbonation. The period of two-month carbonation duration provides clear evidence that the gas-solid route is not effective in reaching complete carbonation. Water is an important agent in dissolving carbon dioxide and increasing its interaction with calcium-bearing components. This process is not fully achievable through gas-solid carbonation under ambient conditions. Literature has shown that it requires very high temperatures, reaching up to 300°C, to carbonate in the gas-solid method [75]. This high-energy addition embeds more carbon into the ash, which can negate the benefits of carbon sequestration. The wet carbonation, on the other hand, shows more promising results. Within just 8 hours, the lime and portlandite contents have completely vanished. These results show the superiority of the wet methods as it can fully carbonate the ash within a limited period of time. These findings are consistent with previous studies, which have shown that water is a critical component in the carbonation process [48] [33].

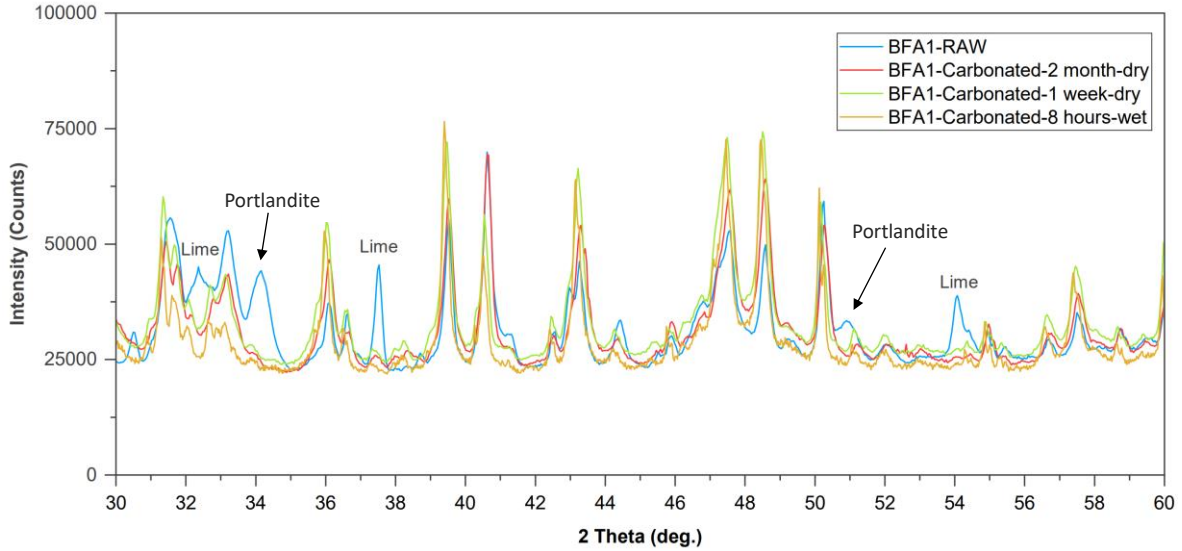

Figure 4.5: XRD patterns of BFA1 in raw and various carbonated states (two months dry, one week dry, and eight hours wet), highlighting the presence of lime peaks to assess carbonation efficiency.

4.3.1.2 Thermogravimetric analysis

The Thermogravimetric (TG) and derivative thermogravimetric (DTG) analyses results of biomass fly ashes BFA1 are presented in Figure 4.6. The TG curve for uncarbonated BFA1 shows a weight loss between 450°C and 500°C, which is indicative for portlandite ($Ca(OH)_2$) decomposition [76]. This peak is absent in the carbonated sample. This shows that the portlandite has been fully carbonated and is transformed into calcium carbonate. A weight loss peak from 550°C to 950°C is also detected in the graph. This peak is linked to the decomposition of calcium carbonate into calcium oxide and carbon dioxide [76]. This peak is observed in the carbonated ash as well as the Raw ash, which shows that calcium carbonate has already been present in the ash before carbonation.

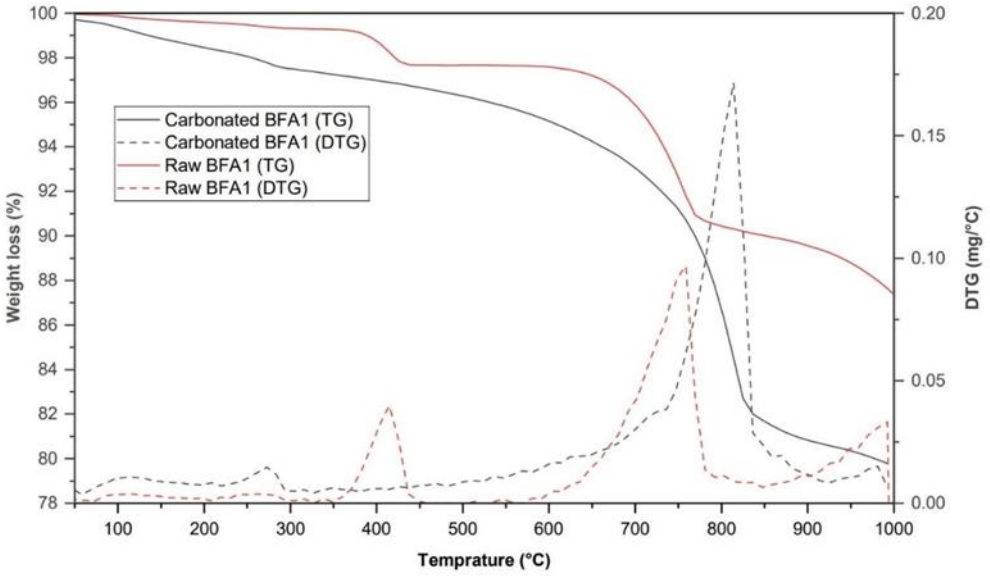

Figure 4.6: Thermogravimetric (TG) and Derivative Thermogravimetric (DTG) Curves of Raw and Carbonated BFA1 Showing Mass Loss and Thermal Decomposition Behaviour.

It is worth noting that the DTG graphs show that there is a sudden weight decrease in the raw BFA1 sample at around 550 °C. This is the range where the more crystalline calcium carbonate starts to decompose. As for the carbonated BFA1, we can see that there is a gradual weight drop that starts at even lower temperatures than 550 °C, which could suggest that some of the earlier weight drop is attributed to poor crystalline or amorphous CaCO3 forms, as have been found in earlier studies [22], [77], [78]. This weight range can also be attributed to Portlandite decomposition; however, the XRD results showed that there is no Portlandite in the carbonated samples, so this is unlikely. These findings suggest that accelerated carbonation not only produces crystalline forms of $CaCO_3$ but also results in the formation of less crystalline or amorphous carbonate phases, as evidenced by the gradual weight loss observed in the DTG curves.

Table 4.1 shows the weight loss observed between 550°C and 950°C. this is a range directly linked to the CO2 content in the ash. This temperature range reveals the CaCO3 content as it decomposes into calcium oxide (CaO) and carbon dioxide (CO2) during the heating process. The molar mass of CO2 is 44 g/mol, and for CaCO3, it is 100 g/mol. During decomposition, CO2 is released, and for each gram of CO2 produced, approximately 2.27 grams of CaCO3 were initially present. Therefore, a sample that loses 15.47 grams as CO2 indicates the original presence of about 35.11 grams of CaCO3 (calculated as 15.47 grams of CO2 × 2.27). This assumption is valid on the basis that the observed weight loss is exclusively due to CaCO3 decomposition within this specific temperature range.

Table 4.1 provides percentages of CO2 released and the corresponding CaCO3 content. By examining the provided table, we see that the raw BFA1 already contained 20.15% $CaCO_3$ before carbonation. This indicates some level of natural carbonation during storage [49]. After carbonation, the $CaCO_3$ content in the ash has increased, showing a rise in content from 20.15% to 35.11%.

Table 4.1 : Comparison of CO2 release, CaCO3 content, and absorption capacity in raw versus carbonated BFA1 illustrating carbonation impact on CO2 sequestration.

Sample	State	CO2 Released [%] (550°C - 950°C)	Corresponding CaCO3 [%]	CO2 Absorption Capacity [wt.%]
BFA1	Raw	8.87	20.15	6.59
BFA1	Carbonated	15.47	35.11	

4.3.2 Influence of water-carbonation pre-treatment on particle size

The particle size distribution of the binder materials used in this study is presented in Figure 4.7.

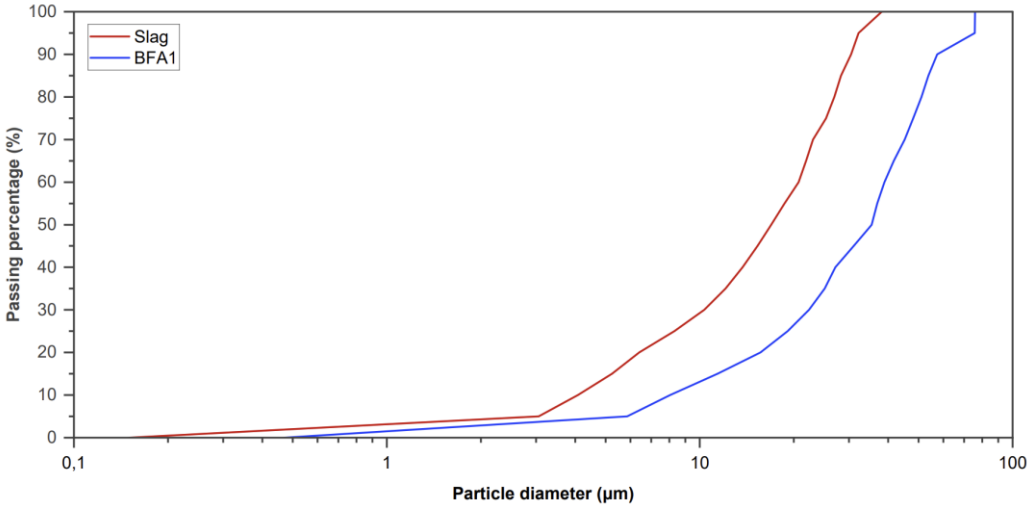

Figure 4.7: Particle size distribution of slag and BFA1.

Table 4.2 presents the volume dimensions of precursors with median sizes. From the particle size distribution results, slag is found to have a smaller particle size compared to BFA1. More precisely, the D10, D50, and D90 of slag are 4.08 µm, 16.9 µm, and 30.45 µm, respectively, indicating a finer material. In contrast, BFA1 shows larger particle sizes with D10, D50, and D90 being 8.05 µm, 35.44 µm, and 57.44 µm, respectively.

Table 4.2 : Volume dimensions of precursors with median size.

	D10 (µm)	D50 (µm)	D90 (µm)
GGBFS	4.08	16.9	30.45
BFA1	8.05	35.44	57.44

Particle size distribution of BFA1 following combined pre-treatment with carbonation and water has been analysed in order to determine changes that will influence reactivity in alkali-activated systems, Figure 4.8. There is a noticeable shift towards coarser particles, probably an effect corresponding to agglomeration of the fines or the creation of denser particles after carbonation. Although the raw ash contained mostly fine particles, the treated sample had a higher percentage of coarser fractions, Figure 4.9. These changes are important, as they will lower the reactivity of the ash during alkaline activation.

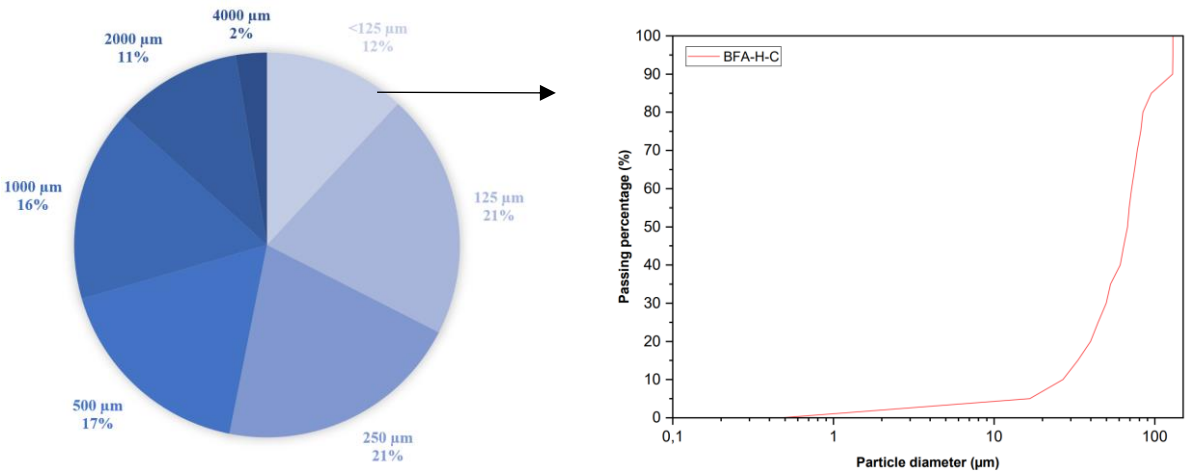

Figure 4.8 : Particle size distribution of carbonated biomass fly ash (BFA-H-C). The left panel presents the percentage of ash retained across different sieve size fractions. The right panel displays the cumulative particle size distribution curve, obtained via la ser diffraction, for the fraction passing below 125 µm from the sieve analysis, which represents 12% of the total ash mass.

Figure 4.9 : Visual representation of the different particle size fractions of carbonated biomass fly ash (BFA-H-C) obtained through sieve analysis.

4.3.3 Effect of pre-treatment on the ash composition

4.3.3.1 Mineralogical composition

QXRD characterization was conducted to analyse the content of the amorphous phase in biomass fly ash (BFA1). This content includes reactive elements such as silica and alumina [79], [80]. These elements are essential since they are soluble and contribute to undergoing reactions through the formation of reaction gels, including CSH and CASH. Figure 4.10 presents the XRD patterns of biomass fly ash (BFA1), which have been subjected to various pretreatment methods. At first look, A broad hump is observed between 25° and 35° 2θ across all the samples. This hump represents the amorphous phase within the ash [81], [82], [83]. The position and shape of the hump is similar among the different samples, however the water-treated ash (BFA-H) shows a more pronounced hump. This slight difference means a slight increase in amorphous content. This is likely caused by the alkaline conditions introduced after the water treatment, which can dissolve some extra phases.

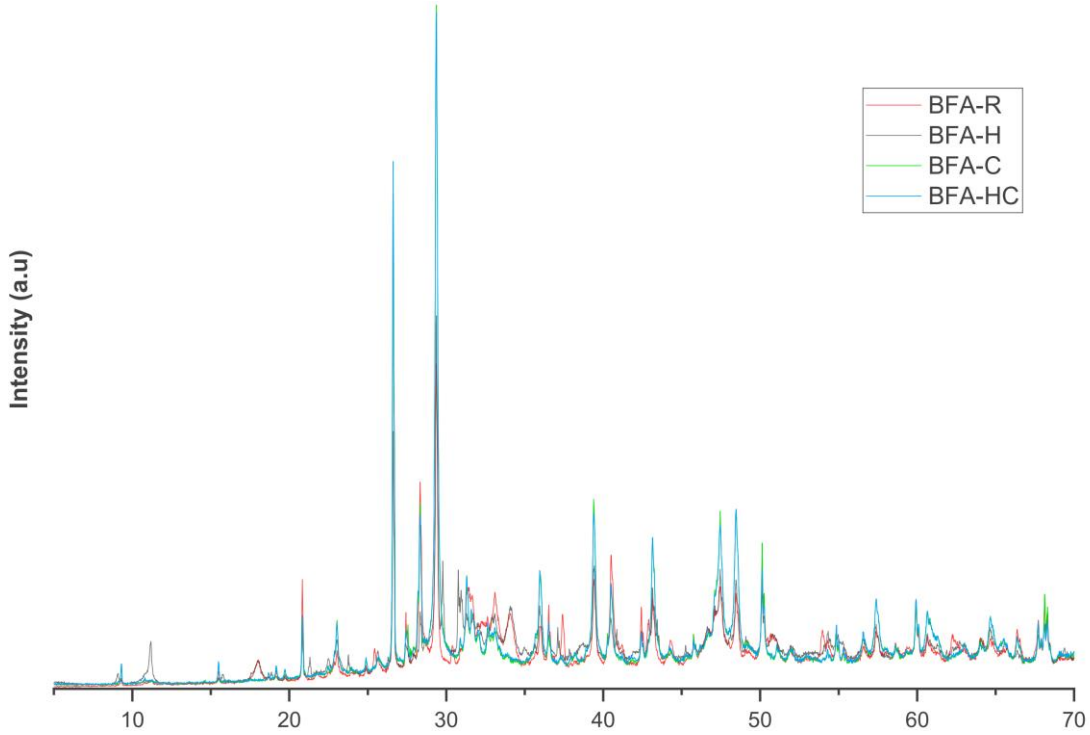

Figure 4.10: XRD patterns of BFA1 following various treatments, highlighting changes in crystalline phases.

The results of the QXRD analysis are shown in Figure 4.11. Across the treatments, certain crystalline phases such as quartz, syngenite, and rutile showed remarkable consistency in their presence. Quartz maintained a concentration of around 10%, syngenite at approximately 5%, and rutile was barely detectable with less than 1% concentration. The stability of these phases across various treatments indicates their non-reactivity under the pretreatment processes. The transition from raw (BFA-RAW) to water-treated (BFA-H) samples showed the most phase changes. Phases like anhydrite, aphthitalite, sylvite, and perovskite were either significantly reduced in content or completely eliminated. This shows that these phases have been dissolved and consumed in the formation of new phases like arcanite, simonkolleite, and apatite. Their new phases were only detected after the water treatment. BFA-RAW contained amounts of lime. However, after the water treatment, this lime is no longer detectable, showing that it has undergone complete hydration. The carbonated samples (BFA-C and BFA-H-C) show a complete absence of lime and portlandite, which implies that these phases have been fully carbonate.

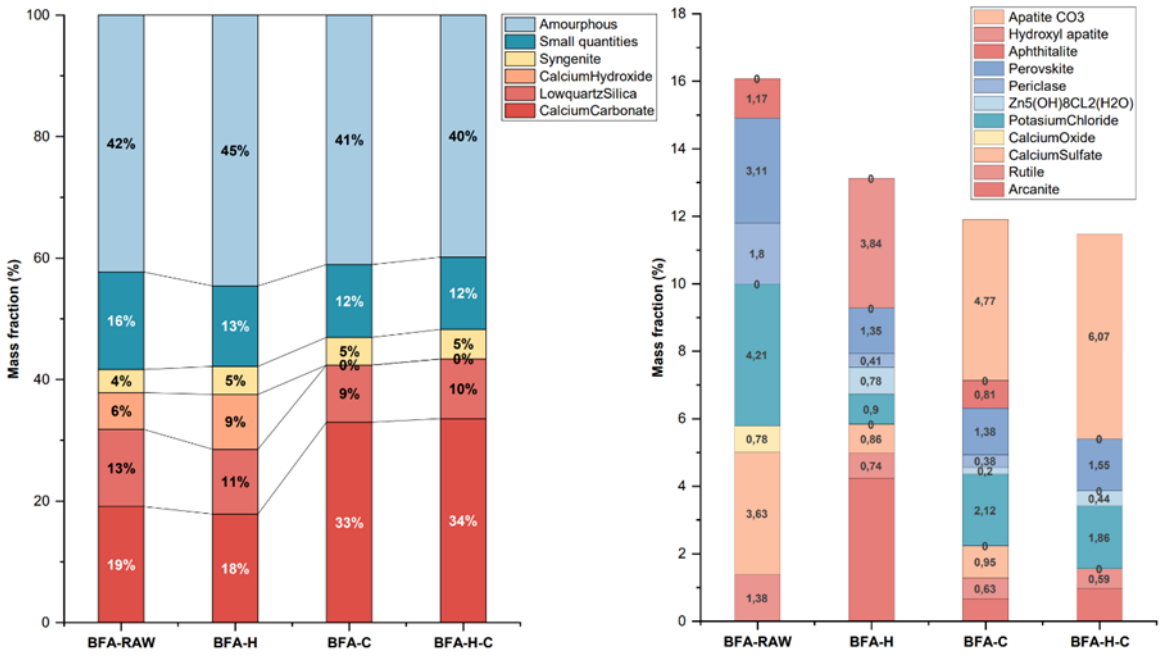

Figure 4.11: Phase composition of BFA1 after various treatments (raw, water treated, carbonated, and water treated plus carbonated), as determined by QXRD analysis. The graphs display the mass fractions of amorphous and crystalline phases, highlighting changes in phases due to treatments.

The amorphous content of Raw BFA1 (BFA-Raw) was quantitatively measured at 42.30%. After the water treatment (BFA-H), a slight increase to 44.6% was observed. This increase can be linked to the formation of hydration products initiated by the wetting of the ash. The increased alkalinity of the ash after water treatment likely initiated these reactions. The samples that have been carbonated (BFA-C and BFA-H-C), showed a slight decrease in amorphous content. This content has dropped to 40% from the initial 43.36% observed in the raw sample. This reduction is mainly due to an increase in calcite content, which is mainly crystalline and will thus increase the crystalline content [22].

Comparative studies of calcite from QXRD and TGA results confirm consistency between the two analyses. TGA reported calcite content in raw fly ash (BFA-Raw) to be 20.15%, in close agreement with the value from the QXRD, which is about 19 %. The calcite content in raw (BFA-RAW) and in the water-treated (BFA-H) samples, measured by the QXRD analysis, is closely matched at about 19 % and 18%. This is likely due to the samples being stored in airtight conditions that prevented atmospheric carbonation during the water-interaction treatment. Carbonated samples showed an increase in calcite content up to 34% according to the QXRD analysis, aligning well with TGA findings of a 35% calcite content after carbonation.

4.3.3.2 FTIR chemical bonds

FTIR spectroscopy was used to analyse changes within the amorphous phases of biomass fly ash following various pretreatments. This analysis, focusing on the 1800 to 600 cm^{-1} spectral range, shows differences between untreated and treated samples. These findings are illustrated in Figure 4.12.

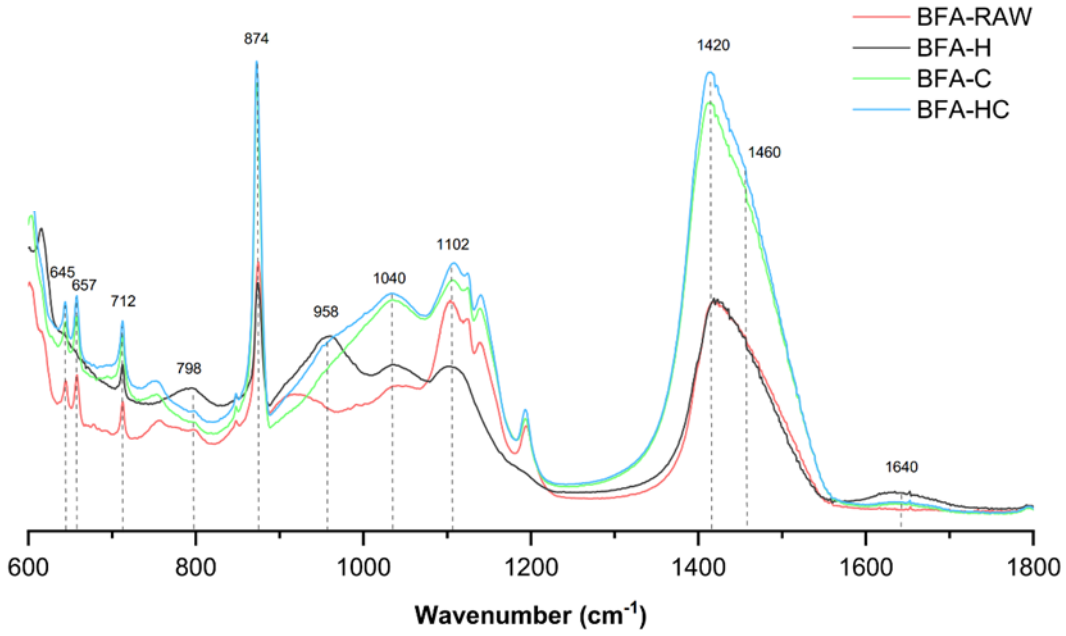

Figure 4.12: FTIR spectra of BFA1 subjected to different treatments (RAW, water-treated, carbonated, and water-treated plus carbonated), highlighting changes in functional groups and bonding environments across the wavenumber range.

Several peaks have been detected that are linked to specific molecular vibrations of the carbonate structures. The peaks at 1420, 874, and 712 cm^{-1} correspond to the out-of-plane bending, asymmetric stretching, and in-plane bending vibrations of calcium carbonate ($CaCO_3$), respectively [84], [85], [86], [87], [88], [89]. These peaks are found in all samples but are more Noticeable in the carbonated samples (BFA-C, BFA-H-C), showing that carbonation intensifies the carbonate bonds. In the carbonated samples, a small shoulder appears around 1460 cm^{-1}. This shoulder may be associated with the presence of amorphous or poorly crystalline $CaCO_3$ [90]. This feature is absent in the raw sample (BFA-Raw), showing that the pre-existing carbonates in the untreated ash are primarily in a more crystalline form. This observation aligns with the earlier TGA results.

The broad peak between 1200 and 950 cm^{-1} is linked to the vibrations of Si-O-Si and Al-O-Si bonds. [91] [92] [89]. This region is linked with the formation of gels such as C–S–H and C–A–S–H [93]. Interestingly, a peak around 958 cm^{-1} is observed only in the BFA-H sample. This peak indicates the potential formation of these gels, showing that water treatment creates an alkaline environment that promotes such reactions. In the carbonated samples (BFA-C and BFA-H-C), a notable peak near 1040 cm^{-1} can be seen. This peak is also linked to the stretching of Si–O–Si and Si–O–Al bonds. Its presence shows the formation of a polymerized silica gel following the carbonation process, likely due to the consumption of the calcium elements. These findings show that during the carbonation process, further reaction product formation takes place. This is likely facilitated by the water used during the carbonation process.

Furthermore, a peak around the wavenumber 1640 is observed in the water-treated sample. This peak is linked to the vibrations of H-OH bonds. This bond is found within the gel phases [94], [95], [96], [97], [98]. This observation further supports the hypothesis that water treatment facilitates the formation of reaction products.

The smaller peaks at 645 and 657 cm^{-1} relate to the vibrations of Si–O–Si bonds [99], [100] . A small peak at 798 cm^{-1} found in all samples, typically associated with Si-O stretching vibrations, confirms the presence of quartz [100], [101], [102]. Further analysis reveals the peak at 1102 cm^{-1}, which is linked with the stretching of Si–O–Si bonds [100], [101], [102]. This peak is associated with the presence of quartz in the sample.

4.3.3.3 Results of pre-treatment on metallic aluminium content

The metallic aluminium content following various treatments is presented in Table 4.3. The raw biomass fly ash (BFA) showed a metallic aluminium content of 0.090%, which had a substantial potential for hydrogen gas generation when subjected to alkaline conditions. Carbonation pretreatment managed to lower the metallic aluminium content to 0.045%. This is a notable improvement, but it still poses some danger of hydrogen gas generation. Water treatment was more effective, having lowered the aluminium content to 0.015% after a period of 7 days of exposure to water. The combination of both water treatment and carbonation completely mitigated the content of metallic aluminium, taking it down to 0.00%. This combination is effectively diminishing the danger of hydrogen gas generation.

Table 4.3 : Metallic Aluminium content in BFA1 under various treatments (raw, exposed to CO2, treated with water, and treated with both CO2 and water), demonstrating the effects of treatment on hydrogen gas release.

	Metallic Aluminium content (%)
BFA1-RAW	0.090
BFA1-C	0.045
BFA1-H	0.015
BFA1-C-H	0

4.3.4 Effects of pre-treatments on reactivity

4.3.4.1 ICP-dissolution Test

The results of the ICP dissolution test, showing the concentrations of key elements (Ca, Si, Al and Mg) released from the ash into solution, are presented in Figure 4.13.

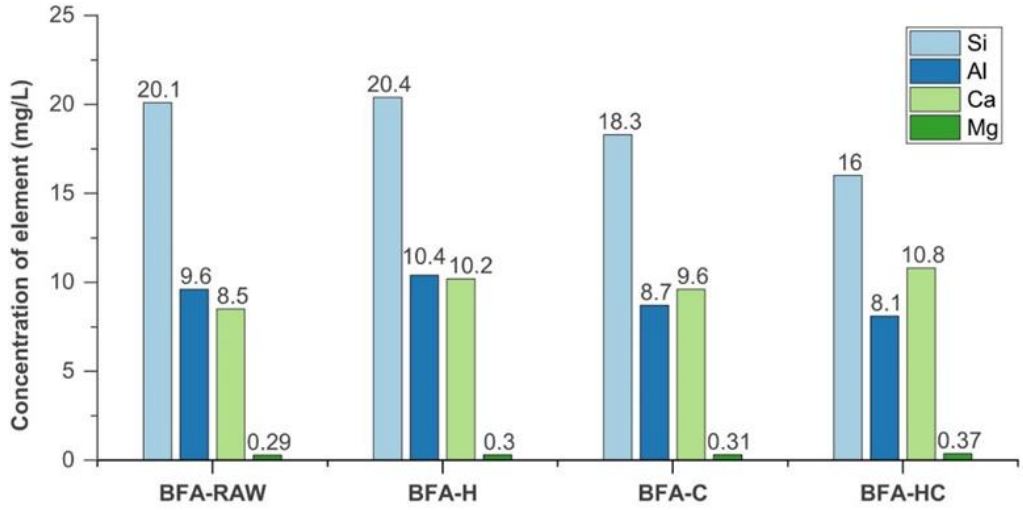

Figure 4.13: Dissolution of Si, Al, Ca, and Mg from BFA1 after various pretreatments (RAW, water-treated, carbonated, and water-treated plus carbonated), indicating the effect of each treatment on elemental solubility.

Raw (BFA-RAW) and water-treated (BFA-H) ash samples showed the maximum elemental dissolution. This is due to the finer particle size distribution in these samples. The smaller particle size leads to an increase in surface area, which increases the solubility in the alkaline solution. Although some agglomeration occurs after water treatment, it is largely physical rather than chemical. This does not significantly reduce the solubility of elements, as the BFA-H results show. The water-treated ash BFA-H showed slightly elevated levels of dissolved elements. By comparison, carbonated sample BFA-C exhibited a decline in element dissolution in relation to both BFA-RAW and BFA-H. This decline was even more pronounced in the BFA-H-C sample. The lower solubility is caused by the formation of a carbonated surface layer, which limits further dissolution of elements.

A notable exception to the overall dissolution trend is calcium, which showed a slight increase in solubility following carbonation treatment. A portion of the newly formed $CaCO_3$ exists in amorphous or poorly crystalline form, as shown by TGA analysis of the ash. These forms of $CaCO_3$ have a more disordered molecular structure, unlike the crystalline forms, which are ordered and have stronger bonds. This could explain the increased leaching of calcium despite an overall reduction of solubility for the other elements. The results of this test show that carbonation reduces the dissolution of elements, and as a consequence, the reactivity of the ash might also decrease.

4.3.4.1 Isothermal calorimetry

Isothermal calorimetry experiments were performed to measure the heat releases of the alkali activation reaction due to the incorporation of the various BFA ashes in the paste sample according to the mix design in Table 4.4.

Table 4.4: Mix design of the alkali activated paste samples.

Paste mix design	Paste-REF	Paste-BFA-RAW	Paste-BFA-W	Paste-BFA-C	Paste-BFA-H-C
Blast furnace slag (kg/m3)	400	300	300	300	300
BFA1 (kg/m3)	0	100	100	100	100
Water (kg/m3)	135.72	135.72	135.72	135.72	135.72
NAOH (50%) (kg/m3)	35.21	35.21	35.21	35.21	35.21
waterglass (kg/m3)	29.07	29.07	29.07	29.07	29.07

Figure 4.14 shows the heat release graphs for the prepared paste samples. The reference sample consists of 100% slag, while the other samples contain 25% of biomass fly ash, undergoing different treatments such as carbonation, water treatment, and a combination of both.

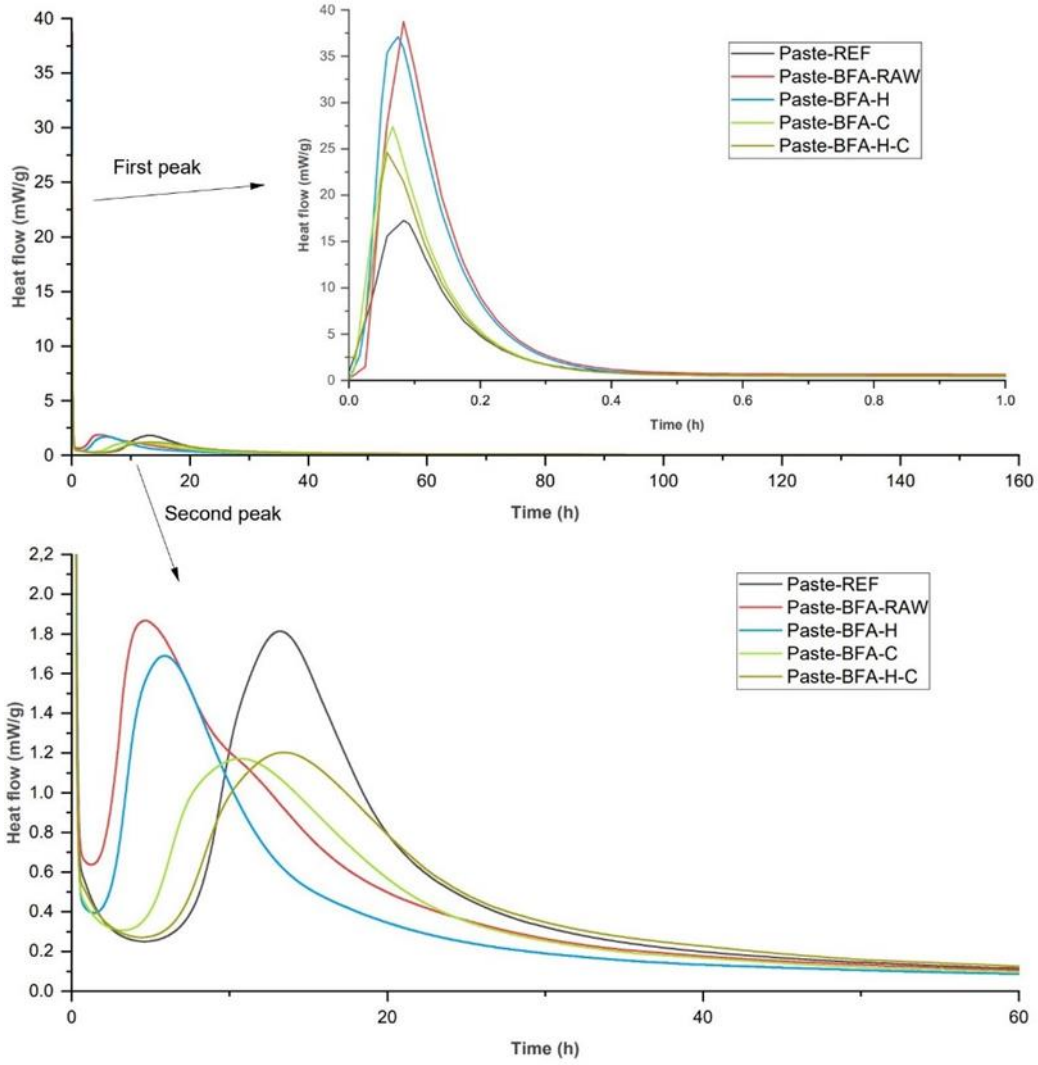

Figure 4.14: Heat flow of pastes incorporating BFA1 in different pre-treatment conditions (raw, water treated, carbonation treated, and combination of water and carbonation treatment).

In Figure 4.14, an initial exothermic peak is shown. This peak is immediately upon mixing the activator with the solid materials, corresponding to the wetting and dissolution of the solid material [103], [104], [105]. This is notably pronounced in the BFA-RAW sample due to the exothermic reaction involving the release of hydrogen gas from metallic aluminium. This reaction is intensely exothermic and occurs early when sodium hydroxide makes contact with the ash [26], [28]. The peak heights vary among samples, indicating differences in the rapid dissolution of components. This initial peak is succeeded by an induction period during which the reaction heat significantly decreases.

The second exothermic peak is attributed to the extensive precipitation of reaction products such as C-A-S-H [106], [107]. This peak is influenced by both the polymerization and condensation of geopolymer gels. The induction period for the non-carbonated samples (BFA-RAW and BFA-H) is notably shorter, showing an earlier formation of reaction products. Their smaller particle size is responsible for the early reactivity, which enhances the dissolution of elements such as SI, Al and Ca. The carbonated samples BFA-C and BFA-H-C exhibit dissolution induction periods comparable with the reference sample, suggesting a comparable timing for reaction product formation. Carbonation has been shown to increase the particle size of the ash. This has caused the reduction of the contact surface in the alkaline environment, thus delaying reaction peaks and aligning the reaction timing with that of the reference slag paste (REF).

Figure 4.15 shows the cumulative heat release for the sample pastes over 160 hours of curing. The initial rise in the curve is the heat released from the wetting and dissolution of the pastes. The second rise in the graph is due to the formation of reaction products [105]. The induction period is shown as a relatively flat region in the cumulative heat release curve. This region is found between the initial dissolution rise and the second acceleration rise. This period spans from the start of the test to 4 hours for the BFA-RAW and BFA-H samples, and extends to 10 hours for the REF, BFA-C, and BFA-H-C pastes.

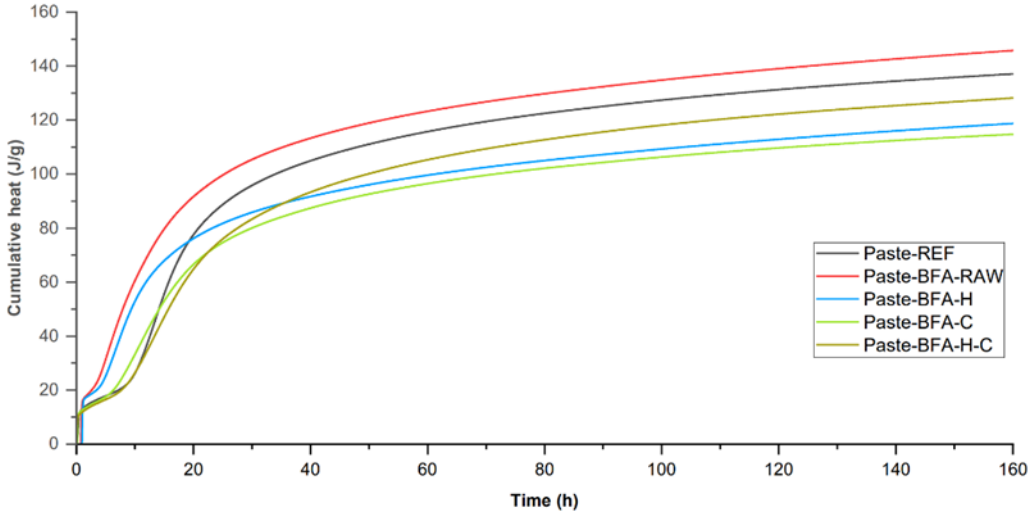

Figure 4.15: Cumulative heat release of pastes incorporating BFA1 in different treatment states (raw, hydrated, carbonated, and hydrated–carbonated), showing the total heat released over time during the reaction process.

Figure 4.16 shows the total heat release for each mixture. In order to have a better insight into the reaction kinetics, the initial heat from the element dissolution is excluded from the total heat release. Overall, reducing the slag content decreases the total heat release of the mixture. However, for the BFA-RAW sample, the cumulative heat flow exceeds that of the reference sample, largely due to the continuous reaction involving metallic aluminium. In addition, due to the absence of any pretreatment, the BFA-RAW sample exhibits a finer particle size distribution and contains a higher proportion of amorphous phases, which participate in the formation of reaction products.

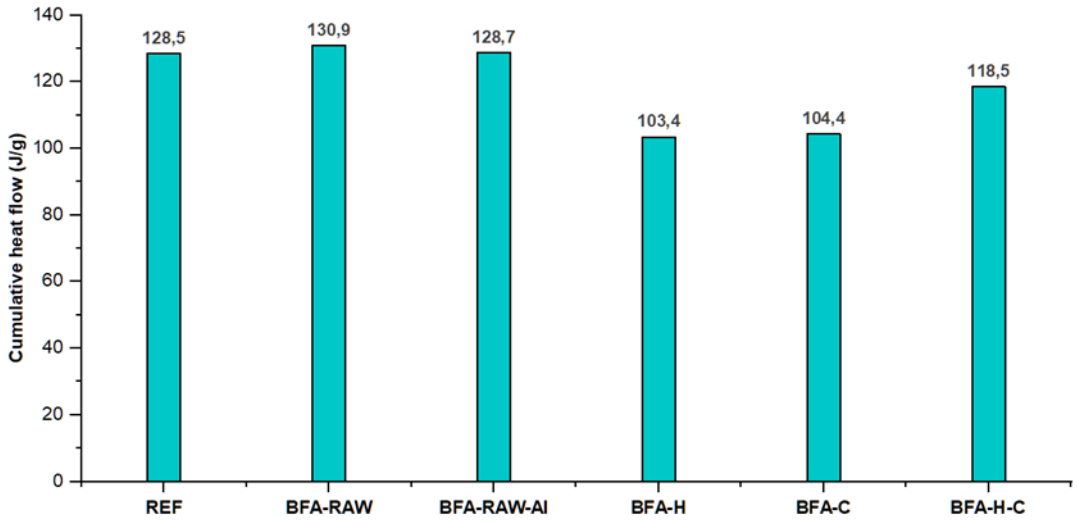

Figure 4.16: Cumulative heat release (J/g) of paste samples after 160 hours of curing with various BFA treatments, excluding the initial dissolution heat release. BFA-RAW-Al refers to the BFA-RAW sample with the heat contribution from metallic aluminium reaction subtracted.

In comparison to the BFA-RAW sample, the water-treated BFA-H sample exhibits a lower cumulative heat release, primarily because reactive metallic aluminium has been removed. Additionally, part of the amorphous content in the ash may have reacted at an early stage during water treatment, forming initial products that limit further reaction once in the paste during alkaline activation. This early reaction and formation of reaction products in the BFA-H sample have been shown in the FTIR analysis. The carbonated samples also exhibit lower cumulative heat release. This decline can be linked not only to the early formation of reaction products, as has been shown in the FTIR analysis, but also to the unreactive nature of carbonation products such as calcite. Moreover, the increase in particle size observed after pretreatment may further reduce reactivity by lowering the available surface area for dissolution.

To investigate the influence of the metallic aluminium reaction on the overall cumulative heat release, a theoretical calculation was performed. For this analysis, the content of metallic aluminium in one gram of paste must be known. One gram of paste consists of approximately 0.6 g of binder, and with a 25% replacement level, this means 0.15 g of BFA is present. From the water displacement method, BFA-RAW contains 0.09% metallic aluminium, resulting in a metallic Al content of:

$$0.15 \times 0.09/100 = 0.000135 \text{ g Al/g paste}$$

Theoretically, the reaction of 1 g of metallic aluminium with water releases 16.3 kJ of heat according to the reaction [108] :

$$2Al + 6H_2O \rightarrow 2Al(OH)_3 + 3H_2$$

Based on this, the heat released from metallic Al in BFA-RAW is about 2.2 J/g paste. The cumulative heat release of the BFA-RAW sample is 128.7 J/g after subtraction of the metallic Al contribution. This heat released is equal to the reference paste (128.5 J/g). These results indicate that BFA-RAW shows the highest reactivity as a precursor among the various treatments. This also shows that the pretreatment of BFA, whether by carbonation, water treatment, or both, causes a reduction in the reactivity of the ash. This is mainly attributed to early product formation during water treatment and the decreased solubility of components following carbonation. Furthermore, carbonation products, which increase after treatment, are chemically stable and do not actively contribute to the alkali activation reaction.

4.3.5 Effect of pre-treatment on heavy metal leaching

Removal of heavy metals from biomass fly ash is important for reducing its environmental risks. Carbonation and water treatments are methods used to immobilize heavy metals. These methods reduce the content of heavy metals to levels below those set by Dutch SQL regulations. The results of the leaching tests are presented in Table 4.5.

Table 4.5: Heavy metal leaching from BFA1 after various treatments compared to standard quality limits (SQL).

	RAW	BFA-C	BFA-H	BFA-H-C	SQL Limit
Barium [mg/kg]	3	1.9	1.3	1.7	200
Cadmium [mg/kg]	0.007	0.007	0.007	0.007	0.8
Chrome [mg/kg]	39	34	20	34	100
Copper [mg/kg]	0.14	0.05	0.05	0.05	36
Lead [mg/kg]	190	0.1	0.22	0.1	85
Nickel [mg/kg]	0.1	0.1	0.1	0.1	35
Zinc [mg/kg]	34	0.2	0.2	0.2	140

The immobilization mechanism is influenced by pH changes. Heavy metals such as Pb and Zn are less soluble under neutral, weak acid and weak base conditions, with solubility increasing with both acidity and alkalinity [59]. Conversely, metals like Cr, Cd, Cu and Ni show the lowest leaching under neutral and alkaline conditions and increase rapidly in strong acids [59].

Water treatment raises the pH through the dissolution of alkalis in the ash, promoting the precipitation of heavy metal hydroxides and reducing their solubility. This is particularly effective for lead (Pb), which forms insoluble hydroxides in alkaline conditions[109]. Chromium and nickel, however, may not precipitate as easily under alkaline conditions. Additionally, the formation of hydration products during water treatment can incorporate some of the heavy metals within their structure, as observed with the formation of simonkolleite phases containing zinc, in section 4.3.3.1.

Carbonation immobilises heavy metals by a number of mechanisms. Adsorption precipitation involves the adsorption of metal ions to fly ash particles surface via carbonate precipitates [59] [60] [116] [117]. This immobilises metals such as Pb, Zn and Cu in surface precipitates. But Cd, Cr and Ni are less effectively immobilised by this process since they do not easily form a precipitate under these conditions. Carbonation also enables direct chemical reactions between heavy metals and CO_2, forming stable carbonates or oxides that significantly reduce leaching, such as $PbCO_3$, $ZnCO_3$ for Pb and Zn [59]. Additionally, the formation of dense carbonate layers around fly ash particles physically encapsulates heavy metals, reducing their mobility and preventing leaching. This physical encapsulation applies to all tested metals, including Pb, Zn, Cu, Cd, Cr and Ni [112].

4.4 Conclusion

Pretreatment of BFA was essential for making the ash suitable for concrete use. The general goals of the treatments were accomplished. During carbonation, the ash was capable of absorbing up to 6.6 wt% CO_2. Additionally, the water and carbonation treatment combined effectively eliminated metallic aluminium content, thus preventing the formation of hydrogen gas. Another important benefit was the stabilization of heavy metals. Leaching decreased below the Dutch Soil Quality Guidelines (SQL) after pre-treatment, thus making the ash more safe environmentally. However, with these benefits, there came some trade-offs. Reactivity of the ash considerably reduced after treatment. This was mostly because there was an increase in particle size that reduced contact surface during alkali activation. Moreover, both water and carbonation treatments appeared to cause formation of early-stage reaction products. These products consumed some of the reactive silica and alumina that were needed later during hardening of the concrete, reducing the contribution of the ash towards strength gain. overall, the slight reduction in reactivity does still justify the use of the pretreatment as the benefits of removing metallic aluminium and immobilizing of heavy metals are very necessary for the production of mechanically and environmentally safer concrete.

5

5 Analysis of mechanical and durability properties of concrete

5.1 Introduction

This chapter describes the design and testing of concrete mixtures with the addition of pretreated biomass fly ash (BFA1). All mix designs considered here contain BFA1 treated with both water and carbonation treatment (BFA-H-C). The treated ash is used to partially replace ground granulated blast furnace slag (GGBFS) at different replacement levels. The chapter describes the test methods applied to determine the mechanical and durability performance of the produced concrete. This is followed by a discussion of the experimental results.

5.2 Materials and methods

5.2.1 materials

Mix design

The mix design is presented in Table 5.1. Central to this design is the varying replacement percentages of biomass fly ash with the binder. Literature review guided the selection of replacement levels. with a decision not to exceed 35% [68]. [119]. [120]. This threshold is critical as higher replacement levels have been shown to significantly diminish the mechanical strength of the concrete due to reduced binder content and decreased reactivity of the biomass fly ash. Conversely. keeping the replacement percentage too low would result in minimal impact on the amount of absorbed carbon dioxide in the sample. For this research. replacement levels of 15%. 25% and 35% of carbonated biomass fly ash were chosen. The geopolymer system comprises a binder composed of Ground Granulated Blast-Furnace Slag (GGBFS). an activator consisting of a solution of Sodium Hydroxide (50% wt%) and Water Glass Solution (37.5% wt%). The remaining components are coarse and fine aggregates.

Table 5.1: Mix design of the alkali activated concrete samples.

Concrete mix design	AAC-REF	AAC-BFA15	AAC-BFA25	AAC-BFA35
Blast furnace slag (kg/m3)	400	340	300	260
BFA1 (kg/m3)	0	60	100	140
Water (kg/m3)	143.86	143.86	143.86	143.86
NAOH (50%) (kg/m3)	37.30	37.30	37.30	37.30
PQ waterglass (kg/m3)	30.80	30.80	30.80	30.80
Gravel (4-16mm) (kg/m3)	946.9	946.9	946.9	946.9
Gravel (4-8mm) (kg/m3)	74.7	74.7	74.7	74.7
Sand(2-4mm) (kg/m3)	62.9	62.9	62.9	62.9
Sand(1-2mm) (kg/m3)	70.8	70.8	70.8	70.8
Sand(0.5-1mm) (kg/m3)	102.3	102.3	102.3	102.3
Sand(0.25-0.5mm) (kg/m3)	346.2	346.2	346.2	346.2
Sand(0.125-0.25mm) (kg/m3)	130.3	130.3	130.3	130.3
Total (kg/m3)	2334.1	2328.1	2324.1	2320.1

Concrete sample preparation

In the preparation of the concrete sample, the initial step involves preparing the activator solution prior to casting. This solution is made by mixing sodium hydroxide solution with water glass solution in the required proportions, followed by the addition of water. The activator solution is then allowed to cool, as the dissolution process generates heat. This preparation of the activator is completed 2 hours before mixing to prevent precipitation of the activator particles if left longer. During the casting process, coarse aggregates are first added and mixed for 1 minute to ensure thorough mixing. The next step involves adding the biomass fly ash. This step is crucial because the ash particles are agglomerated after carbonation pretreatment, and mixing them with the aggregates acts like a milling process. Mixing continues for another minute. Following this, fine aggregates are added, and after thorough mixing, the slag is incorporated. Finally, the activator is added in three stages, adding half a bucket at each step to enhance mixing and prevent agglomeration. The fresh concrete is then cast into moulds measuring 15 x 15 x 15 cm. The samples are left to harden at room temperature (20°C), covered with plastic film to prevent moisture loss. The samples are demoulded after 24 hours and placed in a curing chamber at 20°C and 99% relative humidity. They are covered with plastic film until the testing days, which are day 1, day 7 and day 28.

Concrete performance requirements

The concrete is intended for non-structural applications, specifically for the making of pavement tiles. To ensure suitability, it must meet the following performance requirements by EN 1338 (2003) [115] and NEN-EN 206 + NEN 8005 (2017) [116]: a compressive strength class of at least C30/37, a minimum tensile splitting strength of 3.5 MPa, consistency class of S2-S3 and a maximum surface scaling of 1.0 kg/m² after 28 freeze-thaw cycles.

5.2.3 Methods

5.2.3.1 Slump test

The workability was examined by measuring the slump of different mixes following the addition of different replacement levels of biomass fly ash to slag binder. Slump test was carried out according to the prescribed procedure in ASTM C143/C143M[117]. A standard slump cone was filled in three layers with the concrete mix, each layer being thoroughly compacted using 30 strokes of a tamping rod. Once filled, the cone was carefully lifted vertically, allowing the concrete to slump, and the subsidence was then measured from the original height to the displaced top of the concrete to determine the slump value, Figure 5.1.

Figure 5.1: Slump test for reference concrete (left) and concrete incorporating 25% BFA1 (right), illustrating the workability differences due to ash incorporation.

5.2.3.2 Compressive strength test procedure

The compressive strength test was conducted using a two-column universal compression testing machine in accordance with NEN-EN 12390-3 [118], Figure 5.2, for the test cubic samples with dimensions of 150x150x150 mm³ were prepared according to the standards. Each test consisted of three cubes and the final result was reported as the average of these three measurements.

The test was initiated within 10 hours of removing the samples from the curing chamber, which was maintained at a temperature of 20°C and 99% relative humidity (RH). The surfaces of the cubes were first wiped.

The application of the load began from zero and increased continuously at a rate of 13.5 kN/s until the cube crushed. The compressive strength of each cube was calculated using the following formula:

$$f_c = \frac{F}{A_c}$$

$f_c =$ the compression strenght. in MPa $\left(\frac{N}{mm^2}\right)$;

$F =$ Maximum load at failure. in N

$A_c =$ Cross sectional area. in mm^2

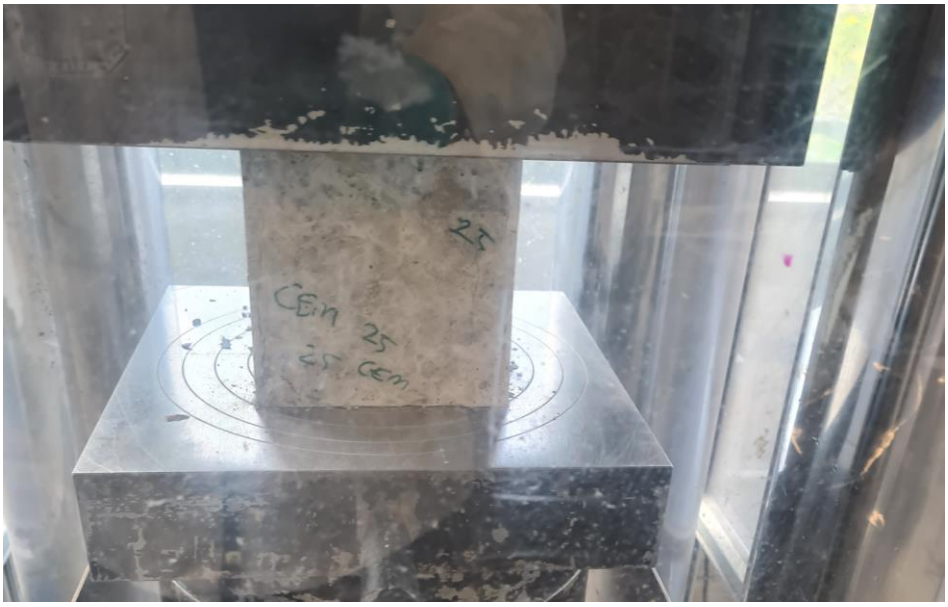

Figure 5.2: Setup of the compressive strength test for a concrete cube specimen.

5.2.3.3 Tensile strength test procedure

The splitting tensile strength test was carried out in compliance with NEN-EN 12390-6 [119]. The cubic samples used for this test had dimensions of 150x150x150 mm³. For this procedure, three cubes were tested, and the average value of the three tests was reported as the tensile strength.

The test was performed 28 days after casting using a two-column universal compression testing machine. Before testing, the samples were removed from the curing chamber, which was maintained at a temperature of 20°C and 99% relative humidity and were carefully wiped to remove any surface water or loose material.

During the test, small wooden slats were placed along the top and bottom surfaces of the cubes, perpendicular to the load direction, to ensure proper load concentration and cracking patterns. The load was applied at a constant rate of 1.1 kN/s until the specimens failed, Figure 5.3.

The tensile strength of each cube was calculated using the following formula:

$$f_{ct} = \frac{2 \times F}{\pi \times L \times d}$$

f_{ct} = Tensile strengh. in MPa

F = Maximum load. in Newtons N

L = The length of the line of contact of the specimen. in millimetres (mm);

d = The designated cross − sectional dimension. in millimetres (mm).

Figure 5.3: Setup of the tensile strength test for a concrete cube specimen.

5.2.3.4 Freeze-thaw testing procedure

The freeze-thaw resistance of the concrete mixtures was evaluated following NVN-CEN/TS 12390-9:2016 [120]. Concrete cubes with dimensions of 150 × 150 × 150 mm were cast, incorporating a polytetrafluoroethylene (PTFE) plate centrally positioned on one surface to serve as a hydrophobic barrier. The PTFE plate was placed without the use of Vaseline to avoid interference with surface interactions during the freeze and thaw test.

Following casting, the specimens were covered with polyethylene sheets and kept in their moulds for 24 hours to prevent early drying. After demoulding, the samples underwent 14 days of wet curing in a controlled curing room maintained at 20°C and 99% relative humidity. This was followed by a 14-day conditioning period in a climate chamber set to 20 ± 2°C and 50 ± 5% relative humidity. At 25 days after casting. The non-test surfaces were sealed with rubber tape, ensuring a watertight seal with additional layers applied around the joints, Figure 5.4. The sealed specimens were returned to the climate chamber until testing commenced.

Figure 5.4: Concrete samples prepared and sealed for freeze–thaw testing.

At 28 days, the specimens were partially immersed (5 mm depth) in a 3% NaCl solution on the exposed test surface. This allowed capillary suction of the solution into the concrete over 7 days at a constant temperature of 20 ± 2°C. On day 35. After refreshing the NaCl solution, the freeze-thaw cycles were initiated. The freeze-thaw regime followed a 12-hour cycle, beginning at +20°C. decreasing to −20°C (held for 3 hours) and then returning to +20°C. The NaCl solution was replaced after every freeze-thaw exposure period. Testing was conducted at 4, 6, 14 and 28 cycles. After each designated cycle, the stainless steel containers holding the specimens were removed and placed in an ultrasonic bath for 3 minutes. This process removed any surface scaling or loose particles, which were collected using filter paper. The filter paper and debris were then oven-dried at 105°C for 24 hours, after which, the dried material was weighed to determine the mass of scaled material.

The freeze-thaw damage was quantified by calculating the cumulative surface scaling per unit area. using the following formula:

$$S_n = M_{s,n} / A \times 10^3$$

where S_n is the surface scaling after *n* cycles (kg/m²). $M_{s,n}$ is the cumulative mass of dried scaled material after *n* cycles (kg). and A is the exposed test surface area (m²).

5.3 Results and discussion

5.3.1 Workability

The test results indicate a consistent decline in slump value with a rise in levels of biomass fly ash, indicating lower workability. AAC-REF gave a slump of 215 mm, reflecting the highest workability. This is followed by AAC-BFA1-15 with a slump value of 185 mm, AAC-BFA1-25 at 145 mm and AAC-BFA1-35 with the lowest slump at 80 mm, Figure 5.5. The substantial decrease in slump as the replacement level increased suggests a significant impact on the fresh properties of the concrete. likely due to the altered particle size distribution of the fly ash and water demand compared to the original slag binder. These results are consistent with previous results found in the literature [68]. [69].

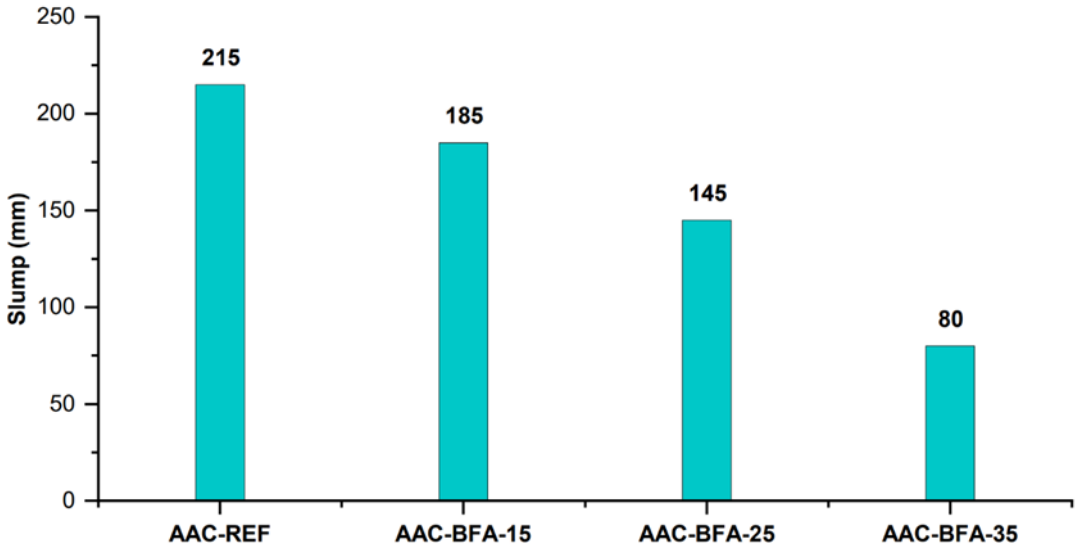

Figure 5.5: Workability of alkali-activated concrete samples incorporating BFA1. as assessed by the slump test.

5.3.2 Compression strength

The compressive strength of alkali-activated concrete was evaluated after 28 days of curing. The results showed a trend of decreasing strength with increasing replacement levels: AAC-REF exhibited the highest strength at 49.7 MPa, followed by AAC-BFA-15 at 48.5 MPa, AAC-BFA-25 at 46.3 MPa and AAC-BFA-35 showing the lowest at 41.2 MPa, Figure 5.6.

These concrete mixtures were designed to achieve a minimum compressive strength of C30/37 after 28 days, compliant with the requirements per NEN 206 [121]. And by accounting for probabilistic variations in the compressive strength. the strength must not fall below 45 MPa. The results indicated that up to a 25% replacement level, the compressive strength does not significantly reduce, remaining above the threshold of 45 MPa. However, increasing the biomass fly ash (BFA) content to 35% resulted in the strength falling below the required minimum, likely due to the reduced reactivity of BFA and the substantial reduction in slag content. Based on the results of the compressive strength tests, a 25% replacement level of BFA-H-C was selected for all subsequent evaluations. This replacement ratio was used consistently across all remaining mechanical, durability and microstructural tests presented in the following sections.

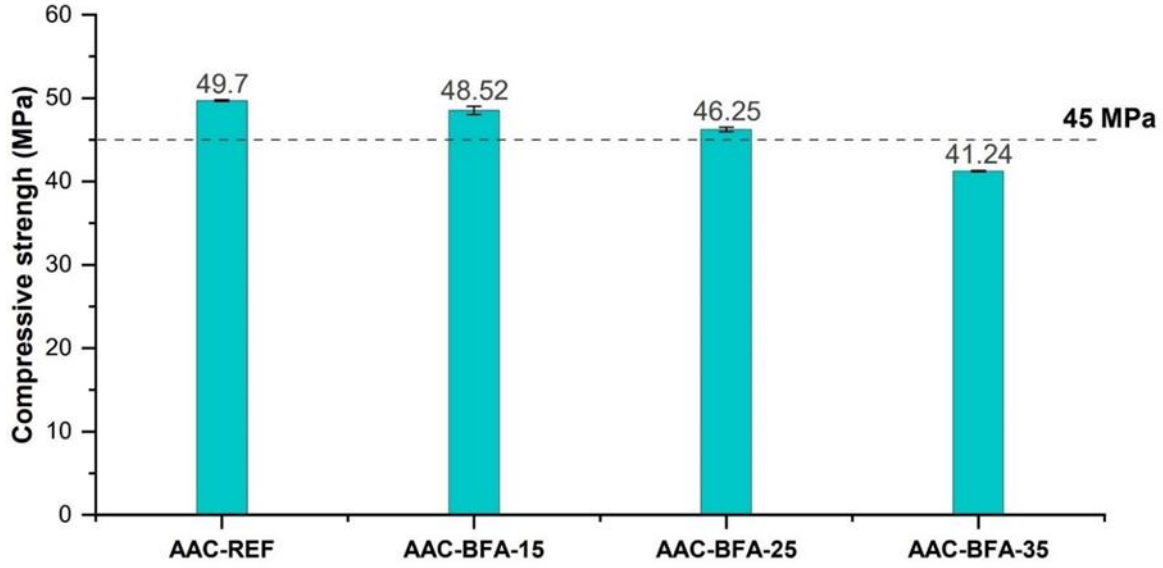

Figure 5.6: Compressive strength of alkali-activated concrete samples incorporating BFA1.

The AAC-BFA-25 sample was further compared to the REF sample. The time-dependent strength development was tested at 1, 7, and 28 days, showing an increase in compressive strength from 15.94 MPa on day 1 to 30.14 MPa at day 7 and 46.3 MPa at 28 days, Figure 5.7. This trend shows a slower initial strength gain but a substantial strength recovery over time, making the 25% replacement a good option for structural applications.

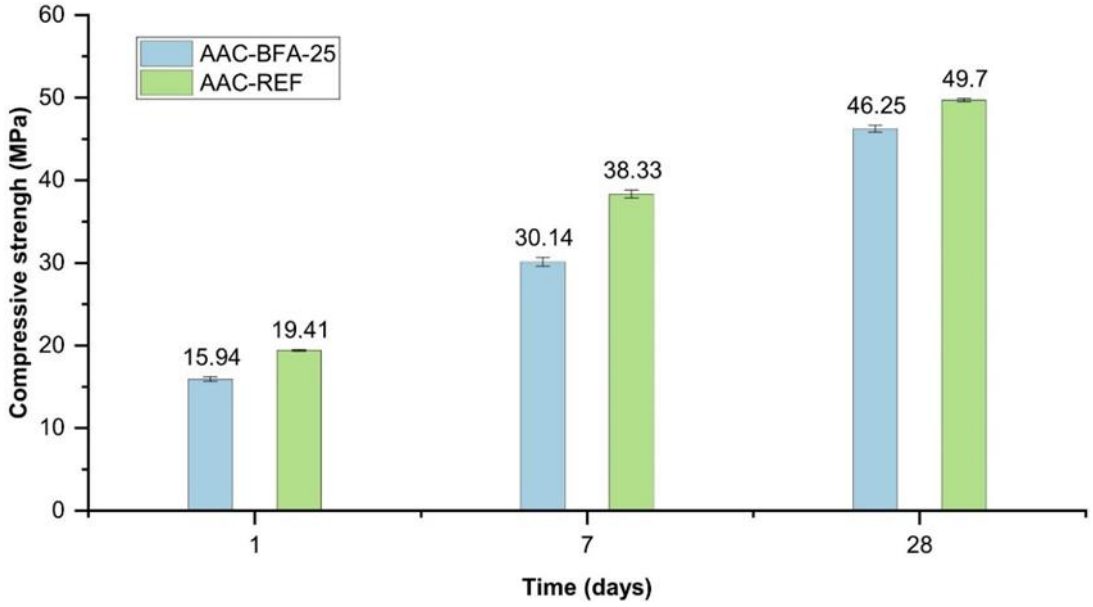

Figure 5.7: Development of compressive strength over time for reference concrete (AAC-REF) and concrete incorporating 25% BFA1 (AAC-BFA-25).

5.3.3 Tensile strength

The tensile strength of alkali-activated concrete (AAC) was assessed after a 28-day curing period to evaluate the impact of varying biomass fly ash replacement levels in the slag binder. The results demonstrated a gradual decrease in tensile strength with increasing biomass fly ash content: AAC-REF presented a tensile strength of 3.39 MPa, followed by AAC-15 at 3.40 MPa, AAC-25 at 3.25 MPa and AAC-35 with the lowest strength at 3.11 MPa, Figure 5.8. The required strength of 3.6 MPa, compliant with the requirements per NEN 1338 (2003), was not reached, even in the REF sample to meet the requirement for pavement blocks. However, the comparison of the BFA-incorporated sample did not show much reduction in tensile strength when compared with the REF sample.

While the tensile strength decreased with increasing BFA content, the reduction as a whole was comparatively modest. In particular, the 15% replacement level resulted in no measurable reduction in tensile strength. these results are consistent with the report of Ghorpade [68] where replacing 10% of the binder with BFA resulted in little or no loss in the tensile performance. These results show that partial replacement of the binder with BFA by 25% could be accomplished without seriously reducing the tensile strength. Although some level of strength reduction should be found at higher replacement levels.

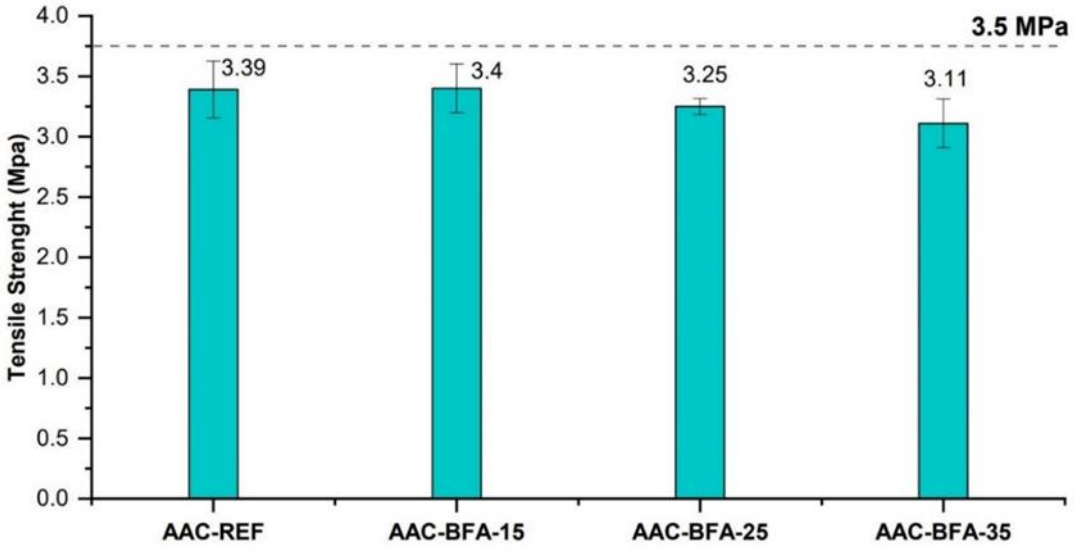

Figure 5.8: Tensile strength of alkali-activated concrete samples incorporating BFA1.

5.3.4 Freeze-thaw resistance

The freeze-thaw resistance of the concrete samples was assessed using the capillary suction of de-icing chemicals and the freeze-thaw (CDF) test method. In this investigation, concrete mixes incorporating 25% biomass fly ash (BFA) as a partial replacement for slag in the alkali-activated cementitious (AAC) system were examined for their resistance to freeze-thaw damage. A 3% NaCl solution was used as the liquid medium in this test.

Figure 5.9 presents the development of surface scaling over 28 freeze-thaw cycles for both the reference mix (AAC-REF) and the BFA-incorporated mix (AAC-BFA25). The AAC-REF mix exhibited significantly lower surface scaling, beginning at 1.47 kg/m² after four cycles and reaching 3.63 kg/m² after 28 cycles. The AAC-BFA-25 mixture showed higher scaling, with an initial value of 2.83 kg/m² after four cycles and a final value of 5.66 kg/m² after 28 cycles. These results highlight a higher susceptibility to degradation in the BFA-containing mix during freeze-thaw conditions, likely due to changes in the pore structure after the introduction of BFA into the mix. Similar results have been reported by Nagrockienė et al. [70], who observed that replacing slag with 25% BFA led to a 50% reduction in freeze-thaw resistance. These results show that the targeted surface scaling of 1 kg/m^2 is not reached, even in the AAC-REF sample.

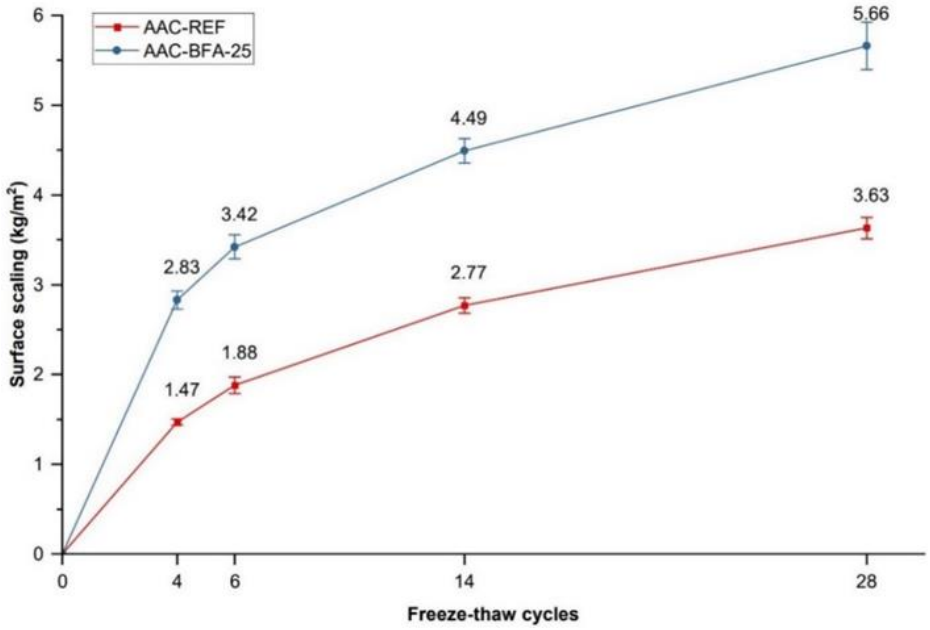

Figure 5.9: Evolution of surface scaling in concrete specimens (REF and BFA-25) subjected to 4, 6, 14 and 28 freeze–thaw cycles.

Furthermore, additional freeze–thaw tests were carried out using water instead of the standard 3% NaCl solution, since the presence of salt is known to potentially intensify surface scaling. In addition, superabsorbent polymer (SAP) was introduced in some mixtures, given its reported ability to enhance freeze-thaw resistance. A SAP content of 0.1% to binder ratio is added as this content has been shown in earlier research to not decrease the compressive strength while increasing the freeze and thaw resistance.

The extra test configurations included the following samples:

- AAC-BFA-25 (Water): exposed to water without SAP
- AAC-BFA-25-SAP (NaCl): exposed to 3% NaCl with 0.1% SAP
- AAC-BFA-25-SAP (Water): exposed to water with 0.1% SAP

The results of the additional freeze-thaw tests are presented in Table 5.2. Overall, the data shows no significant improvement in surface scaling when water was used instead of a NaCl solution, or when SAP was added to the BFA-containing concrete. The AAC-BFA-25 mix showed identical surface scaling after 28 cycles when tested in water or NaCl medium. the scaling was at 5.67 and 5.66 kg/m² respectively. The addition of SAP in the NaCl solution showed more decrease in the freeze and thaw performance, with surface scaling increasing to 6.91 kg/m² in the AAC-BFA-25-SAP sample. A minor improvement was seen when SAP was used in combination with water, where the surface scaling was decreased slightly to 5.64 kg/m². These findings suggest that the inclusion of BFA does not enhance the freeze-thaw resistance under the tested conditions, regardless of the use of SAP or changes in the exposure medium. The durability performance remains consistently lower than the reference mix.

Table 5.2: Surface scaling after 28 freeze and thaw cycles.

Mix Name	Mix Description	Scaling (kg/m²)
AAC-REF (NaCl)	100% slag mix, exposed to 3% NaCl solution	3.63
AAC-BFA-25 (NaCl)	25% BFA, in a 3% NaCl solution	5.66
AAC-BFA-25 (Water)	25% BFA, in a water (no salt)	5.67
AAC-BFA-25-SAP (NaCl)	25% BFA with 0.1% SAP, in a 3% NaCl solution	6.91
AAC-BFA-25-SAP (Water)	25% BFA with 0.1% SAP, exposed to water	5.64

To better understand the reduction in freeze–thaw resistance observed after incorporating BFA, a Mercury Intrusion Porosimeter (MIP) test was carried out on the paste portion of concrete samples after 28 days of curing. The tested samples included the AAC-REF (100% slag) and AAC-BFA-25 (25% BFA, no SAP). The MIP results revealed a total porosity of 7.88 % in the BFA containing sample, while the reference sample showed a reduced total porosity at 6.60 %. This difference can be linked to the reduced reactivity of BFA, resulting in less gel formation during the alkali activation process. This results in a denser matrix in the reference sample compared to the BFA containing mixture. In addition, Figure 5.10 shows a noticeable increase in pore intrusion within the range smaller than 0.03µm. At the same time, pores larger than 1 µm also exhibited consistently higher intrusion values in the BFA mix, suggesting a more open and heterogeneous pore network. This test confirms that an overall increase in porosity results from addition of BFA in the concrete mixture. This porosity can be found in both the fine and coarse pore ranges. This increase in porosity facilitates greater water ingress, which expands in volume after freezing and imposes internal stress on the matrix. Following further freeze/thawing, this condition may result in microcracking, scaling, and overall degradation in durability.

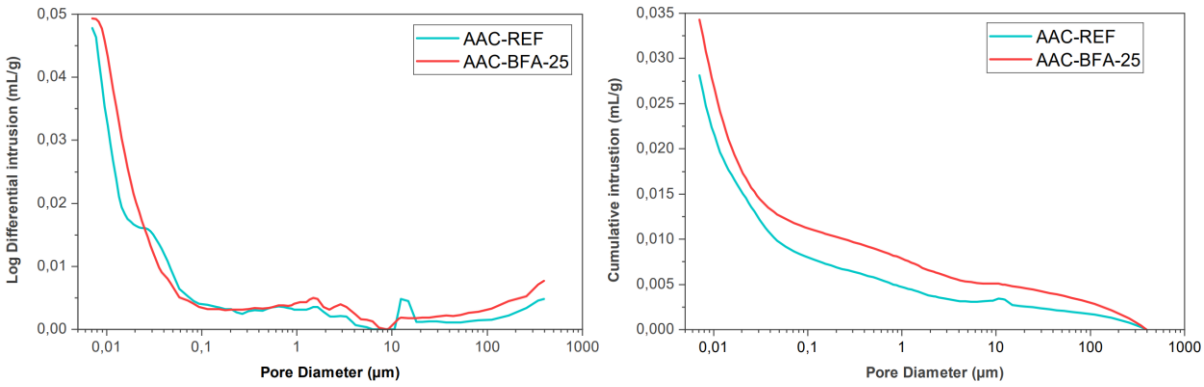

Figure 5.10: MIP results showing the differential (left) and cumulative (right) pore size distributions of AAC-REF and AAC-BFA-25 samples.

6

6 Microstructure and phase assemblage in alkali-activated concrete binders

6.1 Introduction

This chapter investigates the microstructural characteristics of concrete binders incorporating treated biomass fly ash (BFA1). Paste samples were prepared to simulate the binder phase of the concrete mixes. Quantitative X-ray diffraction (QXRD) was carried out to identify and measure the crystalline phases present after alkali activation. Thermogravimetric analysis (TGA) was used to estimate the amount of reaction products formed. To better understand changes in chemical bonding and the level of polymerisation, FTIR spectroscopy was applied. Lastly, SEM-EDX analysis provided insight into the morphology and elemental composition of the binder, allowing for a closer look at the effects of incorporating BFA.

6.2 Materials and methods

6.2.1 Materials

Mix design

In order to understand the microstructural and phase assemblage changes, paste samples were prepared by eliminating the fine and coarse aggregates from the mix design; only the binder and activator were used, in the same proportions as the concrete level. The absorption content of the aggregates was accounted for by adjusting the activator content. In the reference sample, labelled 'Paste-REF,' the binder consists of 100% slag. In contrast, the BFA-incorporated sample, labelled 'Paste-BFA,' uses a binder composed of 75% slag and 25% water–carbonation-treated BFA1. The detailed mix design of the paste samples is provided in Table 6.1.

Table 6.1: Mix design of the alkali-activated paste samples.

Paste mix design	Paste-REF	Paste-BFA
Blast furnace slag (kg/m³)	400	300
BFA1 (kg/m³)	0	100
Water (kg/m³)	135.72	135.72
NAOH (50%) (kg/m³)	35.21	35.21
PQ waterglass (kg/m³)	29.07	29.07

Paste sample preparation

Paste samples are prepared by mixing the alkaline activator solution with the solid precursor at 150 rpm for one minute using a head mixer, followed by hand mixing for an additional minute and a final mix at 500 rpm for one minute to ensure homogeneity. The mixed paste is poured into small plastic containers and sealed with cling film, as shown in Figure 6.1. The paste specimens are first cured at room temperature for 24 hours. After demoulding, the specimens are cut into pieces and sealed with cling film. and cured in a fog room (20°C, 99% relative humidity) until the testing days, which are days 1, 7, and 28. Isopropanol was used to stop the hydration at specific dates for later testing.

Figure 6.1: Paste samples for microstructural analysis, with 'Paste-BFA ' on the left incorporating biomass fly ash and 'Paste-REF' on the right consisting only of slag.

6.2.2 Methods

QXRD

The paste samples were crushed and manually ground using a mortar and pestle to obtain a fine particle size distribution ranging from 1 to 5 µm. For the quantitative analysis of the crystalline phases, 10 wt% of silicon powder was incorporated as an internal standard and uniformly mixed with the ground paste. The identification and quantification of mineral phases were performed using the Rietveld refinement method implemented in the Profex-BGMN software.

TGA

Thermogravimetric analysis was performed using a TG 449 F3 Jupiter instrument. Around 30 mg of crushed paste was placed in an open aluminium crucible and heated from 40 °C to 1000 °C at a rate of 10 °C/min under an argon gas atmosphere. The mass loss was continuously recorded to identify thermal decomposition stages.

FTIR chemical bond

Fourier-transform infrared (FTIR) spectroscopy was employed to identify the functional groups and chemical bonds present in the paste samples. The model of the instrument is PerkinElmer Spectrum 100. Each sample was scanned in the mid-infrared range of 4000–600 cm^{-1} with a spectral resolution of 1 cm^{-1}.

SEM-EDX

Prior to SEM analysis, the sample was impregnated with epoxy resin to protect its microstructure during grinding and polishing, Figure 6.2. The epoxy was allowed to harden for 48 hours at room temperature. The hardened surface was then ground using 2000- and 4000-grit abrasive paper for 15 minutes each, with ethanol used as a wetting agent to prevent the formation of reaction products.

Polishing was performed afterwards and carried out using polishing discs spread with diamond particles of decreasing sizes (6 µm, 3 µm, 1 µm, 0.5 µm, and 0.25 µm), each applied for 3 minutes in succession. After each grinding and polishing session, the sample underwent ultrasonic cleaning in ethanol for 2 minutes to remove surface particles. Following the final polishing step, the sample was carbon-coated 24 hours prior to SEM testing to ensure conductivity during the test.

Figure 6.2: Samples impregnated with epoxy in preparation for the SEM-EDX test.

6.3 Results and discussion

6.3.1 QXRD

QXRD analysis was conducted to measure the phase composition of the pastes after inclusion of BFA. The QXRD analysis showed that the pastes consist mainly of amorphous phases. These phases are mainly composed of C-A-S-H gels for the slag-based alkali-activated system, Table 6.2.

Table 6.2: Phase composition of Paste-REF and Paste-BFA as determined by QXRD analysis.

Phase	Paste-REF	Paste-BFA
Amorphous phase	89.62	77.99
Calcium Carbonate	2.36	11.65
Tobermorite	4.25	4.98
Hydrotalcite	3.78	3.4
Quartz	-	1.98

The results showed a higher amorphous phase content in the Paste-REF sample, with 89.62 % compared to 77.99 % in the Paste-BFA sample. This higher amorphous content can also be seen in the enhanced amorphous hump between 25° and 35° 2θ in the XRD pattern of Paste-REF, Figure 6.3. A higher degree of alkali activation in the slag system is the reason for the increased amorphous content in the Paste-REF.

The Paste-BFA sample shows a higher amount of calcium carbonate at 11.7 %, whereas the Paste-REF sample shows only 2.4 %. This increase is due to the carbonation pretreatment of the BFA, showing its CO_2 sequestration. The presence of calcium carbonate in the Paste-REF sample at low content can originate from natural carbonisation during curing. Quartz is found in the BFA-incorporated paste and was earlier detected in the ash analysis. The two samples showed similar results for the crystalline hydration products, with tobermorite (4.3%, 5.0%) and hydrotalcite (3.4%, 3.8%) being found in similar quantities.

These findings show that although the incorporation of BFA can reduce the overall amorphous gel content, due to the presence of carbonated phases. It still contributes in the formation of reaction products relevant to mechanical performance.

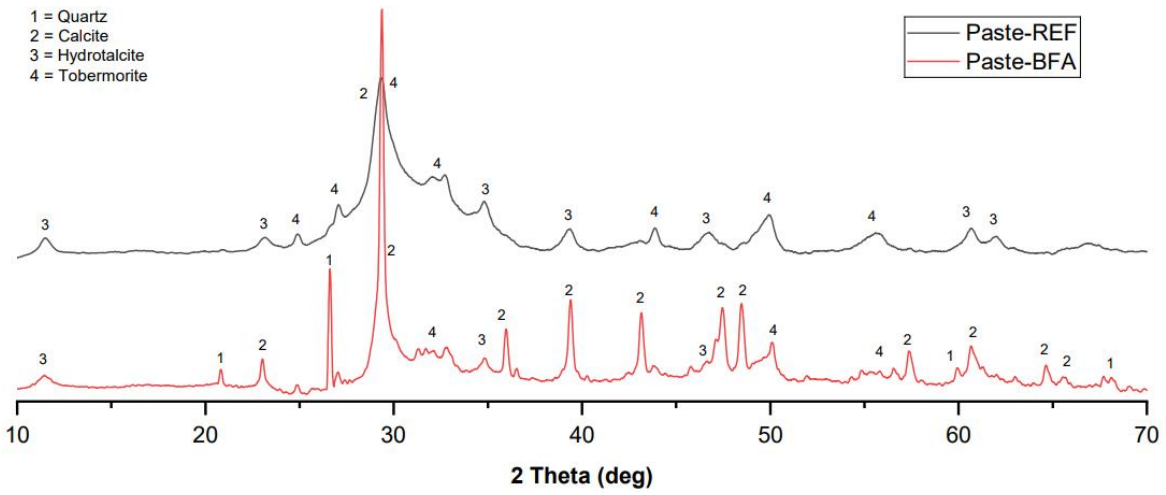

Figure 6.3: XRD patterns of Paste-REF and Paste-BFA samples. The broader amorphous hump between 25° and 35° in the Paste-REF sample indicates a higher proportion of amorphous reaction products compared to the BFA-containing paste.

6.3.2 Thermogravimetric analysis

The thermogravimetric analysis (TGA) and differential thermogravimetric (DTG) curves for the paste samples are shown in Figure 6.4. The samples were analysed at curing ages of 1, 7, and 28 days.

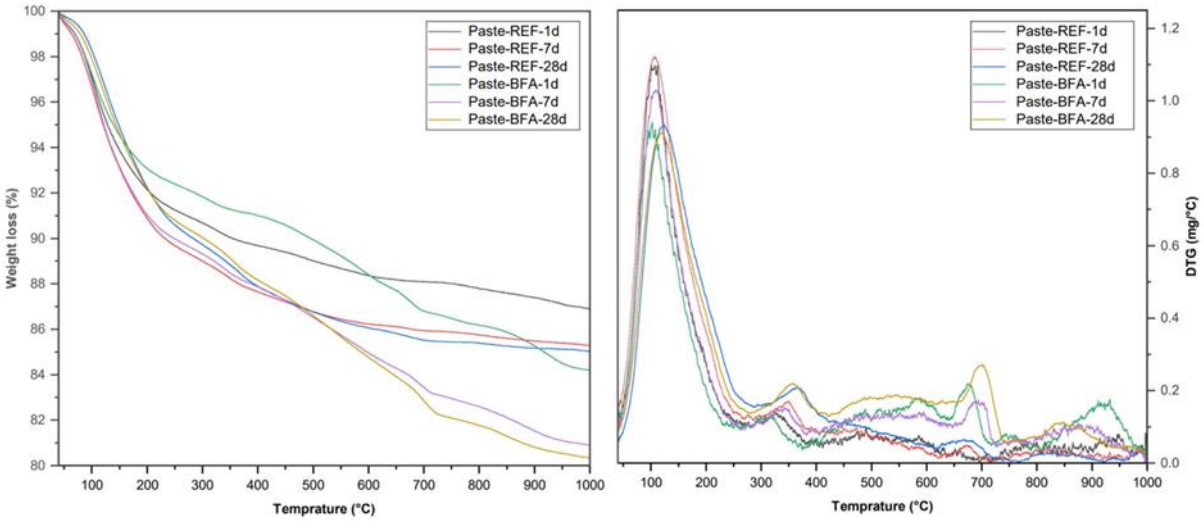

Figure 6.4: Thermogravimetric (TG) and derivative thermogravimetric (DTG) analysis of reference and BFA25 samples at 1, 7, and 28 days. illustrating weight loss behaviour and thermal decomposition characteristics.

The weight loss observed in the temperature range of 105–300°C is attributed to the dehydration of C-A-S-H-type gel, which is the dominant hydration product in alkali-activated pastes [128]. [129]. This region reflects the chemically bound water within the gel network. The results show a higher mass loss in this range for the Paste-REF sample compared to the Paste-BFA sample at day 1, Table 6.3. After 7 days, the mass loss in this range is nearly identical for both samples, showing that the Paste-BFA forms a comparable amount of reaction products. By 28 days, while the Paste-REF samples still show a slightly higher content of reaction products, the Paste-BFA samples is only about 10% lower, confirming the reactivity of BFA in the mixture.

Between 500°C and 850°C, the weight loss is primarily attributed to the decomposition of calcium carbonate [128]. [129]. This weight loss is more pronounced in the Paste-BFA sample, which is a reflection of the high level of calcium carbonate that is brought into the BFA ash during the carbonation process. This difference can also be seen in the DTG curves, where higher peaks in this temperature range can be seen in the Paste-BFA samples.

Table 6.3: Mass loss in the temperature range of 105–300°C.

Mass loss in 105-300◦C	**Paste-REF**	**Paste-BFA**
Mass loss 1 day [%]	5.96	4.96
Mass loss 7 day [%]	7.15	7.11
Mass loss 28 day [%]	8.18	7.44

6.3.3 FTIR chemical bond

In this section, we examine the FTIR spectra of alkali-activated paste samples made with different mixtures of slag and biomass fly ash (BFA). The reference sample (Paste-REF) consists of 100% slag. while the treated sample (Paste-BFA) includes 25% carbonated and water-treated BFA. Analyses were conducted on Days 1, 7 and 28 after curing to gain insights into the gel formation processes and the characteristics of the resulting reaction products.

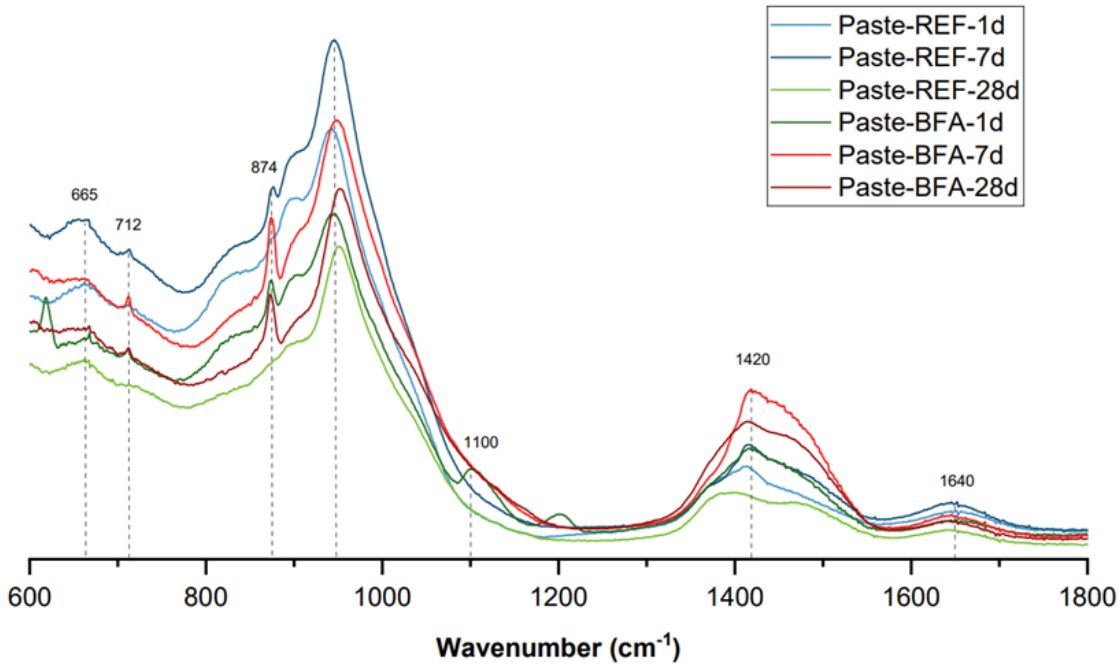

Figure 6.5: FTIR spectra of REF and BFA-HC paste samples at 1, 7 and 28 days of curing.

Figure 6.5 shows the FTIR spectra of the various samples. The absorption band around 1420 cm^{-1} found in all mixes corresponds to the stretching vibrations of O-C-O in carbonates [130] [131] [132], and is more pronounced in the BFA incorporated samples than in the Paste-REF sample. This is representative of the calcite in the fly ash. In addition to that, the carbonate peaks at 875 cm^{-1} and 712 cm^{-1} can only be seen in the BFA-containing samples [85] [90]. They are not detected in the Paste-REF sample, which indicates that calcite is not present initially. However, small peaks in the Paste-REF spectra can be seen at day 7, which are probably due to carbonation during curing.

Around 1640 cm^{-1}, a very small band is attributed to the bending modes of the H-OH groups from interlayer adsorbed water, suggesting the presence of structural water in the samples [96] [98] [99] [133]. Additionally, the signal at 665 cm^{-1} relates to Si-O-Si bending vibrations [128].

A characteristic feature across all tested composites is a broad peak from 800 to 1200 cm^{-1}, mainly due to the asymmetric stretching vibration of Si–O–Si or Si–O–Al, indicating the presence of C–A–S–H gels from alkali activation [90]. [92]. [93]. This band peaks at around 950 cm^{-1} in all the samples at different ages. A shift in the absorption wavenumbers in this peak to a higher value generally indicates an increase in the polymerization degree of a specific group, and an increase in wavenumber suggests a more highly polymerized SiO network [91]. [133]. [135]. [136] .

To gain further insight into the evolution of the geopolymer's three-dimensional structure, the FTIR spectra around this peak were recorded at 1, 7, and 28 days of curing, Figure 6.6. The observations reveal that the position of the main band gradually shifts to higher wavenumbers over time.

On day 1 the main peak was detected at 943 cm^{-1} for the paste-REF as well as the paste-BFA samples. By Day 14, the peak shifted to 946 cm^{-1} for the paste-REF and 948 cm^{-1} for paste-BFA, which indicates an increased polymerization. By Day 28, the peak shifted even further to 951 cm^{-1} for the paste-REF and 952 cm^{-1} for the paste-BFA. This higher peak in the paste-BFA indicates that the incorporation of BFA increases the polymerization degree.

The pre-treatment of BFA, either through water treatment or carbonation, appears to initiate early reactions that lead to the formation of reaction product. Although both the Paste-REF and the Paste-BFA samples begin with similar degrees of polymerization at Day 1, the Paste-BFA sample shows a faster shift in wavenumber by Day 7. This is a result of the fact that partially polymerized phases are initially found in the Paste-BFA particles, through water and carbonation pretreatments. By Day 28 the polymerization difference between the two systems declines, showing that although BFA pretreatment gives an initial advantage in polymerization development, the slag-rich Paste-REF sample achieves a similar level of structural maturity.

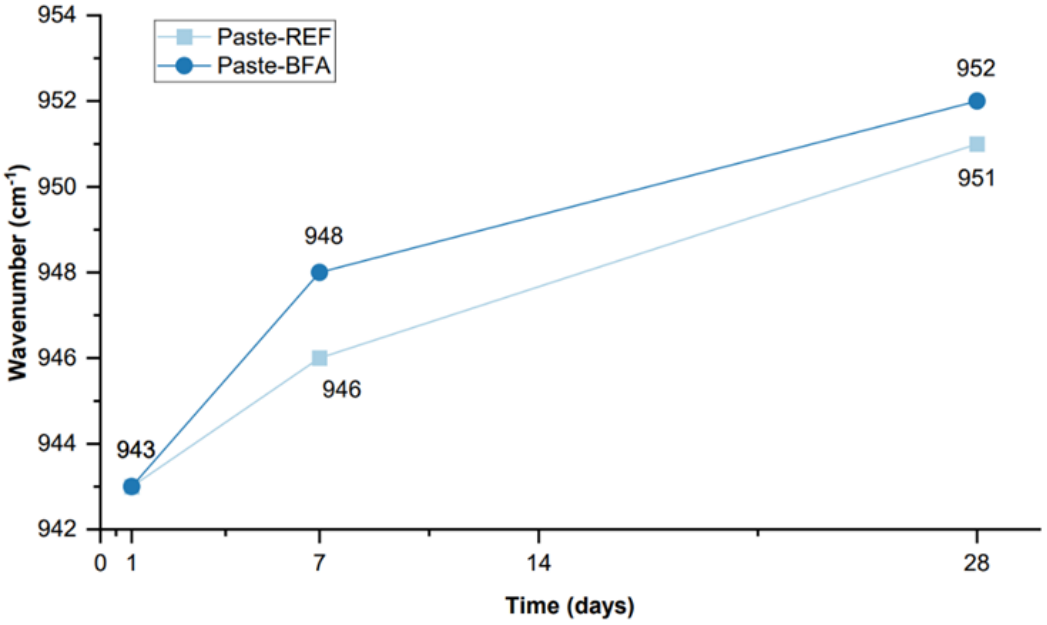

Figure 6.6: Evolution of Main FTIR Band Position Indicating Polymerization degree Over Time in REF and BFA-HC Pastes.

6.3.4 SEM-EDX analysis

The SEM images presented offer a detailed view of the morphological differences between the two alkali-activated paste compositions, Figure 6.7. At a magnification of 1000x, these images highlight the impact of incorporating biomass fly ash (BFA) on the microstructure of the slag-based binder. The reference sample, which is only composed of slag, shows a homogeneous and dense microstructure. In contrast, the sample including BFA shows a more heterogeneous and irregular microstructure. This blend of slag and BFA particles shows regions rich in BFA particles and a greater variety of particle sizes.

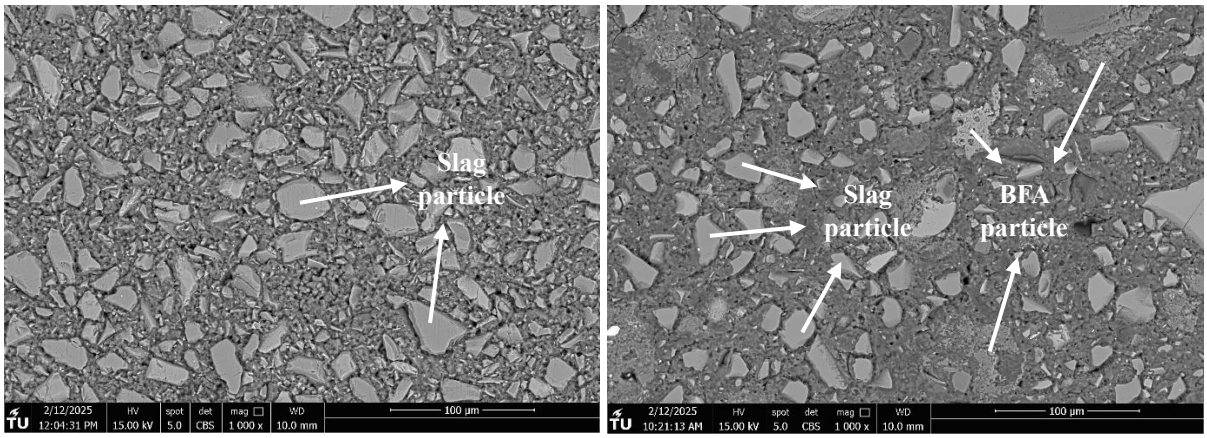

Figure 6.7: SEM images of slag-only paste (left) and paste incorporating 25% BFA1 (right), showing the difference in particle distribution and matrix homogeneity at 1000× magnification.

Figure 6.8 presents a SEM image taken at 500× magnification. This image shows a large BFA particle embedded in the alkali-activated matrix. A clear interfacial gap between the BFA particle and the surrounding binder matrix can be seen. This indicates a possible weak bond at the interface between the BFA particle and the matrix. Furthermore, internal cracking is visible inside the BFA particle itself. These microstructural imperfections might negatively affect the mechanical integrity of the paste, which causes a reduction in mechanical properties for the system including BFA.

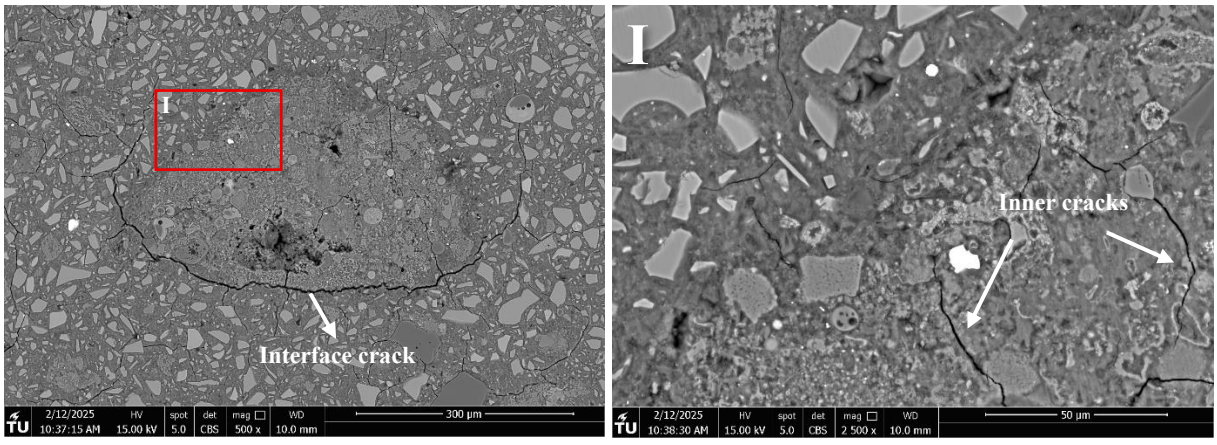

Figure 6.8 : SEM micrographs showing interface and inner cracking within a BFA-containing alkali-activated paste. The left image highlights an interface crack between the particle and surrounding matrix, while the magnified region I on the right shows internal microcracks within the BFA particle.

Elemental spot analysis

In order to determine the chemical composition of the reaction products in the alkali-activated pastes, SEM-EDX spot analysis of three different regions was performed, as presented in Figure 6.9. The analysis focused on:

- BFA-Inner: Points located inside biomass fly ash (BFA) particles to examine the reaction products formed internally after alkali activation.
- BFA-Outer: Points located in the binder matrix surrounding the BFA and slag particles, to analyse the gels formed here.
- REF-Outer: Points were selected from the binder matrix between slag particles to analyse the gel composition in the absence of BFA.

In each region, 100 random spots, at a magnification of 1000x, were analysed at a curing age of 28 days, excluding unreacted precursor particles. The elemental compositions obtained via the SEM-EDX test were normalized to CaO-SiO_2-Al_2O_3 (oxide basis) and plotted in a ternary diagram, shown in Figure 6.10.

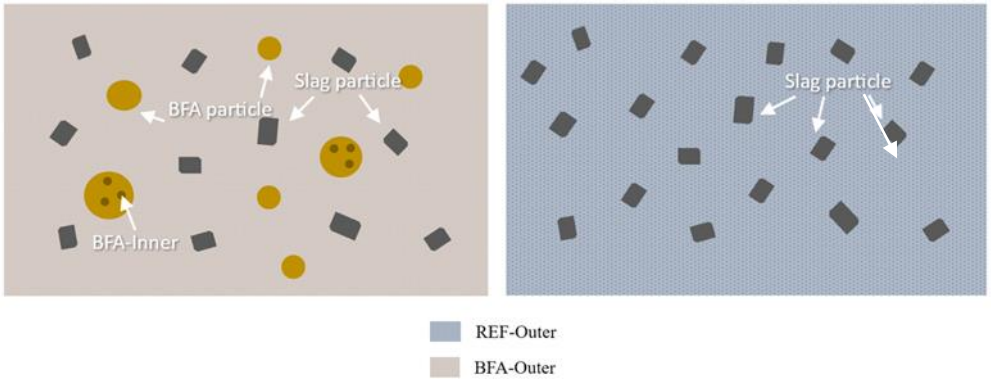

Figure 6.9: Illustration of SEM-EDX spot analysis points. The left image represents the sample containing biomass fly ash (BFA), while the right image shows the reference sample made with slag only. In the BFA sample, points labelled BFA-inner are located inside BFA particles to examine internal reaction products, while BFA-outer points are in the surrounding gel matrix. In the reference sample, REF-outer points are placed in the matrix between slag particles to analyse the binder composition in the absence of BFA.

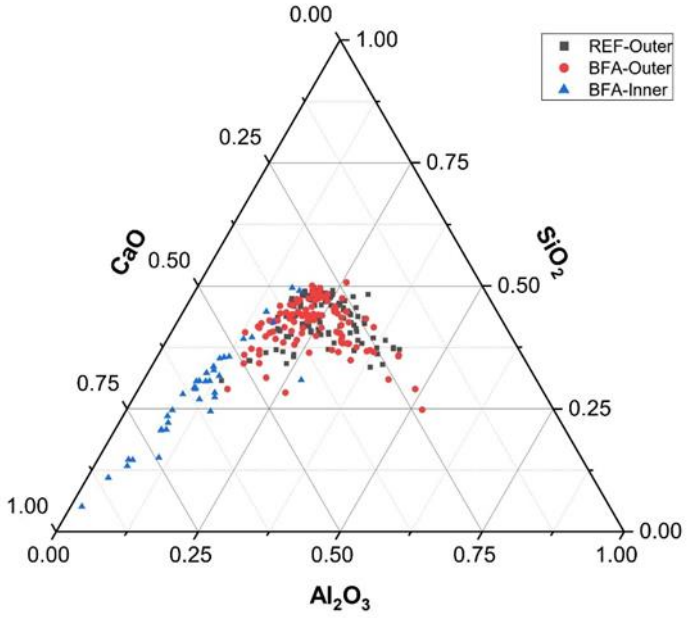

Figure 6.10: Ternary plot of CaO–SiO_2–Al_2O_3 atomic ratios in reaction products of REF-Outer, BFA-Outer, and BFA-25-Inner samples based on SEM-EDX analysis.

The reaction gel formed in the reacted regions of both the REF-Outer and BFA-Outer falls within the compositional domain typically associated with C–A–S–H gels [137]. [138]. [139]. [140], as shown in the ternary diagram, Figure 6.10. Notably, the overall gel chemistry remains relatively consistent following the incorporation of BFA as a partial slag replacement. The BFA-Inner points are scattered more towards a higher content of CaO. This is mainly due to the higher concentration of calcium carbonate in the BFA.

Other types of gel phases, such as N–A–S–H gels, which are typically observed in low-calcium alkali-activated fly ash systems, were not detected in either sample. This absence is probably due to the dominant presence of calcium in the precursor materials, whether in the form of slag or BFA. Although the alkaline activator provides a rich supply of sodium, the chemical situation is still not favourable for N–A–S–H gel stability. García-Lodeiro et al [133], that highly alkaline conditions (pH > 12) favour the exchange of calcium and sodium ions in solid phases, promoting C–A–S–H gel formation and destabilising N–A–S–H structures. Therefore, the system favours C–A–S–H gel formation, driven by the high calcium availability introduced through BFA incorporation.

A noticeable shift is observed in the Ca/Si ratio, Table 6.4 and Figure 6.11. To make the results more representative, the average value of the 25th to 75th percentile range of all the points is measured. The REF sample exhibits a median Ca/Si value of 1.07, while the BFA-containing mix displays a higher Ca/Si median ratio of 1.18. Although the BFA incorporated sample is slightly higher, it still falls within the same range as the REF sample. The measured calcium content in the BFA incorporated sample is overestimated since EDX analysis measures the total elemental concentrations and cannot distinguish between calcium incorporated into reaction products and calcium found in carbonate phases. As a consequence, the Ca/Si ratio measured from the EDX analysis cannot accurately reflect the true binder gel composition.

Table 6.4: Atomic ratios of the elements in the matrix.

	REF-Outer (Average)	REF-Outer (Std)	BFA-Outer (Average)	BFA-Outer (Std)	BFA-Inner (Average)	BFA-Inner (Std in)
Ca/Si	1.07	0.11	1.18	0.10	3.09	0.56

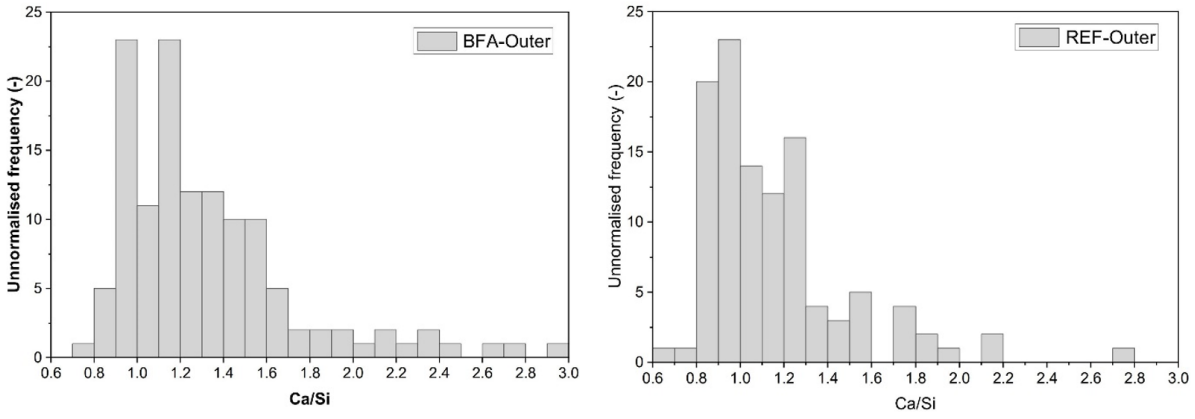

Figure 6.11: Histogram of the SEM-EDS points showing the Ca/Si distribution in the REF-Outer and BFA-Outer samples.

Line scans of individual slag and biomass fly ash (BFA) particles embedded within the alkali-activated paste matrix were conducted using energy-dispersive X-ray spectroscopy (EDX) to determine the distribution of elemental composition across selected regions, Figure 6.12. The EDX line scan performed on a BFA particle revealed distinct peaks in calcium concentration at specific locations along the line. These calcium peaks consistently coincided with local reductions in both silicon and aluminium, indicating the presence of Ca-rich, aluminosilicate-poor phases. This elemental distribution is characteristic of calcium carbonate ($CaCO_3$) formations rather than conventional alkali-activated reaction products such as C–A–S–H gels. These results indicate that most of the ash is composed of stable $CaCO_3$ phases, which occupy a major fraction of the BFA particle. In contrast, the line scan of the slag particle exhibited a consistent elemental composition across the tested section.

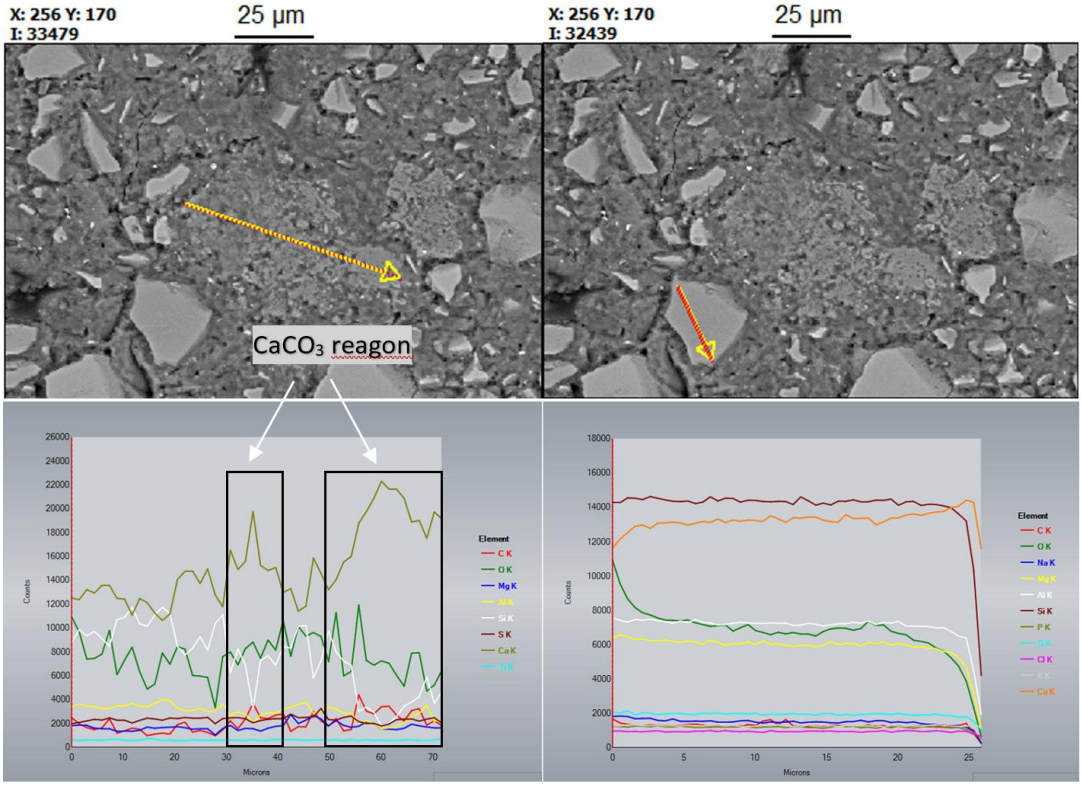

Figure 6.12: Line scan profiles obtained from SEM-EDX analysis of individual slag (right) and biomass fly ash (BFA) (left) particles.

7

7 Life cycle assessment of biomass fly ash in concrete production

7.1 Introduction to life cycle assessment

This study aims to measure the environmental impact of concrete mix designs containing BFA. The LCA is used in accordance with the ISO 14040 [137]. In the Netherlands, the Environmental Cost Indicator (ECI) is commonly used as a standardized method to quantify the total environmental cost of a product or process. It is a method based on the SBK method, measuring environmental performance through a total of 11 impact categories. These are given in unit equivalents (UE) and in terms of related shadow costs in euros/UE. Table 7.1 gives an overview of the considered environmental impact categories.

Table 7.1: Environmental impact categories whit their associated shadow costs.

Impact category:	**Abbreviation:**	**equivalent Unit:**	**Shadow costs per UE in Euro:**
Abiotic depletion non-fuel	ADP-non fuel	kg Antimone	0.16
Abiotic depletion fuel	ADP-fuel	kg Antimone (4.81E-4 kg antimone/MJ)	0.16
Global warming	GWP100	kg CO2	0.05
Ozone layer depletion	ODP	kg CFC-11	30
Photochemical oxidation	POCP	kg Ethene	2
Acidification	AP	kg SO2	4
Eutrophication	EP	kg PO43-	9
Human toxicity	HTP	kg 1.4-dichloro benzene	0.09
Fresh water aquatic ecotoxicity	FAETP	kg 1.4-dichloro benzene	0.03
Marine aquatic ecotoxicity	MAETP	kg 1.4-dichloro benzene	0.0001
Terrestrial ecotoxicity	TAETP	kg 1.4-dichloro benzene	0.06

7.2 Goal and Scope of the LCA

The goal of this LCA is to quantify the carbon footprint of concrete incorporating biomass fly ash at various replacement levels. Although the LCA covers all 11 impact categories, the primary emphasis lies on global warming potential (GWP) due to its direct correlation with CO_2 emissions. This research aims to determine whether adding BFA1 into concrete can effectively minimize the carbon footprint and whether a huge carbon emission reduction is possible. The life cycle study can also indicate the most critical components of the mix design in impacting the environment.

The functional unit is defined as 1 cubic meter (m^3) of concrete with the same compressive strength class (C30/37 at 28 days). The assessment follows a cradle-to-gate approach. focusing on the product stage (A1-A3). This includes [135]:

- A1: Raw material extraction and processing.
- A2: Transportation of raw materials to the manufacturing site.
- A3: Manufacturing of the concrete mix.

The LCA excludes the construction process (A4-A5), the use phase (B1-B7), and the end-of-life stage (C1-C4), Figure 7.1. The environmental impact during the operational phase, such as energy consumption for heating or cooling, is beyond the scope of this study.

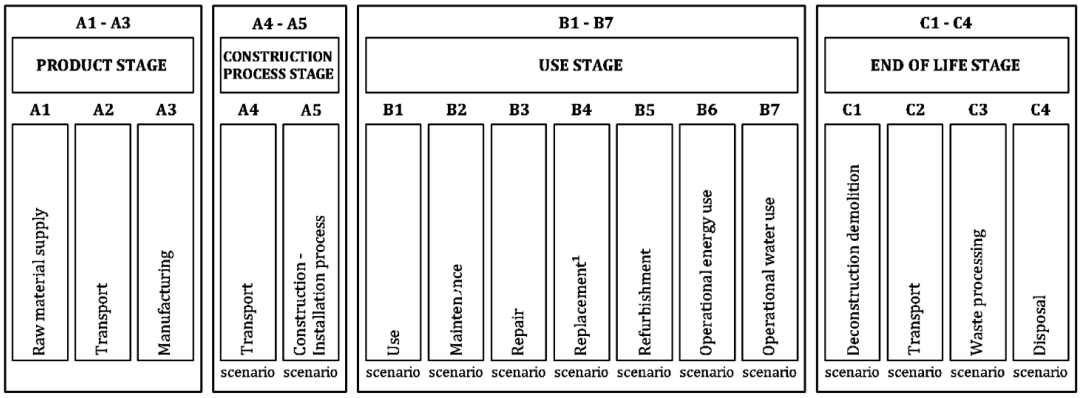

Figure 7.1 Life cycle stages of a construction product as defined in EN 15804. encompassing the product stage (A1–A3). construction process stage (A4–A5), use stage (B1–B7). and end-of-life stage (C1–C4) [135].

7.3 Life cycle inventory

All material data used in this study is taken from the NIBE database [136]. The materials include ground granulated blast furnace slag (GGBFS), sodium hydroxide (50% wt% solid), water glass solution (48% wt% solid), river sand and gravel. For biomass fly ash (BFA1), the inventory data is derived from an MRPI report specifically covering fly ash production. It is important to note that the sodium hydroxide and sodium silicate data from the NIBE database reflect only the solid content of the solutions. For accuracy, the active content is considered by adjusting the values accordingly. For instance, sodium hydroxide (50%) is calculated at half the listed values to account for the actual solid component, and the same adjustment is applied to the water glass solution (48%). The mix design for the concrete samples varies based on the replacement level of BFA1 for slag, while all other materials remain constant, Table 7.2. This approach allows for a direct comparison of environmental impacts across different replacement levels.

Table 7.2: Mix design compositions of alkali-activated concretes incorporating varying amounts of BFA1 used for the Life Cycle Assessment study.

Composition	AAC-REF	AAC-15	AAC-25	AAC-35
Blast furnace slag	400.0	340.0	300.0	260.0
BFA1	0.0	60.0	100.0	140.0
Water	143.9	143.9	143.9	143.9
NAOH (50%)	37.3	37.3	37.3	37.3
PQ waterglass	30.8	30.8	30.8	30.8
Gravel (4-16mm)	1021.7	1021.7	1021.7	1021.7
Sand(0-4mm)	712.5	712.5	712.5	712.5

7.4 Results and discussion

The Environmental Cost Indicator (ECI) reflects the total environmental cost expressed in monetary terms. The shadow cost from the Life Cycle Assessment (LCA) study is presented in Table 7.3. This table demonstrates that the addition of biomass fly ash (BFA) to the concrete mix design can indeed reduce the total environmental cost of the produced sample. This reduction is quantified in monetary terms per cubic meter of concrete produced. As shown in the table, while there is a reduction, it is not particularly significant, given that slag-based geopolymer concrete is already an environmentally favourable material compared to Portland cement concrete.

Table 7.3: Environmental Cost Indicator (ECI) values representing the shadow costs (€) of the alkali-activated concrete mixtures incorporating different proportions of BFA1.

Mixture	ECI (€)
AAC-REF	7.84
AAC-BFA-15	7.33
AAC-BFA-25	7.00
AAC-BFA-35	6.66

Figure 7.2 shows the contribution per impact category. The major contributors to the environmental cost are Global Warming Potential (GWP), Acidification Potential (AP), and Human Toxicity (HT). The other impact categories, such as Eutrophication Potential (EP) and Ozone Depletion Potential (ODP) show much smaller contributions, indicating that the environmental impact from these aspects is limited and does not constitute a significant risk.

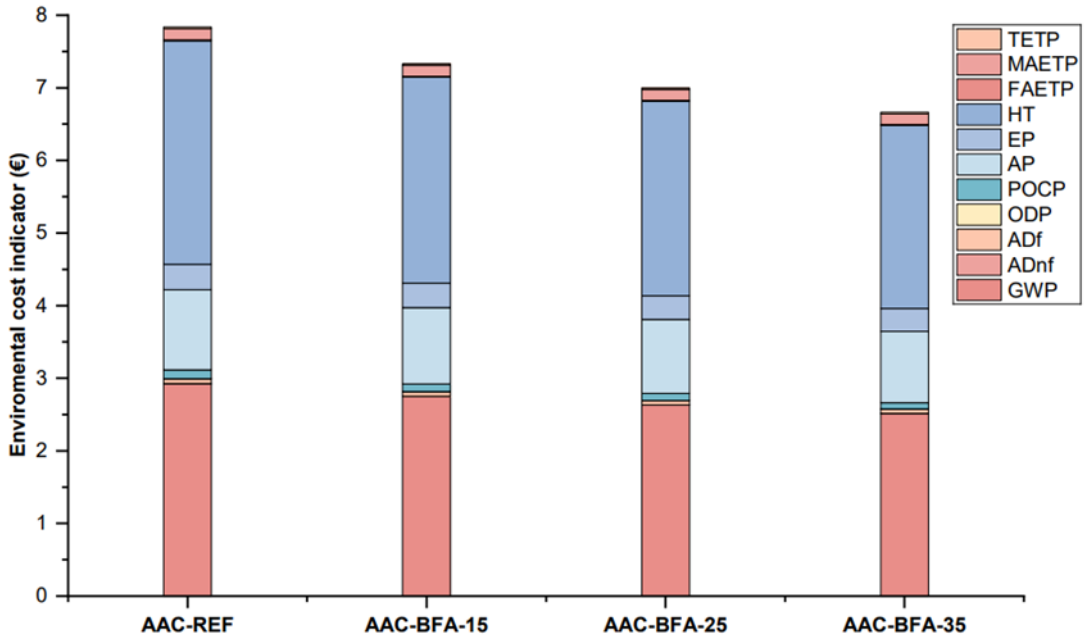

Figure 7.2: Environmental cost indicator (ECI) for the various concrete mixtures. illustrating the individual contributions of different impact categories to the total environmental cost.

In Figure 7.3, we see the contribution of every material to the environmental footprint of the mix design. Interestingly, the activator, which is a combination of sodium hydroxide and sodium silicate, contributes most to it [137]. This is due to the extensive amount of energy consumed in the manufacturing process and the energy-intensive raw material extraction, which has a great amount of environmental impact.

Following the activator, slag also has a considerable environmental impact. Its production and subsequent processes, such as drying and grinding, are energy-intensive and contribute to CO2 emissions [144] [145]. In contrast, aggregates and sand contribute significantly less to the environmental impact, despite their abundance in the mix. This reduced impact is due to their lower energy-consuming extraction processes, which also do not involve chemical processes. Finally, biomass fly ash seems to have the minimal effect among all the materials.

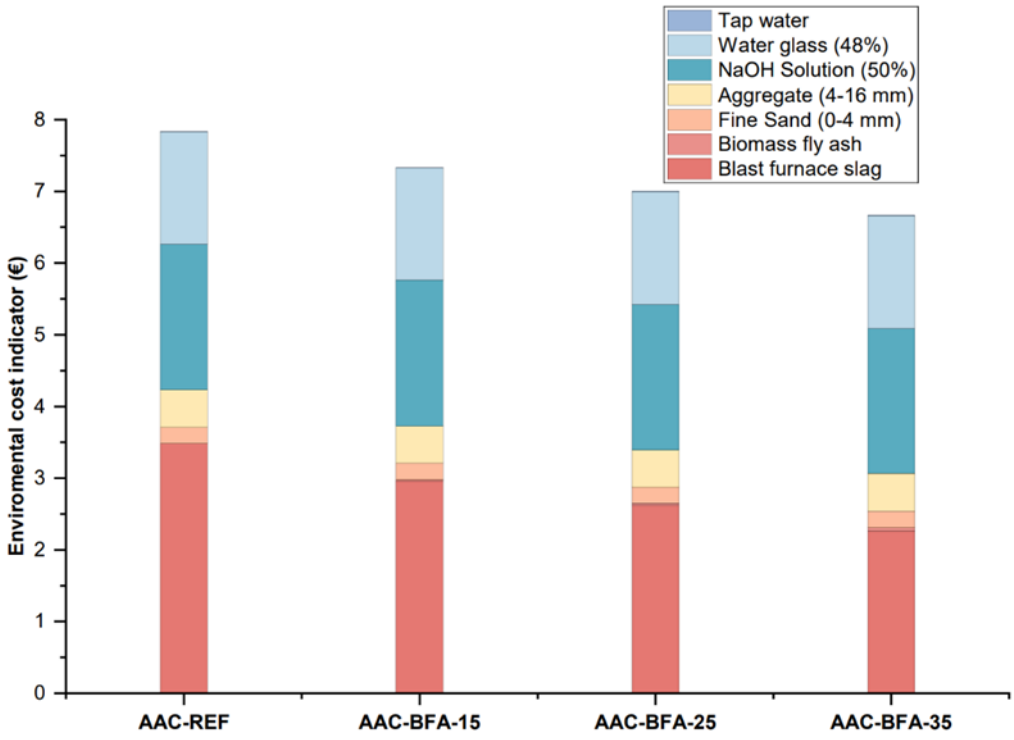

Figure 7.3: Environmental cost indicator for the various concrete mixes. highlighting the contribution of each ingredient in the mix design to the total environmental cost.

Carbon emission

The amount of absorbed carbon is calculated based on the impact category global warming potential (GWP) as this category is equivalent to the amount of emitted carbon dioxide in kg. The equivalent emitted carbon in kg by the various components in concrete is shown in Table 7.4:

Table 7.4: Carbon emission in kg/ton as derived from the GWP impact category for each ingredient in the mix design

Component	Carbon emission (kg/ton)
Blast furnace slag	61.80
Coal fly ash	3.26
Fine Sand (0-4 mm)	2.41
Aggregate (4-16 mm)	3.88
NaOH Solution (50%. only active content)	872.98
Water glass (48%. only active content)	795.78
Tap water	0.34

By using the inventory data presented in Table 7.4, the carbon footprint for each mixture is calculated with the following equation [140]:

$$C = \sum_{i=1}^{n} c_i \cdot r_i$$

In this equation, C represents the carbon footprint of the mixture. The variable c_i denotes the unit carbon emissions associated with each component i (where i ranges from 1 to 7, as detailed in Table 7.4 and r_i refers to the mass of component i as specified in Table 7.2.

Figure 7.4 shows the carbon emissions (in kg CO_2 equivalent) associated with each component of the concrete mix designs. The data shows that the primary reduction in carbon emissions results from the partial replacement of slag with BFA. Since BFA has a significantly lower carbon footprint compared to slag, this substitution is the main contributor to the observed reduction in global warming potential. The carbon contributions of the other mix components, such as the alkaline activator, aggregates, water, and fine sand, remain constant across all mixes, as their proportions were not changed during the substitution process. Thus, the environmental benefit is directly linked to the use of BFA in place of slag.

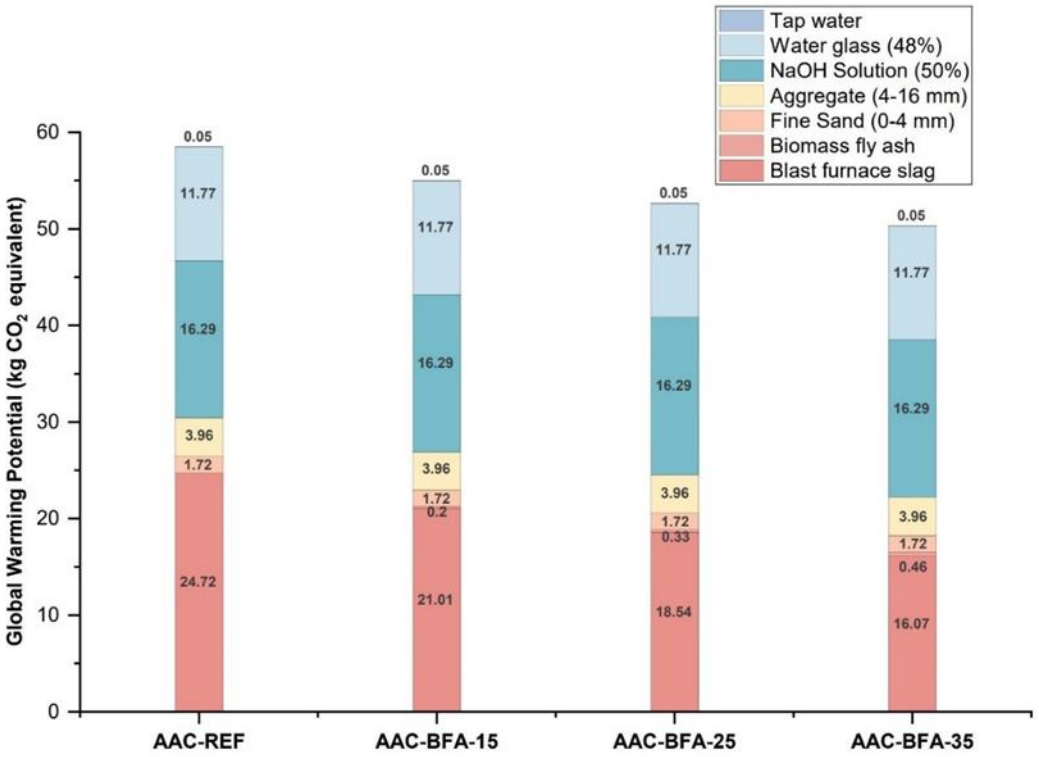

Figure 7.4 : Carbon emission in kg for the various ingredients in the mix design.

Net emission calculations

Table 7.5 summarizes the CO_2 emissions of alkali-activated concrete mixtures using BFA. The total CO_2 emission is estimated for the production of one m^3 of concrete. As indicated from Table 7.5, using carbonated biomass fly ash (BFA1) in alkali-activated mixtures results in a substantial decrease in CO_2 emissions. Mixes AAC-BFA-15 and AAC-BFA-25 not only achieved compressive strengths that meet the requirements of the C30/35 strength class, but also reduced total CO_2 emissions by 12.77% and 21.28%, respectively, when compared to the reference mix (AAC-REF). This shows that carbonated BFA is an effective low-carbon binder that maintains structural performance. Although AAC-BFA-35 did not meet the target compressive strength, it achieved the highest emission reduction of 29.80%, suggesting that higher BFA replacement levels offer considerable environmental advantages. This mix may be suitable for non-structural or low-load-bearing applications.

Table 7.5: Results of the accelerated carbonation only, presenting CO2 emissions, sequestrated CO2 ,net CO2, and the corresponding reduction percentage for each concrete mix design.

Mix Design	CO_2 Emissions (kg/m^2)	Sequestrated CO_2 (kg)	Net CO_2 (kg)	Reduction (%)
AAC-REF	58.51	0	58.52	0
AAC-BFA-15	55.00	3.96	51.05	12.77
AAC-BFA-25	52.66	6.60	46.06	21.28
AAC-BFA-35	50.32	9.24	41.08	29.80

These results show a substantial decrease in carbon emissions through the use of carbonated BFA in the concrete mixture. Future research should investigate the potential of using alternative ashes with greater carbon sequestration capacity and adequate reactivity in obtaining the necessary compressive strength with increased levels of BFA. This is a challenge in particular. High-calcium ashes will absorb more CO_2 based on the presence of calcium-rich phases. however, these ashes are less reactive since they have reduced amounts of reactive alumina and silica, both of which are needed for higher reactivity in alkali-activated systems.

For industrial application of mineral CO_2 sequestration, consideration needs to be given to the energy consumption of the carbonation processes. The most substantial contributor in this regard is the consumption of electricity to conduct accelerated carbonation. The Global Warming Potential (GWP) of electricity is usually between 0.34 and 0.95 kg CO_2 equivalent per kWh, averaging about 0.5 kg CO_2 eq./kWh [141]. Actual power consumption is a function of carbonation time, temperature, pressure, and design of the carbonation setup. Existing studies indicate that, despite CO_2 uptake in carbonation, the net environmental advantage can be negative. In one study, for instance, carbonation of slag resulted in carbon uptake of 0.09 kg CO_2/kg, whereas the corresponding emissions from the consumption of electricity was equal to 0.208 kg CO_2 eq./kg [143]. This points out that although carbonation has potential for carbon capture, its energy consumption has to be addressed carefully to achieve true environmental benefits.

8

8 Conclusion and recommendations

CHARACTERIZATION OF BIOMASS FLY ASHES

The chemical and mineralogical characterization of the raw biomass fly ash samples BFA1, BFA2, BFA3, and WA4 showed their suitability for CO_2 sequestration. The availability of reactive calcium-bearing phases, particularly free lime (CaO) and portlandite are the main factors determining their carbonation potential. Although magnesium-bearing compounds could also be involved in the carbonation process. The limited presence of these compounds in the examined ashes led to them not being considered in the selection process.

XRF results showed that BFA1 and WA4 had the highest levels of CaO at 51.12% and 46.81%, respectively. Although this content is significant, this Figure by itself proved insufficient to predict the overall carbonation efficiency. A significant portion of the CaO in these samples was found in calcite ($CaCO_3$), indicating partial pre-carbonation had already taken place. This naturally pre-carbonated situation reduced the sequestration capacity of the ashes. Further XRF investigation of BFA2 and BFA3 revealed a total CaO content of 27.26% and 18.25%, respectively. This lower calcium availability showed more limited potential for carbonation in these ashes. XRD Phase analysis of BFA3 revealed further that its CaO content is entirely found within non-reactive phases, such as anhydrite or already carbonated phases as calcite, clearly showing its unsuitability for CO_2 sequestration.

Free lime quantification further clarified these findings. BFA1 had the highest content 5.61%, while BFA2 and WA4 showed values of 1.43% and 1.01%, respectively. Despite WA4's high total CaO, its low free lime content, due to a high calcite fraction, confirmed its limited sequestration potential. BFA1, in contrast, combined a high reactive CaO phase content with minimal pre-carbonation, confirming it as the most promising candidate for CO_2 capture among the samples tested.

The carbonation treatment of BFA1 under gas-solid and aqueous conditions showed differences in reactivity. Gas-solid carbonation of BFA1 was slow, and the lime was still present after two months of carbonation. This result highlighted the kinetic limitations of this method. On the other hand, the wet carbonation (L/S 0.3) achieved full lime conversion in just eight hours, indicating a more efficient reaction mechanism. TGA analysis showed that the $CaCO_3$ content in BFA1 increased from 20.15% in raw BFA1 to 35.11% in the carbonated BFA1.

REACTIVITY OF BIOMASS FLY ASH AFTER TREATMENT

The mechanical performance and durability of alkali-activated BFA containing concrete were highly affected by the replacement levels of the ash and were correlated with the underlying microstructural changes. The C30/37 compressive strength requirement was reached at a replacement level of 25%. Further BFA content increase led to a decline in strength with mix designs above a replacement level of 25% not satisfying the threshold compressive strength. Tensile strength also declines with an increase in BFA replacement level. The freeze-thaw resistance of the concretes containing BFA was severely undermined when compared to the reference mix.

The deterioration in mechanical and durability properties is related to the decreased reactivity of treated (water treatment and carbonation treatment) BFA and the detrimental effect of its addition on the microstructure. The introduction of BFA added more heterogeneity in the matrix and promoted the development of internal micro-cracks. These microscopic discontinuities compromised the cohesiveness of the matrix and its strength and resistance to environmental degradation mechanisms. The SEM analysis supported these findings. The reference mix exhibited a compact and homogeneous matrix containing well-distributed slag particles. However, the mix containing 25% BFA1 showed a more irregular structure with evident microstructural defects, which negatively influenced the properties on the concrete level.

The reactivity of the treated biomass fly ash (BFA1) is another factor in the reduced mechanical integrity of the concrete samples. In this study, the effect of different pre-treatment methods, namely water treatment, accelerated carbonation treatment, and their combination, on the reactivity of BFA was investigated using a combination of quantitative X-ray diffraction (QXRD), elemental dissolution via ICP-OES, Fourier-transform infrared spectroscopy (FTIR), and isothermal calorimetry. These techniques provided a comprehensive understanding of how physical and chemical transformations influence the behaviour of the ash in reactive environments.

The amorphous phase in fly ash is widely recognized as the reactive fraction responsible for participating in the formation of reaction products in alkali-activated systems. Quantitative XRD analysis indicated that raw ash (BFA-RAW) contained an amorphous component of 42.3%, which is marginally increased to 44.6% after treatment with water (BFA-H). Conversely, carbonated samples (BFA-C and BFA-H-C) displayed a decline in the proportion of the amorphous component to about 40%. The decline is a result of the formation of crystalline carbonate phases, mainly $CaCO_3$, during carbonation.

Dissolution of the major alkali activation elements (Ca, Si, Al and Mg) was quantified by ICP-OES. The maximum dissolution values were found for the raw (BFA-RAW) and water-treated ashes (BFA-H), indicating higher reactivity. This enhanced dissolution is reached due to the finer size distribution of these samples, increasing the surface area and facilitating greater contact between ash particles and the alkaline solution. In contrast, carbonated ashes (BFA-C and BFA-H-C) showed lower dissolution rates in particular for Si and Al. This reduction is mainly due to two main factors: the increase in particle size after carbonation treatment and the formation of a carbonated layer on the ash particles, which limits the dissolution of these elements. A notable exception to the general trend was observed with calcium, which showed slightly increased solubility after carbonation treatment. This increase in solubility can be explained by the fact that during carbonation, most of the carbonates fall within the crystalline phase, however, some of the formation of amorphous or poorly crystalline $CaCO_3$ can take place, as confirmed by TGA and FTIR analysis. These carbonates have a less ordered molecular structure and therefore show higher solubility.

Isothermal calorimetry was used to determine the heat released related to the alkali activation reaction of paste samples containing BFA. The raw BFA paste (BFA-RAW) revealed a cumulative heat released at 130.9 J/g, greater than the reference paste (128.5 J/g). A portion of this heat release was attributed to the reaction of metallic aluminium present in the raw ash, which can produce hydrogen gas and additional heat. However, calculation based on thermodynamics showed that the present metallic aluminium in the ash contributed only for 2.2 J/g. The cumulative heat release of the BFA-RAW sample without metallic aluminium was 128.7 J/g, which was equal to the reference sample. This shows that raw BFA has a high chemical reactivity. This reactivity is due to the smaller particle size of the ash and the higher solubility of elements.

The water-treated (BFA-H) and carbonated (BFA-C and BFA-H-C) samples exhibited lower cumulative heat release at 103.4 J/g for BFA-H, 104.4 J/g for BFA-C and 118.5 J/g for BFA-H-C. This is attributed to the reduced reactivity due to the formation of reaction products of these ashes during pretreatments, as have been shown in the FTIR analysis. FTIR analysis revealed changes in the ash following treatment. As the water-treated BFA-H sample showed a peak at 958 cm^{-1} , which indicates the early formation of reaction products, initiated by the alkaline environment created during the treatment. A similar finding was also observed in the carbonated samples at peak 1040 cm^{-1}, which was also linked to reaction products formation. These reaction products make the ash less reactive during the alkali activation in paste and concrete samples as these reactions consume elements needed for alkali activation.

In the carbonated samples (BFA-C and BFA-H-C), the decline in total reactivity is also attributed to the creation of carbonation products, notably calcite. Calcite is a thermodynamically stable mineral, and under alkaline conditions, is chemically inert and will not engage in additional geopolymerization reactions. While the core concept of carbon sequestration relies on this stability, by ensuring that captured CO_2 is permanently stored within the concrete matrix in the form of calcite, the downside is that this process also compromises the reactive fraction of the ash. TGA results demonstrated that up to 36% of the ash mass in carbonated samples consists of calcite, which no longer contributes to binder formation.

However, a more nuanced interpretation is necessary. The initial calcite concentration in the raw ash (BFA-RAW) was around 20%, yet this sample showed a notably greater cumulative heat release than the reference sample. This indicates that despite a high concentration of calcite presence, a substantial portion of the ash remained chemically active and capable of contributing to the alkali activation process. While carbonation itself reduces the reactivity potential of BFA, the true reduction in reactivity occurs from the early formation of reaction product, which absorbs the reactive alumina and silica elements. The proof for this statement is that the concentration of calcite in both the BFA-RAW and BFA-H is around 20%. However, BFA-RAW is far more reactive due to the preservation of its reactive elements, like silica and alumina.

HEAVY METAL AND METALLIC ALUMINIUM CONTENT

Both carbonation and water treatment efficiently reduced levels of the heavy metals below the Dutch Soil Quality Limit (SQL). Although the initial concentration of most of these elements (Ba, Ca, Cr, Cu, Ni, and Zn) were below threshold levels. However, Pb concentration was above the allowed limit in the Raw BFA1 ash. All the measured heavy metals, including Pb were successfully reduced to acceptable levels following both treatments.

Furthermore, combining carbonation with water treatment removed metallic aluminium in its entirety. This is an important result, as it prevents the formation of hydrogen gas during of alkali activation and as a consequence reduces the mechanical degradation of the produced concrete.

ENVIRONMENTAL IMPACT AND CO_2 EMISSIONS

The life cycle study conducted in this research verifies that the use of carbonated BFA at a replacement level of 25% leads to a substantial reduction of alkali-activated concrete carbon footprint. In the reference mix, containing only ground granulated blast furnace slag as a binder, the CO_2 emissions were equal to 58.51 kg CO_2/m^2 of concrete. After substitution of a portion of the slag binder by 25% of carbonated BFA, the emissions were brought down to 46.06 kg CO_2/m^2. This constitutes to a reduction of 21.28% of carbon emission, which is a direct consequence of the carbonation pretreatment.

Importantly, the incorporation of the 25% BFA did not compromise the compressive strength the concrete, meeting the C30/37 class requirements. This confirms the suitability for structural applications. However, when lower strength class is not a problem, for example in non-structural or low-strength applications, a higher replacement level of up to 35% can be considered. In this cases, the total carbon emission can be further reduced by as much as 29.8%.

A detailed analysis of the emission sources in the mix indicates that the most dominant contributor to the total emissions is the alkali activator, responsible for about 48% of the total CO_2 produced. Notably, this is despite the fact that the activator is in mass a relatively small portion of the mix, showing a high emission intensity. Following this is the slag itself, which accounts for about 42% of total emissions. These two components dominate the environmental impact of alkali-activated systems, highlighting the need for low-carbon activators and binder alternatives to be developed.

In conclusion, the results of this research establish the feasibility of using pretreated biomass fly ash as a replacement for a portion of the slag binder. In addition to having carbon permanently embodied in concrete, the mechanical performance is still sustained. This represents a realistic option for further reduction of the carbon footprint in alkali-activated concrete.

RECOMMENDATIONS

The findings of this study highlight several critical aspects that should guide future research and development concerning the use of carbonated biomass fly ash as a partial binder in alkali-activated materials. The effects of pre-treatment on both material reactivity and environmental behaviour of the ash need to be further researched. Despite the highest reactivity of raw BFA in this research, its direct use in concrete is challenged by the presence of metallic aluminium and the possibility of heavy metals leaching, both of which are detrimental to concrete durability and environmental safety. These points need to be addressed through specific treatments that reduce the risks they pose while not reducing the contribution of the ash towards gel formation significantly. A major implication of this work is that pretreatment techniques involving moisture, including wet carbonation for CO_2 water-treatment for removal of metallic aluminium, are critical in reducing reactivity from the ash. Future studies, therefore, need to investigate alternative approaches that minimize or completely avoid prior exposure of the ash to water, since early hydration may initiate undesirable initial reactions. The technique of pretreatment needs to be optimized to conserve the ash's reactive and amorphous phases, while still delivering the benefits such as immobilization of heavy metals and neutralization of metallic aluminium.

Besides, another factor responsible for the reduction in reactivity after the treatments is the increase in particle size. Grinding, a mechanical activation process, can reverse this development by increasing reactivity and facilitating a greater replacement rate. It is, however, an energy-requiring process and involves extra CO_2 emissions, which have the potential to negate the environmental gain during carbonation. There is a need for a systematic study of the grinding time that will equate enhanced reactivity and replacement rate with overall carbon production. Such a balance would facilitate greater ash utilization while keeping the mechanical strength intact, marking a substantial advancement in sustainable concrete design.

It is also important to mention that most studies on the carbonation of fly ash have considered mainly application as carbon capture and stabilization of heavy metals, and not the effect of using carbonated ashes in binder systems. There is still a gap in knowledge on how to include carbonated ashes in AAC systems without compromising their mechanical performance.

Finally, as in most alkali-activated systems, the major contributor to environmental impact is still the alkali activator. Future studies should focus on the design of low-carbon, high-efficiency activators with lower emissions. Sustainable activator development still offers considerable room for innovation.

References

[1] F. Winnefeld, A. Leemann, A. German, and B. Lothenbach, "CO2 storage in cement and concrete by mineral carbonation," *Curr Opin Green Sustain Chem*, vol. 38, p. 100672, Dec. 2022, doi: 10.1016/J.COGSC.2022.100672.

[2] J. H. A. Rocha, R. D. Toledo Filho, and N. G. Cayo-Chileno, "Sustainable alternatives to CO2 reduction in the cement industry: A short review," *Mater Today Proc*, vol. 57, pp. 436–439, Jan. 2022, doi: 10.1016/J.MATPR.2021.12.565.

[3] E. Gartner and H. Hirao, "A review of alternative approaches to the reduction of CO2 emissions associated with the manufacture of the binder phase in concrete," *Cem Concr Res*, vol. 78, pp. 126–142, Dec. 2015, doi: 10.1016/J.CEMCONRES.2015.04.012.

[4] E. Aprianti S, "A huge number of artificial waste material can be supplementary cementitious material (SCM) for concrete production – a review part II," *J Clean Prod*, vol. 142, pp. 4178–4194, Jan. 2017, doi: 10.1016/J.JCLEPRO.2015.12.115.

[5] J. Hubert, S. Grigoletto, F. Michel, Z. Zhao, and L. Courard, "Development and Properties of Recycled Biomass Fly Ashes Modified Mortars," *Recycling 2024, Vol. 9, Page 46*, vol. 9, no. 3, p. 46, May 2024, doi: 10.3390/RECYCLING9030046.

[6] K. D. Hannam, L. Venier, E. Hope, D. McKenney, D. Allen, and P. W. Hazlett, "AshNet: Facilitating the use of wood ash as a forest soil amendment in Canada," *Forestry Chronicle*, vol. 93, no. 1, pp. 17–20, Jan. 2017, doi: 10.5558/TFC2017-006;CTYPE:STRING:JOURNAL.

[7] R. Rajamma, R. J. Ball, L. A. C. Tarelho, G. C. Allen, J. A. Labrincha, and V. M. Ferreira, "Characterisation and use of biomass fly ash in cement-based materials," *J Hazard Mater*, vol. 172, no. 2–3, pp. 1049–1060, Dec. 2009, doi: 10.1016/J.JHAZMAT.2009.07.109.

[8] X. Liang, Z. Li, H. Dong, and G. Ye, "A review on the characteristics of wood biomass fly ash and their influences on the valorization in cementitious materials," 2024, doi: 10.1016/j.jobe.2024.110927.

[9] R. Siddique, "Utilization of wood ash in concrete manufacturing," *Resour Conserv Recycl*, vol. 67, pp. 27–33, Oct. 2012, doi: 10.1016/J.RESCONREC.2012.07.004.

[10] O. J. Olatoyan, M. A. Kareem, A. U. Adebanjo, S. O. A. Olawale, and K. T. Alao, "Potential use of biomass ash as a sustainable alternative for fly ash in concrete production: A review," *Hybrid Advances*, vol. 4, p. 100076, Dec. 2023, doi: 10.1016/J.HYBADV.2023.100076.

[11] A. Kicí Nska, G. Caba, E. Arato, and C. Vlachokostas, "Leaching of Chlorides, Sulphates, and Phosphates from Ashes Formed as a Result of Burning Conventional Fuels, Alternative Fuels, and Municipal Waste in Household Furnaces," *Energies 2021, Vol. 14, Page 3936*, vol. 14, no. 13, p. 3936, Jun. 2021, doi: 10.3390/EN14133936.

[12] M. Pazalja *et al.*, "Heavy metals content in ashes of wood pellets and the health risk assessment related to their presence in the environment," *Scientific Reports 2021 11:1*, vol. 11, no. 1, pp. 1–9, Sep. 2021, doi: 10.1038/s41598-021-97305-4.

[13] H. Y. Jo, J. H. Kim, Y. J. Lee, M. Lee, and S. J. Choh, "Evaluation of factors affecting mineral carbonation of CO2 using coal fly ash in aqueous solutions under ambient conditions," *Chemical Engineering Journal*, vol. 183, pp. 77–87, Feb. 2012, doi: 10.1016/J.CEJ.2011.12.023.

[14] N. L. Ukwattage, P. G. Ranjith, M. Yellishetty, H. H. Bui, and T. Xu, “A laboratory-scale study of the aqueous mineral carbonation of coal fly ash for CO2 sequestration,” *J Clean Prod*, vol. 103, pp. 665–674, Sep. 2015, doi: 10.1016/J.JCLEPRO.2014.03.005.

[15] Q. Yuan, G. Yang, Y. Zhang, T. Wang, J. Wang, and C. E. Romero, “Supercritical CO2 coupled with mechanical force to enhance carbonation of fly ash and heavy metal solidification,” *Fuel*, vol. 315, p. 123154, May 2022, doi: 10.1016/J.FUEL.2022.123154.

[16] S. V. Vassilev, C. G. Vassileva, and N. L. Petrova, “Mineral Carbonation of Biomass Ashes in Relation to Their CO2Capture and Storage Potential,” *ACS Omega*, vol. 6, no. 22, pp. 14598–14611, Jun. 2021, doi: 10.1021/ACSOMEGA.1C01730/ASSET/IMAGES/LARGE/AO1C01730_0006.JPEG.

[17] F. Agrela, M. Cabrera, M. M. Morales, M. Zamorano, and M. Alshaaer, “Biomass fly ash and biomass bottom ash,” *New Trends in Eco-efficient and Recycled Concrete*, pp. 23–58, Jan. 2019, doi: 10.1016/B978-0-08-102480-5.00002-6.

[18] A. K. James, R. W. Thring, P. M. Rutherford, and S. S. Helle, “Characterization of Biomass Bottom Ash from an Industrial Scale Fixed-Bed Boiler by Fractionation,” *Energy and Environment Research*, vol. 3, no. 2, p. p21, Jul. 2013, doi: 10.5539/EER.V3N2P21.

[19] J. L. Provis, A. Palomo, and C. Shi, “Advances in understanding alkali-activated materials,” *Cem Concr Res*, vol. 78, pp. 110–125, Dec. 2015, doi: 10.1016/J.CEMCONRES.2015.04.013.

[20] L. Stefanini, S. Ghorbani, G. De Schutter, S. Matthys, B. Walkley, and J. L. Provis, “Evaluation of copper slag and stainless steel slag as replacements for blast furnace slag in binary and ternary alkali-activated cements,” *J Mater Sci*, vol. 58, no. 31, pp. 12537–12558, Aug. 2023, doi: 10.1007/S10853-023-08815-7/METRICS.

[21] F. Matalkah, P. Soroushian, S. Ul Abideen, and A. Peyvandi, “Use of non-wood biomass combustion ash in development of alkali-activated concrete,” *Constr Build Mater*, vol. 121, pp. 491–500, Sep. 2016, doi: 10.1016/J.CONBUILDMAT.2016.06.023.

[22] G. Deng *et al.*, “Pozzolanic reactivity of carbonated high-calcium fly ash: A mechanism study,” *Constr Build Mater*, vol. 446, p. 138015, Oct. 2024, doi: 10.1016/J.CONBUILDMAT.2024.138015.

[23] E. E. ; Cwirzen *et al.*, “The Effects of Partial Replacement of Ground Granulated Blast Furnace Slag by Ground Wood Ash on Alkali-Activated Binder Systems,” *Materials 2023, Vol. 16, Page 5347*, vol. 16, no. 15, p. 5347, Jul. 2023, doi: 10.3390/MA16155347.

[24] S. K. Adhikary, T. Luukkonen, M. A. H. Bhuyan, Y. Yu, and P. Perumal, “A method of pretreating incineration ashes containing metallic aluminium using NaOH to mitigate volume expansion under highly alkaline conditions,” *Constr Build Mater*, vol. 450, p. 138639, Nov. 2024, doi: 10.1016/J.CONBUILDMAT.2024.138639.

[25] T. Luukkonen, Y. Yu, S. K. Adhikary, S. Kauppinen, M. Finnilä, and P. Perumal, “Metallic aluminium in municipal solid waste incineration fly ash as a blowing agent for porous alkali-activated granules,” *R Soc Open Sci*, vol. 11, no. 8, Aug. 2024, doi: 10.1098/RSOS.240598.

[26] D. Xuan and C. S. Poon, “Removal of metallic Al and Al/Zn alloys in MSWI bottom ash by alkaline treatment,” *J Hazard Mater*, vol. 344, pp. 73–80, Feb. 2018, doi: 10.1016/J.JHAZMAT.2017.10.002.

[27] B. Chen *et al.*, “Characterization and mechanical removal of metallic aluminum (Al) embedded in weathered municipal solid waste incineration (MSWI) bottom ash for application as

supplementary cementitious material," *Waste Management*, vol. 176, pp. 128–139, Mar. 2024, doi: 10.1016/J.WASMAN.2024.01.031.

[28] N. Saikia, G. Mertens, K. Van Balen, J. Elsen, T. Van Gerven, and C. Vandecasteele, "Pre-treatment of municipal solid waste incineration (MSWI) bottom ash for utilisation in cement mortar," *Constr Build Mater*, vol. 96, pp. 76–85, Oct. 2015, doi: 10.1016/J.CONBUILDMAT.2015.07.185.

[29] A. Nithiya, A. Saffarzadeh, and T. Shimaoka, "Hydrogen gas generation from metal aluminum-water interaction in municipal solid waste incineration (MSWI) bottom ash," *Waste Management*, vol. 73, pp. 342–350, Mar. 2018, doi: 10.1016/J.WASMAN.2017.06.030.

[30] S. Mizutani, S. Sakai, and H. Takatsuki, "Investigation of hydrogen generation from municipal solid waste incineration fly ash," *Journal of Material Cycles and Waste Management 2000 2:1*, vol. 2, no. 1, pp. 16–23, 2000, doi: 10.1007/S10163-999-0016-3.

[31] E. Miao, Y. Du, H. Wang, Z. Xiong, Y. Zhao, and J. Zhang, "Experimental study and kinetics on CO2 mineral sequestration by the direct aqueous carbonation of pepper stalk ash," *Fuel*, vol. 303, p. 121230, Nov. 2021, doi: 10.1016/J.FUEL.2021.121230.

[32] L. Li and M. Wu, "An overview of utilizing CO2 for accelerated carbonation treatment in the concrete industry," *Journal of CO2 Utilization*, vol. 60, p. 102000, Jun. 2022, doi: 10.1016/J.JCOU.2022.102000.

[33] N. L. Ukwattage, P. G. Ranjith, M. Yellishetty, H. H. Bui, and T. Xu, "A laboratory-scale study of the aqueous mineral carbonation of coal fly ash for CO2 sequestration," *J Clean Prod*, vol. 103, pp. 665–674, Sep. 2015, doi: 10.1016/J.JCLEPRO.2014.03.005.

[34] S. Y. Pan, E. E. Chang, and P. C. Chiang, "CO2 Capture by Accelerated Carbonation of Alkaline Wastes: A Review on Its Principles and Applications," *Aerosol and Air Quality Research 2012 12:5*, vol. 12, no. 5, pp. 770–791, Nov. 2024, doi: 10.4209/AAQR.2012.06.0149.

[35] L. Jiang, L. Cheng, Y. Zhang, G. Liu, and J. Sun, "A Review on CO2 Sequestration via Mineralization of Coal Fly Ash," *Energies 2023, Vol. 16, Page 6241*, vol. 16, no. 17, p. 6241, Aug. 2023, doi: 10.3390/EN16176241.

[36] R. R. Tamilselvi Dananjayan, P. Kandasamy, and R. Andimuthu, "Direct mineral carbonation of coal fly ash for CO2 sequestration," *J Clean Prod*, vol. 112, pp. 4173–4182, Jan. 2016, doi: 10.1016/J.JCLEPRO.2015.05.145.

[37] E. R. Bobicki, Q. Liu, Z. Xu, and H. Zeng, "Carbon capture and storage using alkaline industrial wastes," *Prog Energy Combust Sci*, vol. 38, no. 2, pp. 302–320, Apr. 2012, doi: 10.1016/J.PECS.2011.11.002.

[38] S. Eloneva, S. Teir, J. Salminen, C. J. Fogelholm, and R. Zevenhoven, "Fixation of CO2 by carbonating calcium derived from blast furnace slag," *Energy*, vol. 33, no. 9, pp. 1461–1467, Sep. 2008, doi: 10.1016/J.ENERGY.2008.05.003.

[39] F. L. Pundsack and N. J. Somerville, "United States Patent Office RECOVERY OF SILICA, IRON OXDE AND MAG NESUM CARBONATE FROM THE TREATMENT OF SERPENTANE WITH AMMONUM BISULFATE," 1967.

[40] S. Teir, H. Revitzer, S. Eloneva, C. J. Fogelholm, and R. Zevenhoven, "Dissolution of natural serpentinite in mineral and organic acids," *Int J Miner Process*, vol. 83, no. 1–2, pp. 36–46, Jul. 2007, doi: 10.1016/J.MINPRO.2007.04.001.

[41] S. Kodama, T. Nishimoto, N. Yamamoto, K. Yogo, and K. Yamada, “Development of a new pH-swing CO2 mineralization process with a recyclable reaction solution,” *Energy*, vol. 33, no. 5, pp. 776–784, May 2008, doi: 10.1016/J.ENERGY.2008.01.005.

[42] G. Costa, R. Baciocchi, A. Polettini, R. Pomi, C. D. Hills, and P. J. Carey, “Current status and perspectives of accelerated carbonation processes on municipal waste combustion residues,” *Environ Monit Assess*, vol. 135, no. 1–3, pp. 55–75, Dec. 2007, doi: 10.1007/S10661-007-9704-4/METRICS.

[43] S. N. Lekakh, C. H. Rawlins, D. G. C. Robertson, V. L. Richards, and K. D. Peaslee, “Kinetics of aqueous leaching and carbonization of steelmaking slag,” *Metallurgical and Materials Transactions B: Process Metallurgy and Materials Processing Science*, vol. 39, no. 1, pp. 125–134, Jan. 2008, doi: 10.1007/S11663-007-9112-8/METRICS.

[44] N. L. Ukwattage, P. G. Ranjith, and X. Li, “Steel-making slag for mineral sequestration of carbon dioxide by accelerated carbonation,” *Measurement*, vol. 97, pp. 15–22, Feb. 2017, doi: 10.1016/J.MEASUREMENT.2016.10.057.

[45] E. E. Chang, C. H. Chen, Y. H. Chen, S. Y. Pan, and P. C. Chiang, “Performance evaluation for carbonation of steel-making slags in a slurry reactor,” *J Hazard Mater*, vol. 186, no. 1, pp. 558–564, Feb. 2011, doi: 10.1016/J.JHAZMAT.2010.11.038.

[46] W. J. J. Huijgen, G. J. Witkamp, and R. N. J. Comans, “Mineral CO2 sequestration by steel slag carbonation,” *Environ Sci Technol*, vol. 39, no. 24, pp. 9676–9682, Dec. 2005, doi: 10.1021/ES050795F/SUPPL_FILE/ES050795FSI20051109_103746.PDF.

[47] W. J. J. Huijgen, G. J. Witkamp, and R. N. J. Comans, “Mechanisms of aqueous wollastonite carbonation as a possible CO2 sequestration process,” *Chem Eng Sci*, vol. 61, no. 13, pp. 4242–4251, Jul. 2006, doi: 10.1016/J.CES.2006.01.048.

[48] L. Wang, Y. Jin, and Y. Nie, “Investigation of accelerated and natural carbonation of MSWI fly ash with a high content of Ca,” *J Hazard Mater*, vol. 174, no. 1–3, pp. 334–343, Feb. 2010, doi: 10.1016/J.JHAZMAT.2009.09.055.

[49] N. L. Ukwattage, P. G. Ranjith, and S. H. Wang, “Investigation of the potential of coal combustion fly ash for mineral sequestration of CO2 by accelerated carbonation,” *Energy*, vol. 52, pp. 230–236, Apr. 2013, doi: 10.1016/J.ENERGY.2012.12.048.

[50] X. Li, M. F. Bertos, C. D. Hills, P. J. Carey, and S. Simon, “Accelerated carbonation of municipal solid waste incineration fly ashes,” *Waste Management*, vol. 27, no. 9, pp. 1200–1206, Jan. 2007, doi: 10.1016/J.WASMAN.2006.06.011.

[51] L. Ji *et al.*, “Effects of fly ash properties on carbonation efficiency in CO2 mineralisation,” *Fuel Processing Technology*, vol. 188, pp. 79–88, Jun. 2019, doi: 10.1016/J.FUPROC.2019.01.015.

[52] A. Polettini, R. Pomi, and A. Stramazzo, “Carbon sequestration through accelerated carbonation of BOF slag: Influence of particle size characteristics,” *Chemical Engineering Journal*, vol. 298, pp. 26–35, Aug. 2016, doi: 10.1016/J.CEJ.2016.04.015.

[53] S. Kumar and R. Kumar, “Mechanical activation of fly ash: Effect on reaction, structure and properties of resulting geopolymer,” *Ceram Int*, vol. 37, no. 2, pp. 533–541, Mar. 2011, doi: 10.1016/J.CERAMINT.2010.09.038.

[54] J. Temuujin, R. P. Williams, and A. van Riessen, “Effect of mechanical activation of fly ash on the properties of geopolymer cured at ambient temperature,” *J Mater Process Technol*, vol. 209, no. 12–13, pp. 5276–5280, Jul. 2009, doi: 10.1016/J.JMATPROTEC.2009.03.016.

[55] A. Fuller *et al.*, “Use of wood dust fly ash from an industrial pulverized fuel facility for rendering,” *Constr Build Mater*, vol. 189, pp. 825–848, Nov. 2018, doi: 10.1016/J.CONBUILDMAT.2018.09.016.

[56] A. S. Faried, S. A. Mostafa, B. A. Tayeh, and T. A. Tawfik, “The effect of using nano rice husk ash of different burning degrees on ultra-high-performance concrete properties,” *Constr Build Mater*, vol. 290, p. 123279, Jul. 2021, doi: 10.1016/J.CONBUILDMAT.2021.123279.

[57] A. M. Zeyad, I. S. Agwa, M. H. Abd-Elrahman, and S. A. Mostafa, “Engineering characteristics of ultra-high performance concrete containing basil plant ash,” *Case Studies in Construction Materials*, vol. 21, p. e03422, Dec. 2024, doi: 10.1016/J.CSCM.2024.E03422.

[58] J. Popławski and M. Lelusz, “Assessment of Sieving as a Mean to Increase Utilization Rate of Biomass Fly Ash in Cement-Based Composites,” *Applied Sciences 2023, Vol. 13, Page 1659*, vol. 13, no. 3, p. 1659, Jan. 2023, doi: 10.3390/APP13031659.

[59] P. Ni *et al.*, “Influence of carbonation under oxy-fuel combustion flue gas on the leachability of heavy metals in MSWI fly ash,” *Waste Management*, vol. 67, pp. 171–180, Sep. 2017, doi: 10.1016/J.WASMAN.2017.05.023.

[60] T. Sicong, J. Jianguo, and Z. Chang, “Influence of flue gas SO2 on the toxicity of heavy metals in municipal solid waste incinerator fly ash after accelerated carbonation stabilization,” *J Hazard Mater*, vol. 192, no. 3, pp. 1609–1615, Sep. 2011, doi: 10.1016/J.JHAZMAT.2011.06.085.

[61] Q. Yuan, X. Guo, and S. Ma, “The influence mechanism of mechanical modification on fly ash carbonation to solidify heavy metals,” *J Environ Chem Eng*, vol. 12, no. 6, p. 114714, Dec. 2024, doi: 10.1016/J.JECE.2024.114714.

[62] J. Chen *et al.*, “Accelerated carbonation of ball-milling modified MSWI fly ash: Migration and stabilization of heavy metals,” *J Environ Chem Eng*, vol. 11, no. 2, p. 109396, Apr. 2023, doi: 10.1016/J.JECE.2023.109396.

[63] S. Tian, J. Li, F. Liu, J. Guan, L. Dong, and Q. Wang, “Behavior of Heavy Metals in the Vitrification of MSWI Fly Ash with a Pilot-scale Diesel Oil Furnace,” *Procedia Environ Sci*, vol. 16, pp. 214–221, Jan. 2012, doi: 10.1016/J.PROENV.2012.10.030.

[64] H. Mattenberger *et al.*, “Sewage sludge ash to phosphorus fertiliser (II): Influences of ash and granulate type on heavy metal removal,” *Waste Management*, vol. 30, no. 8–9, pp. 1622–1633, Aug. 2010, doi: 10.1016/J.WASMAN.2010.03.037.

[65] G. Fraissler, M. Jöller, H. Mattenberger, T. Brunner, and I. Obernberger, “Thermodynamic equilibrium calculations concerning the removal of heavy metals from sewage sludge ash by chlorination,” *Chemical Engineering and Processing: Process Intensification*, vol. 48, no. 1, pp. 152–164, Jan. 2009, doi: 10.1016/J.CEP.2008.03.009.

[66] D. Lindberg, C. Molin, and M. Hupa, “Thermal treatment of solid residues from WtE units: A review,” *Waste Management*, vol. 37, pp. 82–94, Mar. 2015, doi: 10.1016/J.WASMAN.2014.12.009.

[67] I. Gabrijel, M. Skazlić, and N. Štirmer, “Long-Term Behavior of Concrete Containing Wood Biomass Fly Ash,” *Applied Sciences 2022, Vol. 12, Page 12859*, vol. 12, no. 24, p. 12859, Dec. 2022, doi: 10.3390/APP122412859.

[68] V. G. Ghorpade, “Effect of Wood Waste Ash on the Strength Characteristics of Concrete Nature Environment and Pollution Technology An International Quarterly Scientific Journal,” vol. 11, pp. 121–124, 2012, Accessed: Apr. 15, 2025. [Online]. Available: www.neptjournal.com

[69] A. N. Givi, S. A. Rashid, F. N. A. Aziz, and M. A. M. Salleh, “Assessment of the effects of rice husk ash particle size on strength, water permeability and workability of binary blended concrete,” *Constr Build Mater*, vol. 24, no. 11, pp. 2145–2150, Nov. 2010, doi: 10.1016/J.CONBUILDMAT.2010.04.045.

[70] D. Nagrockienė and A. Daugėla, “Investigation into the properties of concrete modified with biomass combustion fly ash,” *Constr Build Mater*, vol. 174, pp. 369–375, Jun. 2018, doi: 10.1016/J.CONBUILDMAT.2018.04.125.

[71] “NEN-EN 451-1:2017 en.” Accessed: Apr. 16, 2025. [Online]. Available: https://www.nen.nl/nen-en-451-1-2017-en-233607

[72] L. Ji *et al.*, “CO2 sequestration by direct mineralisation using fly ash from Chinese Shenfu coal,” *Fuel Processing Technology*, vol. 156, pp. 429–437, Feb. 2017, doi: 10.1016/J.FUPROC.2016.10.004.

[73] U. Müller and K. Rübner, “The microstructure of concrete made with municipal waste incinerator bottom ash as an aggregate component,” *Cem Concr Res*, vol. 36, no. 8, pp. 1434–1443, Aug. 2006, doi: 10.1016/J.CEMCONRES.2006.03.023.

[74] R. Yu, P. Tang, P. Spiesz, and H. J. H. Brouwers, “A study of multiple effects of nano-silica and hybrid fibres on the properties of Ultra-High Performance Fibre Reinforced Concrete (UHPFRC) incorporating waste bottom ash (WBA),” *Constr Build Mater*, vol. 60, pp. 98–110, Jun. 2014, doi: 10.1016/J.CONBUILDMAT.2014.02.059.

[75] G. Montes-Hernandez, A. Pommerol, F. Renard, P. Beck, E. Quirico, and O. Brissaud, “In situ kinetic measurements of gas–solid carbonation of Ca(OH)2 by using an infrared microscope coupled to a reaction cell,” *Chemical Engineering Journal*, vol. 161, no. 1–2, pp. 250–256, Jul. 2010, doi: 10.1016/J.CEJ.2010.04.041.

[76] S. Tominc and V. Ducman, “Methodology for Evaluating the CO2 Sequestration Capacity of Waste Ashes,” *Materials 2023, Vol. 16, Page 5284*, vol. 16, no. 15, p. 5284, Jul. 2023, doi: 10.3390/MA16155284.

[77] B. Lu, C. Shi, J. Zhang, and J. Wang, “Effects of carbonated hardened cement paste powder on hydration and microstructure of Portland cement,” *Constr Build Mater*, vol. 186, pp. 699–708, Oct. 2018, doi: 10.1016/J.CONBUILDMAT.2018.07.159.

[78] P. Shen *et al.*, “Phase assemblance evolution during wet carbonation of recycled concrete fines,” *Cem Concr Res*, vol. 154, p. 106733, Apr. 2022, doi: 10.1016/J.CEMCONRES.2022.106733.

[79] Z. Sun and A. Vollpracht, “Isothermal calorimetry and in-situ XRD study of the NaOH activated fly ash, metakaolin and slag,” *Cem Concr Res*, vol. 103, pp. 110–122, Jan. 2018, doi: 10.1016/J.CEMCONRES.2017.10.004.

[80] G. Wei, B. Dong, G. Fang, and Y. Wang, “Understanding reactive amorphous phases of fly ash through the acidolysis,” *Cem Concr Compos*, vol. 140, p. 105102, Jul. 2023, doi: 10.1016/J.CEMCONCOMP.2023.105102.

[81] I. Ismail, S. A. Bernal, J. L. Provis, R. San Nicolas, S. Hamdan, and J. S. J. Van Deventer, “Modification of phase evolution in alkali-activated blast furnace slag by the incorporation of fly ash,” *Cem Concr Compos*, vol. 45, pp. 125–135, Jan. 2014, doi: 10.1016/J.CEMCONCOMP.2013.09.006.

[82] W. Y. Lin, A. K. Prabhakar, B. C. Mohan, and C. H. Wang, “A factorial experimental analysis of using wood fly ash as an alkaline activator along with coal fly ash for production of geopolymer-cementitious hybrids,” *Science of The Total Environment*, vol. 718, p. 135289, May 2020, doi: 10.1016/J.SCITOTENV.2019.135289.

[83] W. Mozgawa, M. Król, J. Dyczek, and J. Deja, “Investigation of the coal fly ashes using IR spectroscopy,” *Spectrochim Acta A Mol Biomol Spectrosc*, vol. 132, pp. 889–894, Nov. 2014, doi: 10.1016/J.SAA.2014.05.052.

[84] A. Feriancová, M. Pajtášová, K. Moricová, and B. Pecušová, “Using of wood ash as the alternative filler for preparation of rubber mixtures,” *IOP Conf Ser Mater Sci Eng*, vol. 776, no. 1, p. 012087, Feb. 2020, doi: 10.1088/1757-899X/776/1/012087.

[85] B. Lu, C. Shi, J. Zhang, and J. Wang, “Effects of carbonated hardened cement paste powder on hydration and microstructure of Portland cement,” *Constr Build Mater*, vol. 186, pp. 699–708, Oct. 2018, doi: 10.1016/J.CONBUILDMAT.2018.07.159.

[86] G. Deng *et al.*, “Pozzolanic reactivity of carbonated high-calcium fly ash: A mechanism study,” *Constr Build Mater*, vol. 446, p. 138015, Oct. 2024, doi: 10.1016/J.CONBUILDMAT.2024.138015.

[87] A. Ćwik, I. Casanova, K. Rausis, and K. Zarębska, “Utilization of high-calcium fly ashes through mineral carbonation: The cases for Greece, Poland and Spain,” *Journal of CO2 Utilization*, vol. 32, pp. 155–162, Jul. 2019, doi: 10.1016/J.JCOU.2019.03.020.

[88] L. Regev, K. M. Poduska, L. Addadi, S. Weiner, and E. Boaretto, “Distinguishing between calcites formed by different mechanisms using infrared spectrometry: archaeological applications,” *J Archaeol Sci*, vol. 37, no. 12, pp. 3022–3029, Dec. 2010, doi: 10.1016/J.JAS.2010.06.027.

[89] P. Shen *et al.*, “Phase assemblance evolution during wet carbonation of recycled concrete fines,” *Cem Concr Res*, vol. 154, p. 106733, Apr. 2022, doi: 10.1016/J.CEMCONRES.2022.106733.

[90] P. Shen *et al.*, “Phase assemblance evolution during wet carbonation of recycled concrete fines,” *Cem Concr Res*, vol. 154, p. 106733, Apr. 2022, doi: 10.1016/J.CEMCONRES.2022.106733.

[91] Z. Zhang, H. Wang, J. L. Provis, F. Bullen, A. Reid, and Y. Zhu, “Quantitative kinetic and structural analysis of geopolymers. Part 1. The activation of metakaolin with sodium hydroxide,” *Thermochim Acta*, vol. 539, pp. 23–33, Jul. 2012, doi: 10.1016/J.TCA.2012.03.021.

[92] I. García Lodeiro, D. E. Macphee, A. Palomo, and A. Fernández-Jiménez, “Effect of alkalis on fresh C–S–H gels. FTIR analysis,” *Cem Concr Res*, vol. 39, no. 3, pp. 147–153, Mar. 2009, doi: 10.1016/J.CEMCONRES.2009.01.003.

[93] X. Gao, Q. L. Yu, and H. J. H. Brouwers, “Reaction kinetics, gel character and strength of ambient temperature cured alkali activated slag–fly ash blends,” *Constr Build Mater*, vol. 80, pp. 105–115, Apr. 2015, doi: 10.1016/J.CONBUILDMAT.2015.01.065.

[94] X. Gao, Q. L. Yu, and H. J. H. Brouwers, “Reaction kinetics, gel character and strength of ambient temperature cured alkali activated slag–fly ash blends,” *Constr Build Mater*, vol. 80, pp. 105–115, Apr. 2015, doi: 10.1016/J.CONBUILDMAT.2015.01.065.

[95] S. K. Nath and S. Kumar, “Influence of iron making slags on strength and microstructure of fly ash geopolymer,” *Constr Build Mater*, vol. 38, pp. 924–930, Jan. 2013, doi: 10.1016/J.CONBUILDMAT.2012.09.070.

[96] H. K. Tchakouté, C. H. Rüscher, S. Kong, E. Kamseu, and C. Leonelli, “Geopolymer binders from metakaolin using sodium waterglass from waste glass and rice husk ash as alternative activators: A comparative study,” *Constr Build Mater*, vol. 114, pp. 276–289, Jul. 2016, doi: 10.1016/J.CONBUILDMAT.2016.03.184.

[97] H. Xu, Q. Li, L. Shen, M. Zhang, and J. Zhai, “Low-reactive circulating fluidized bed combustion (CFBC) fly ashes as source material for geopolymer synthesis,” *Waste Management*, vol. 30, no. 1, pp. 57–62, Jan. 2010, doi: 10.1016/J.WASMAN.2009.09.014.

[98] B. Lu, C. Shi, J. Zhang, and J. Wang, “Effects of carbonated hardened cement paste powder on hydration and microstructure of Portland cement,” *Constr Build Mater*, vol. 186, pp. 699–708, Oct. 2018, doi: 10.1016/J.CONBUILDMAT.2018.07.159.

[99] M. Dener, M. Karatas, and M. Mohabbi, “Sulfate resistance of alkali-activated slag/Portland cement mortar produced with lightweight pumice aggregate,” *Constr Build Mater*, vol. 304, p. 124671, Oct. 2021, doi: 10.1016/J.CONBUILDMAT.2021.124671.

[100] S. S. Narani, S. Siddiqua, and P. Perumal, “Wood fly ash and blast furnace slag management by alkali-activation: Trace elements solidification and composite application,” *J Environ Manage*, vol. 354, p. 120341, Mar. 2024, doi: 10.1016/J.JENVMAN.2024.120341.

[101] V. Gupta, D. K. Pathak, S. Siddique, R. Kumar, and S. Chaudhary, “Study on the mineral phase characteristics of various Indian biomass and coal fly ash for its use in masonry construction products,” *Constr Build Mater*, vol. 235, p. 117413, Feb. 2020, doi: 10.1016/J.CONBUILDMAT.2019.117413.

[102] I. Ismail, S. A. Bernal, J. L. Provis, R. San Nicolas, S. Hamdan, and J. S. J. Van Deventer, “Modification of phase evolution in alkali-activated blast furnace slag by the incorporation of fly ash,” *Cem Concr Compos*, vol. 45, pp. 125–135, Jan. 2014, doi: 10.1016/J.CEMCONCOMP.2013.09.006.

[103] Z. Sun and A. Vollpracht, “Isothermal calorimetry and in-situ XRD study of the NaOH activated fly ash, metakaolin and slag,” *Cem Concr Res*, vol. 103, pp. 110–122, Jan. 2018, doi: 10.1016/J.CEMCONRES.2017.10.004.

[104] S. K. Nath and S. Kumar, “Reaction kinetics, microstructure and strength behavior of alkali activated silico-manganese (SiMn) slag – Fly ash blends,” *Constr Build Mater*, vol. 147, pp. 371–379, Aug. 2017, doi: 10.1016/J.CONBUILDMAT.2017.04.174.

[105] X. Gao, Q. L. Yu, and H. J. H. Brouwers, “Reaction kinetics, gel character and strength of ambient temperature cured alkali activated slag–fly ash blends,” *Constr Build Mater*, vol. 80, pp. 105–115, Apr. 2015, doi: 10.1016/J.CONBUILDMAT.2015.01.065.

[106] X. Yao, Z. Zhang, H. Zhu, and Y. Chen, “Geopolymerization process of alkali–metakaolinite characterized by isothermal calorimetry,” *Thermochim Acta*, vol. 493, no. 1–2, pp. 49–54, Sep. 2009, doi: 10.1016/J.TCA.2009.04.002.

[107] S. Chithiraputhiran and N. Neithalath, “Isothermal reaction kinetics and temperature dependence of alkali activation of slag, fly ash and their blends,” *Constr Build Mater*, vol. 45, pp. 233–242, Aug. 2013, doi: 10.1016/J.CONBUILDMAT.2013.03.061.

[108] B. Chen, “Utilization of mswi bottom ash as a mineral resource for low-carbon construction materials,” 2023, doi: 10.4233/0793986F-B875-4693-A0F9-568978F2D632.

[109] Y. yan WANG, L. yuan CHAI, H. CHANG, X. yu PENG, and Y. de SHU, “Equilibrium of hydroxyl complex ions in Pb2+-H2O system,” *Transactions of Nonferrous Metals Society of China*, vol. 19, no. 2, pp. 458–462, Apr. 2009, doi: 10.1016/S1003-6326(08)60295-2.

[110] H. Ecke, N. Menad, and A. Lagerkvist, “Carbonation of Municipal Solid Waste Incineration Fly Ash and the Impact on Metal Mobility,” *Journal of Environmental Engineering*, vol. 129, no. 5, pp. 435–440, May 2003, doi: 10.1061/(ASCE)0733-9372(2003)129:5(435).

[111] A. Polettini, R. Pomi, and A. Stramazzo, “CO2 sequestration through aqueous accelerated carbonation of BOF slag: A factorial study of parameters effects,” *J Environ Manage*, vol. 167, pp. 185–195, Feb. 2016, doi: 10.1016/J.JENVMAN.2015.11.042.

[112] S. Sakita and K. Nishimura, “Physical containment of municipal solid waste incineration bottom ash by accelerated carbonation,” *J Mater Cycles Waste Manag*, vol. 18, no. 4, pp. 687–694, Sep. 2016, doi: 10.1007/S10163-015-0369-8/METRICS.

[113] # Rimvydas Kaminskas and V. Cesnauskas, “INFLUENCE OF ACTIVATED BIOMASS FLY ASH ON PORTLAND CEMENT HYDRATION,” *Ceramics-Silikáty*, vol. 58, no. 4, pp. 260–268, 2014.

[114] C. B. Cheah and M. Ramli, “Mechanical strength, durability and drying shrinkage of structural mortar containing HCWA as partial replacement of cement,” *Constr Build Mater*, vol. 30, pp. 320–329, May 2012, doi: 10.1016/J.CONBUILDMAT.2011.12.009.

[115] “NEN-EN 1338:2003 nl.” Accessed: Apr. 20, 2025. [Online]. Available: https://www.nen.nl/nen-en-1338-2003-nl-99353

[116] “NEN-EN 206+NEN 8005:2017 nl.” Accessed: Apr. 20, 2025. [Online]. Available: https://www.nen.nl/nen-en-206-nen-8005-2017-nl-242684

[117] “ASTM C143/C143M - 20 en.” Accessed: Apr. 16, 2025. [Online]. Available: https://www.nen.nl/en/astm-c143-c143m-20-en-8444126

[118] “NEN-EN 12390-3:2019 en.” Accessed: Apr. 16, 2025. [Online]. Available: https://www.nen.nl/nen-en-12390-3-2019-en-260976

[119] “NEN-EN 12390-6:2022 Ontw. en.” Accessed: Apr. 16, 2025. [Online]. Available: https://www.nen.nl/nen-en-12390-6-2022-ontw-en-298761

[120] “NVN-CEN/TS 12390-9:2016 en.” Accessed: Apr. 16, 2025. [Online]. Available: https://www.nen.nl/nvn-cen-ts-12390-9-2016-en-228436

[121] “NEN-EN 206:2014+A2:2021 nl.” Accessed: Apr. 16, 2025. [Online]. Available: https://www.nen.nl/nen-en-206-2014-a2-2021-nl-288142

[122] Y. Luo, H. J. H. Brouwers, and Q. Yu, “Understanding the gel compatibility and thermal behavior of alkali activated Class F fly ash/ladle slag: The underlying role of Ca availability,” *Cem Concr Res*, vol. 170, p. 107198, Aug. 2023, doi: 10.1016/J.CEMCONRES.2023.107198.

[123] S. Zhang, Z. Li, B. Ghiassi, S. Yin, and G. Ye, “Fracture properties and microstructure formation of hardened alkali-activated slag/fly ash pastes,” *Cem Concr Res*, vol. 144, p. 106447, Jun. 2021, doi: 10.1016/J.CEMCONRES.2021.106447.

[124] C. Finocchiaro, G. Barone, P. Mazzoleni, C. Leonelli, A. Gharzouni, and S. Rossignol, “FT-IR study of early stages of alkali activated materials based on pyroclastic deposits (Mt. Etna, Sicily, Italy) using two different alkaline solutions,” *Constr Build Mater*, vol. 262, p. 120095, Nov. 2020, doi: 10.1016/J.CONBUILDMAT.2020.120095.

[125] H. K. Tchakouté, C. H. Rüscher, S. Kong, E. Kamseu, and C. Leonelli, “Geopolymer binders from metakaolin using sodium waterglass from waste glass and rice husk ash as alternative activators: A comparative study,” *Constr Build Mater*, vol. 114, pp. 276–289, Jul. 2016, doi: 10.1016/J.CONBUILDMAT.2016.03.184.

[126] S. K. Nath and S. Kumar, “Evaluation of the suitability of ground granulated silico-manganese slag in Portland slag cement,” *Constr Build Mater*, vol. 125, pp. 127–134, Oct. 2016, doi: 10.1016/J.CONBUILDMAT.2016.08.025.

[127] X. Gao, Q. L. Yu, and H. J. H. Brouwers, “Reaction kinetics, gel character and strength of ambient temperature cured alkali activated slag–fly ash blends,” *Constr Build Mater*, vol. 80, pp. 105–115, Apr. 2015, doi: 10.1016/J.CONBUILDMAT.2015.01.065.

[128] Y. Luo, H. J. H. Brouwers, and Q. Yu, “Understanding the gel compatibility and thermal behavior of alkali activated Class F fly ash/ladle slag: The underlying role of Ca availability,” *Cem Concr Res*, vol. 170, p. 107198, Aug. 2023, doi: 10.1016/J.CEMCONRES.2023.107198.

[129] I. F. Sáez Del Bosque, S. Martínez-Ramírez, and M. T. Blanco-Varela, “FTIR study of the effect of temperature and nanosilica on the nano structure of C–S–H gel formed by hydrating tricalcium silicate,” *Constr Build Mater*, vol. 52, pp. 314–323, Feb. 2014, doi: 10.1016/J.CONBUILDMAT.2013.10.056.

[130] Y. Zhao, X. Hu, Q. Yuan, and C. Shi, “The change of phase assemblage and desorption of bound chloride for seawater cement paste under sulfate attack,” *Cem Concr Compos*, vol. 139, p. 105033, May 2023, doi: 10.1016/J.CEMCONCOMP.2023.105033.

[131] I. Ismail, S. A. Bernal, J. L. Provis, R. San Nicolas, S. Hamdan, and J. S. J. Van Deventer, “Modification of phase evolution in alkali-activated blast furnace slag by the incorporation of fly ash,” *Cem Concr Compos*, vol. 45, pp. 125–135, Jan. 2014, doi: 10.1016/J.CEMCONCOMP.2013.09.006.

[132] H. Miraki, N. Shariatmadari, P. Ghadir, S. Jahandari, Z. Tao, and R. Siddique, “Clayey soil stabilization using alkali-activated volcanic ash and slag,” *Journal of Rock Mechanics and Geotechnical Engineering*, vol. 14, no. 2, pp. 576–591, Apr. 2022, doi: 10.1016/J.JRMGE.2021.08.012.

[133] I. Garcia-Lodeiro, A. Palomo, A. Fernández-Jiménez, and D. E. MacPhee, “Compatibility studies between N-A-S-H and C-A-S-H gels. Study in the ternary diagram Na2O–CaO–Al2O3–SiO2–H2O,” *Cem Concr Res*, vol. 41, no. 9, pp. 923–931, Sep. 2011, doi: 10.1016/J.CEMCONRES.2011.05.006.

[134] G. Fang and M. Zhang, “The evolution of interfacial transition zone in alkali-activated fly ash-slag concrete,” *Cem Concr Res*, vol. 129, p. 105963, Mar. 2020, doi: 10.1016/J.CEMCONRES.2019.105963.

[135] “NEN-EN-ISO 14040:2006 en.” Accessed: Apr. 16, 2025. [Online]. Available: https://www.nen.nl/nen-en-iso-14040-2006-en-109085

[136] “NIBE EPD.” Accessed: Apr. 15, 2025. [Online]. Available: https://www.nibe-sustainability-experts.com/nl/epd-tool

[137] L. K. Turner and F. G. Collins, “Carbon dioxide equivalent (CO2-e) emissions: A comparison between geopolymer and OPC cement concrete,” *Constr Build Mater*, vol. 43, pp. 125–130, Jun. 2013, doi: 10.1016/J.CONBUILDMAT.2013.01.023.

[138] G. Habert, J. B. D’Espinose De Lacaillerie, and N. Roussel, “An environmental evaluation of geopolymer based concrete production: reviewing current research trends,” *J Clean Prod*, vol. 19, no. 11, pp. 1229–1238, Jul. 2011, doi: 10.1016/J.JCLEPRO.2011.03.012.

[139] J. L. Provis, A. Palomo, and C. Shi, “Advances in understanding alkali-activated materials,” *Cem Concr Res*, vol. 78, pp. 110–125, Dec. 2015, doi: 10.1016/J.CEMCONRES.2015.04.013.

[140] J. Du, Z. Liu, C. Christodoulatos, M. Conway, Y. Bao, and W. Meng, “Utilization of off-specification fly ash in preparing ultra-high-performance concrete (UHPC): Mixture design, characterization, and life-cycle assessment,” *Resour Conserv Recycl*, vol. 180, p. 106136, May 2022, doi: 10.1016/J.RESCONREC.2021.106136.

[141] L. Li and M. Wu, “An overview of utilizing CO2 for accelerated carbonation treatment in the concrete industry,” *Journal of CO2 Utilization*, vol. 60, p. 102000, Jun. 2022, doi: 10.1016/J.JCOU.2022.102000.